©Copyright 2019
Lauren Michelle Saunders

Thyroid hormone regulation of pigment cell lineages in Zebrafish

Lauren Michelle Saunders

A dissertation
submitted in partial fulfillment of the
requirements for the degree of

Doctor of Philosophy

University of Washington

2019

Reading Committee:

David M. Parichy, Chair

Cole Trapnell, Chair

Andrea E. Wills

Program Authorized to Offer Degree:
Molecular and Cellular Biology

University of Washington

Abstract

Thyroid hormone regulation of pigment cell lineages in Zebrafish

Lauren Michelle Saunders

Co-Chairs of the Supervisory Committee:
Professor David M. Parichy
Biology

Assistant Professor Cole Trapnell
Genome Sciences

During the generation of adult form, circulating endocrine factors are important orchestrators of complex developmental processes. One such factor, thyroid hormone (TH), is essential for proper development and coordinates diverse, often contrasting, cellular events via mechanisms that are poorly understood. Pigmentation of adult zebrafish offers an unusually tractable model in which to address these issues as two neural crest-derived lineages – black melanophores and yellow/orange xanthophores – differ dramatically in their TH-dependence. I sought to define how TH elicits seemingly disparate outcomes in the abundance of these two pigment cell classes during pigment pattern formation. By profiling individual transcriptomes from thousands of neural crest-derived cells, including pigment cells, using single cell RNA-sequencing, I reconstructed developmental trajectories and identified lineage-specific responses to TH. Rather than acting on multipotent progenitors or directing specification towards one lineage or another, we find that TH promotes the maturation of both cell types in distinct ways. Additionally, to better understand how TH signaling differentially modulates gene expression programs in these lineages, I evaluated roles for TH nuclear receptors (TR), which classically repress gene expression in their unliganded form but activate target genes when ligand is present. By combining genetic analyses and thyroid ablation-induced hypothyroidism, we identify roles for TR-dependent repression during zebrafish post-embryonic

development. Together, these studies provide insights into how TH defines and maintains diverse cell lineages during development and deepen our understanding of the neural crest-derived cell types that contribute to adult pigmentation in zebrafish.

In this dissertation, I first introduce zebrafish pigment pattern formation as a model for studying diverse outcomes of global endocrine signaling during development. In Chapter 2, I detail our new understanding of how TH drives lineage-specific outcomes during pigment pattern formation. Specifically, we identify distinct roles for TH in the maturation of both melanophores and xanthophores. In melanophores TH drives a state of terminal differentiation and proliferative arrest, limiting the final number of these cells. In xanthophores, TH is required for the accumulation of yellow, carotenoid-based pigment as cells exit a cryptic phase. Moreover, I present findings that these maturation programs are gated by TRs. In a final chapter, I reflect on future directions for this work as well as promises and limitations of single-cell genomics for studying how global signals are translated into cell-type specific outcomes.

TABLE OF CONTENTS

LIST OF FIGURES

LIST OF TABLES

ACKNOWLEDGMENTS

I am deeply grateful to the community of friends, colleagues, and mentors who supported me during the preparation of this dissertation. Thank you to members of the UW MCB program, Genome Sciences, and the developmental biology community for creating a genuinely inspiring environment to do science.

I thank my mentors, Dave Parichy and Cole Trapnell, who gave me the freedom and financial support to pursue this collaborative thesis project. I am truly thankful for their willingness to co-advise me despite the challenges in doing so. To Dave, thank you for your exhaustive dedication to my training and for leading by example. To Cole, thank you for your optimism and your contagious enthusiasm for asking harder questions. Your ability to attract brilliant, engaging, fun scientists to the lab creates an environment that I look forward to doing research in (almost) every day.

I thank my committee members, Andrea Wills, Dave Raible, and Jay Parrish for generously providing expertise, guidance, and perspective. I also thank them for offering lab space and reagents when my fish moved across the country. I feel incredibly lucky to be part of the rich, inclusive developmental biology community at UW, to which they have all contributed.

I thank my incredible past scientific mentors, especially Kevin Mouillesseaux, Vicki Bautch, Eric Cole, Aaron Turkewitz, and Erica Zweifel, without whom I would not have pursued a career in science.

Completing a dissertation is both an independent enterprise and one that suffers from too much independence. This work would have been impossible without an incredible group of colleagues and friends, of which I am glad there is much overlap. To members of the Parichy and Trapnell labs - especially Andy Aman, Sanjay Srivatsan, Hannah Pliner, Vic Lewis, and Jonathan Packer - thank you for teaching me most of the useful things I learned during this process (and some less

useful things too). Your generosity of time, patience, and scientific insight constantly inspire me to be a better colleague and scientist.

A huge thanks to my friends for keeping me grounded and getting me outside. I thank my fellow “fish doctor”, Sophie Archembeault, for helping me maintain sanity by keeping my head underwater or overseas. And Hannah Pliner for getting me off the grid and teaching me true wilderness survival skills. I thank Kristen Mittelsteadt, Sanjay Srivatsan, and Rebecca Resnick for numerous forms of support and friendship. And I especially thank Mike Dorrity, whose humor and endless creativity makes time inside and outside the lab far more fun and rewarding.

Finally, I thank my family for their unquestioning support and for not taking it personally when I spent holidays caring for fish instead of spending time with them.

Chapter 1: INTRODUCTION

Development from a single cell into a functional adult organism requires precise coordination of cellular events across multiple life stages. In the embryo, local paracrine signaling is sufficient to drive much of early development. The subsequent transition from larval-to-adult stages – whether in the drastic body plan remodeling of frogs or in the more subtle fetal-to-adult transition of mammals – requires coordination of these developmental events by global endocrine signals. These signals are capable of eliciting both systemic and tissue-specific responses in distant regions. A prominent signal regulating body remodeling and maturation during the larval-to-adult transition is thyroid hormone (TH) (Shi, 1999; Brent, 2012). The pigment pattern of zebrafish, *Danio rerio*, has emerged as an excellent system to study the mechanisms of TH signaling because two pigment cell lineages, black melanophores and yellow/orange xanthophores, respond differentially to TH (McMenamin et al., 2014). Mechanisms of TH-dependent responses are difficult to resolve *in vivo* as they involve broad-scale heterogeneous responses across cell types through the action of hundreds of TH target genes. Recent advances in single cell genomics enabling the measurement of whole transcriptomes in thousands of individual cells have provided a unique opportunity to resolve mechanisms of TH action across diverse cell types during post-embryonic development. In this introduction, I will discuss (1) zebrafish pigmentation as a model for studying pattern formation and developmental plasticity of adult, neural-crest derived lineages; (2) the role of TH during the larval-to-adult transition in zebrafish; and (3) the use of single-cell genomics to resolve cell-specific responses underlying these processes.

1.0.1 Pigment pattern formation and neural crest-derived pigment cell lineages in Zebrafish

Vertebrate pigment cells are derived from the embryonic neural crest. The neural crest is a transient, vertebrate-specific tissue that contributes to peripheral nerves and glia, craniofacial cartilage and

bone, and other derivatives (Gans and Northcutt, 1983; Bronner and Simões-Costa, 2016). Differences in the development of NC-derivatives contributes to much of the phenotypic diversity across vertebrates. Birds and mammals have just one pigment cell type – the black melanocyte – which transfers pigment granules to the skin, hair and feathers. In contrast, zebrafish and other teleost fishes, amphibians and reptiles have multiple pigment cell types, or chromatophores. Both the class and spatial arrangement of these chromatophores contribute to the diversity of pigmentation patterns seen in nature. Pigmentation patterns are ecologically relevant for inter- and intraspecific interactions like mate choice, species recognition and predation avoidance (Santos et al., 2003; Salis et al., 2018; Kodric-Brown, 1985; Engeszer et al., 2008).

Zebrafish chromatophores reside in the hypodermis between the skin and muscle, and three main classes comprise their distinctive striped pattern: black melanophores, yellow/orange xanthophores, and iridescent iridophores. During formation of the adult striped pigment pattern, the less distinctive larval pattern is either remodeled or replaced by new pigment cells in a series of precisely coordinated morphogenetic and differentiation events. Previous work has elucidated many of the key signaling molecules and cellular behaviors that contribute to the establishment of stripes, yet substantial gaps remain in our understanding.

While the development of the neural crest has captivated biologists for nearly 150 years, recent studies using genetic lineage tracing have added to our understanding of the multipotent nature of both early neural crest cells and, in some instances, the derivatives that contribute to organism-wide changes during post-embryonic development (Baggiolini et al., 2015; Singh et al., 2016; Adameyko et al., 2009; Petersen and Adameyko, 2017). For example, recent work showed that late-stage, multipotent progenitors contribute to many of the melanophores and iridophores, and at least some of the xanthophores of the adult pattern in zebrafish (Singh et al., 2016), consistent with the requirement for latent NC-derived precursors that associate with dorsal root ganglia (DRG) near the spinal cord during pattern remodeling (Parichy et al., 1999; Budi et al., 2008, 2011; Dooley et al., 2013a). While the early larval melanophore and iridophore populations have only minor contributions to the adult pattern, many early xanthophores persist and continue to proliferate over the flank, entering a “cryptic” unpigmented period during the early stages of adult pattern forma-

tion. However, the relative proportions of early vs. stem cell derived xanthophores is not known (Mahalwar et al., 2014; McMenamin et al., 2014) (Figure 1.1). During the period of adult pattern formation, which unfolds over ∼3 weeks, the constituent cell populations are extremely heterogeneous. At any given time, there are multiple pigment progenitor cell types, committed intermediates, and fully differentiated melanophores, iridophores, and xanthophores (McMenamin et al., 2014; Singh et al., 2016; Eom et al., 2015; Parichy et al., 2003; Johnson et al., 1995). Moreover, within each lineage there is evidence of phenotypically cryptic subpopulations with distinct molecular profiles (e.g., Kit ligand-dependent and independent melanophores (Parichy et al., 1999)). Despite our current knowledge of the lineage relationships and cellular heterogeneity of pigment cells during this complex process, our understanding of the molecular profiles of these cell populations through developmental time or in response to stimuli remains incomplete.

While fundamental questions remain about the mechanisms underlying post-embryonic pigment pattern formation, some key signaling molecules and gene regulatory networks required for the specification and differentiation of each pigment cell class are known (Parichy and Spiewak, 2015; Petratou et al., 2018). Melanophore fate specification relies on the melanocyte inducing transcription factor a (*mitfa*), a homologue of Mitf which serves as the master regulator of melanocyte fate in mammals and other amniotes (Lister et al., 1999; Opdecamp et al., 1997; Levy et al., 2006). The repression of *mitfa* by the forkhead transcription factor, *foxd3*, in conjunction with the expression of a basic-helix-loop-helix transcription factor, *tfec*, is required for iridophore fate specification (Lister et al., 2001; Petratou et al., 2018; Mahony et al., 2016). In xanthophores, specification from early neural crest cells depends on the paired box homeodomain transcription factors, *pax7a/b* and *pax3a*, though their downstream effectors and their requirement for specifying late-stage progenitor-derived xanthophores is unknown (Nord et al., 2016; Minchin and Hughes, 2008). Differentiation of cryptic xanthophores is facilitated by signaling through the receptor tyrosine kinase Colony stimulating factor receptor 1 (*csf1ra*); its ligands, *csf1a* and *csf1b*, are expressed by iridophores and other cells in the hypodermis (Parichy et al., 2000b; Patterson et al., 2014). Genetic studies have uncovered local signaling pathways with roles for proper pattern formation and maintenence, including Wnt, Endothelin, Delta-Notch and Melanocortin (Greenhill et al., 2011;

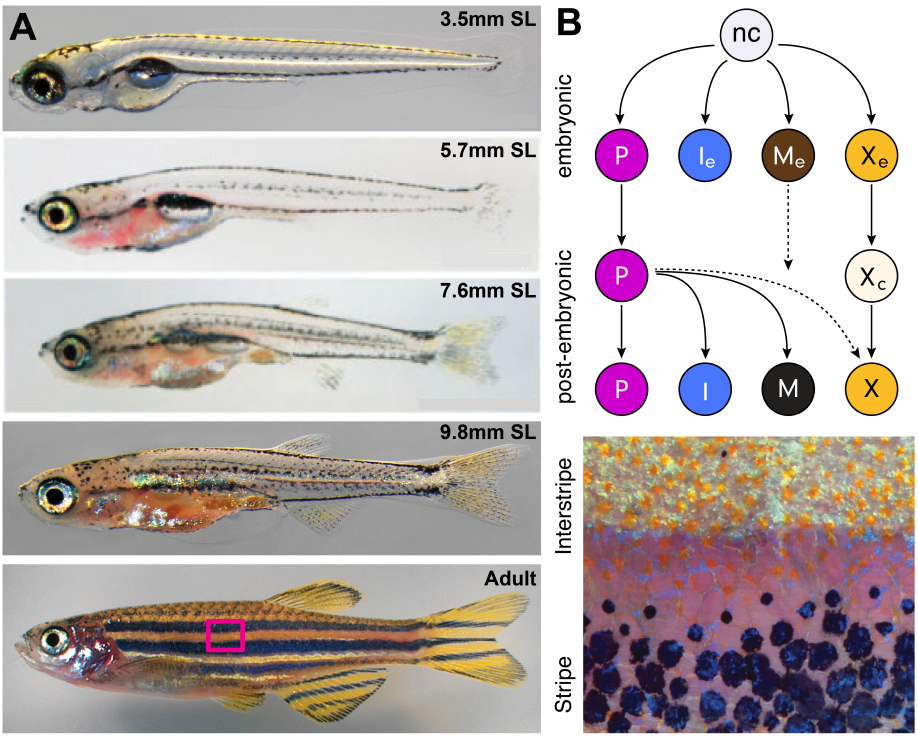

Figure 1.1: ***D. rerio* post-embryonic pigment cell lineages and pattern.** A) Established lineage relationships of embryonic and post-embryonic pigment cells. Multipotent pigment cell progenitors (P) in the peripheral nervous system generate adult iridophores (I), melanophores (M) and some xanthophores (X). A few embryonic melanophores (Me) persist whereas embryonic xanthophores (Xe) proliferate and lose their pigment to enter a cryptic phase (Xc), and then reacquire pigment late in pattern formation to form most adult xanthophores (Patterson et al., 2014).

Lee et al., 2003; Spiewak et al., 2018; Dooley et al., 2013a; Hamada et al., 2014; Eom et al., 2015; Ceinos et al., 2015). Long range hormone signals, including TH (McMenamin et al., 2014) and insulin signaling (Zhang et al., 2018), also coordinate the process of pattern formation. An outstanding question in our understanding of the mechanisms through which adult patterns are formed and maintained is how global signals are integrated with local cell-cell interactions across multiple cell types in different states of differentiation. Much of our understanding about pigment-cell autonomous and non-autonomous factors affecting stripe formation have been discovered through analysis of pigmentation mutants recovered from forward genetic screens or serendipitously in

the lab or pet shops (Haffter et al., 1996; Kelsh et al., 1996; Patton and Zon, 2001; Parichy and Spiewak, 2015). While fruitful, there are limitations to this approach: each mutant often requires years of analysis to understand the gene and cell types affected, mutations do not target specific mechanisms or processes of interest, and mutations in genes with pleiotropic roles in development may result in premature death or uninterpretable phenotypes. Recent advances in single cell genomics and CRISPR/Cas9-based genome editing have rapidly increased the pace of discovery for genes and pathways involved in complex trait formation. For my dissertation, I aimed to resolve mechanisms by which a critical endocrine signal, TH, regulates the specification and differentiation of particular pigment cell lineages from a multipotent progenitor. To this end, I used conditional ablation of the thyroid gland combined with single-cell genomic and reverse genetic techniques. In Chapter 2, I directly address outstanding questions related to TH regulation of melanophore and xanthophore lineages during post-embryonic pigment pattern formation.

1.0.2 The role of thyroid hormone during post-embryonic development

Adult pigmentation in zebrafish has emerged as a powerful model system to study how TH induces proper organization of an entire lineage of cells. Zebrafish do not undergo such dramatic metamorphic changes as frogs or some other teleost species, such as flatfish; yet, there are still major morphological and physiological changes that occur and this subtler transformation is more reminiscent of the fetal-to-adult transition in placental mammals (Parichy et al., 2009a; McMenamin and Parichy, 2013). The larval-to-adult transition in zebrafish begins at $\sim$10 days post fertilization and unfolds over $\sim$3 weeks; during this time the adult pigment pattern is established and refined, the axial skeleton is ossified, scales develop to fully armor the body, and many organs mature and are remodeled, including the gut, kidneys, and peripheral nervous system (Parichy et al., 2009a; Larson et al., 2010; Robertson et al., 2007; McMenamin and Parichy, 2013). The endocrine signal, TH, is a key orchestrator of these developmental events, yet the specific mechanisms by which it drives such diverse outcomes remain essentially unknown. During post-embryonic development in zebrafish, the NC-derived pigment cell lineages display strikingly different responses to TH (Mc-

Menamin et al., 2014). TH promotes xanthophore population expansion via increased proliferation and differentiation; fish lacking TH develop only unpigmented xanthophore precursors. By contrast, TH represses melanophore proliferation and differentiation; in fish lacking TH, additional melanophores differentiate and continue to divide, resulting in twice the normal number. During my dissertation work, I leveraged this *in vivo* system to elucidate how TH regulates cell plasticity and maturation in a lineage-specific way.

Broadly, TH regulates cellular metabolism by stimulating the basal metabolic rate and has various cell-type specific effects on neurons, glia, intestinal crypt cells and more (Brent, 2012; Vella et al., 2014). Dysregulation of TH signaling leading to a hypo- or hyperthyroid state can result in a myriad of health issues including obesity, infertility, peripheral neuropathies, and physical retardation. Additionally, congenital thyroid disorders are one of the most common endocrine diseases in humans and are associated with a wide range of neurological and neuromuscular disorders in children and adolescents (Brent, 2012; Nandi-Munshi and Taplin, 2015). TH production and signaling in zebrafish is similar to that of tetrapods, and genes involved gland formation as well as cellular responses to TH are conserved between fish and mammals (Porazzi et al., 2009; Marelli et al., 2016; Takayama et al., 2008). TH is produced solely in the thyroid follicle cells of the thyroid gland, which develops around 4dpf in zebrafish, as the prohormone Thyroxine (T4) and is transported to distal tissues through the blood stream. Early embryonic requirements for TH rely on maternal deposits of the hormone (Campinho et al., 2014). Conversion of T4 to its less stable but more active form, T3, occurs via the deiodinase 2 (Dio2) enzyme in receptive tissues. An additional deiodinase enzyme, Dio3, can inactivate both T4 and T3 (Figure 1.2). In this way, cells can independently modulate the amount of bioactive hormone available for signaling. This is important because local regulation of deiodinase expression allows for temporal- and tissue-specific control of TH signaling independent of changes in circulating T4.

Additional layers of cell type-specific TH signaling are present at the level of TH receptors and receptor cofactors. Canonical thyroid hormone signaling occurs through the nuclear TH receptors (TRs), a highly conserved set of proteins that dimerize with other nuclear receptors and bind TH-responsive elements (TRE) throughout the genome to modulate the transcription of hun-

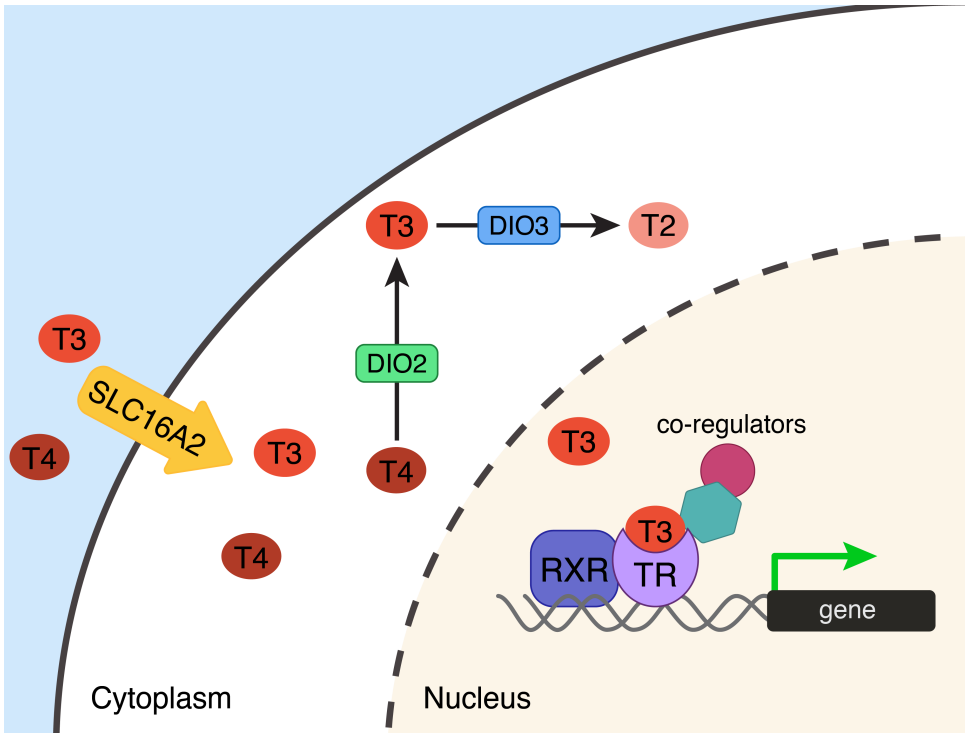

Figure 1.2: **Mechanisms of Thyroid hormone signaling.** Mechanism of TH signaling at the cellular level include intracellular transport of circulating T3 and T4 via the TH transporter, Slc16a2. Within cells, T3 can be converted to T4 by the enzyme, deiodinase 2 (Dio2). Alternatively, the active ligand, T3, can be converted into inactive T2 by the enzyme deiodinase 3 (Dio3). In the presence of T3, TH nuclear receptors (TR) heterodimerize with retinoid-X receptors (RXR), bind TH responsive elements (TRE), and cooperate with co-regulator proteins to activate gene expression.

dreds of genes (Evans and Mangelsdorf, 2014; Brent, 2012; Grøntved et al., 2015)(Figure 1.2). In zebrafish, there are three TR genes: the paralogues *thraa*, *thrab*, as well as *thrb*, (homologous to human THRA and THRB, respectively). In the absence of T3, TRs function primarily to repress transcription by binding to co-repressors; in the presence of ligand, target gene transcription is typically activated, with the recruitment of co-activators instead (Astapova, 2016; Grøntved et al., 2015; Chatonnet et al., 2013). Differential expression of TRs and their multiple isoforms has been shown to mediate tissue-specific responses to TH in multiple systems including the mammalian intestinal epithelium, lung, liver, and some neurons (Flamant and Samarut, 2003). While

spatiotemporal expression of TRs has been observed during early zebrafish development (Marelli et al., 2016), late-stage expression across tissues has yet to be determined. In some systems, the ability of TRs to act as transcriptional repressors in the absence of ligand (T3) prevents inappropriate activation of metamorphic gene expression programs during early stages when TH is not present (Choi et al., 2015; Shi, 2013). This dual-switch role for TRs is important for regulating the abrupt metamorphic onset in amphibians, and mutation of THRA in frogs leads to precocious development (Choi et al., 2015). Moreover, congenitally hypothyroid mice die early during postnatal life, but compounded loss of THRA partially rescues this phenotype, allowing mice to survive into adulthood (Flamant et al., 2002). The importance of unliganded TRs in regulating post-embryonic development in mice and frogs led us to hypothesize that these receptors were serving a related function in zebrafish. To address this question, I generated mutants for the three zebrafish TRs and ablated TH signaling in these backgrounds. In Chapter 2, I detail our findings that multiple TRs are important for gating developmental progression in the absence of ligand during zebrafish post-embryonic development.

1.0.3 Resolving cell type heterogeneity and cell state dynamics with single cell RNA-sequencing

Tissues are complex mixtures of multiple cell types in various differentiated states. Earlier in this chapter, I discussed the complex interplay between cell types during formation of the adult pigment pattern in zebrafish and highlighted the need for high resolution measurements within these cell populations.

Traditionally, whole-transcriptome sequencing has provided the ability to discern molecular differences between groups of cells and tissues. These techniques link organismal phenotype to a molecular phenotype. Bulk RNA-sequencing studies provide an average transcriptional measurement that masks gene expression differences between cell types within a constituent population. Single cell RNA-sequencing (scRNA-seq) addresses this problem by capturing transcriptomic data from individual cells within a population, allowing for the high-resolution characterization of complex, heterogeneous biological processes.

When I started my thesis work in 2014, scRNA-seq was a new technique – publications contained data sets with only hundreds or a few thousands of cells. Rapid improvements in these technologies have allowed researchers to profile thousands to millions of cells in a single experiment (Packer and Trapnell, 2018; Cao et al., 2019). Increased throughput has resulted in-part from two methods that enable the unique barcoding of mRNAs from individual cells of a pool: 1) droplet based technologies wherein single cells are captured with beads containing uniquely barcoded poly-dT oligos that allow unique tagging of mRNAs from individual cells during reverse transcription (Kivioja et al., 2011; Macosko et al., 2015; Pijuan-Sala et al., 2019) and 2) single-cell combinatorial indexing (sci-), which applies split-pool barcoding to fixed cells or nuclei to uniquely tag mRNAs of each cell without ever isolating cells individually (Cao et al., 2017; Rosenberg et al., 2018; Cao et al., 2019).

The abundance of large, high-dimensional scRNA-seq data sets has spurred the development of new computational tools. Principally, these computational tools focus on condensing the data while preserving its intrinsic structure, enabling practical inference from biological data. These tools have facilitated generation of comprehensive atlases and molecular catalogs for cell types in whole developing embryos, including worms, frogs, mice, and zebrafish Cao et al. (2017); Farrell et al. (2018); Wagner et al. (2018); Briggs et al. (2018); Cao et al. (2019). Numerous studies have additionally characterized cell-specific responses to perturbations, such as disease states and drug treatments. In addition to cell type classification, computational tools for "Pseudotemporal" analysis can order cells along a continuous trajectory that reflects changes during a given biological process, such as differentiation (Trapnell et al., 2014; Bendall et al., 2014; Qiu et al., 2017a,b; Packer and Trapnell, 2018). As most tissues are formed from the asynchronous differentiation of one or more cell types, the ability to reconstruct continuous developmental trajectories *in silico* is a critical advance towards understanding the development of complex tissues. These analyses facilitate the discovery of sets of genes with shared dynamics across differentiation or shared responses to various stimuli, and this approach can potentially be applied to many other biological processes. Together, these advances offer the unprecedented ability to resolve heterogeneous, cell-type specific activities in complex tissues in a single experiment.

In my thesis work I applied these technologies to catalog the cell types that constitute pigment pattern formation and to resolve the responses of these cells to perturbations in global TH signaling. These results informed testable hypotheses that ultimately led to the discovery of cell-type specific mechanisms of TH action, the details of which are described in Chapter 2.

Chapter 2: THYROID HORMONE REGULATES DISTINCT PATHS TO MATURATION IN PIGMENT CELL LINEAGES

Chapter 2 is adapted with minimal modification from:

Saunders, L.M., Mishra, A.K., Aman, A.J., Lewis, V.M., Toomey, M.B., Packer, J.S., Qiu, X., McFaline-Figueroa, J.L., Corbo, J.C., Trapnell, C.* and Parichy, D.M.* (2019) Thyroid hormone regulates distinct paths to maturation in pigment cell lineages. *in Revision*, eLife.

2.1 ABSTRACT

Thyroid hormone (TH) regulates diverse developmental events and can drive disparate cellular outcomes. In zebrafish, TH has opposite effects on neural crest derived pigment cells of the adult stripe pattern, limiting melanophore population expansion, yet increasing yellow/orange xanthophore numbers. To learn how TH elicits seemingly opposite responses in cells having a common embryological origin, we analyzed individual transcriptomes from thousands of neural crest derived cells, reconstructed developmental trajectories, identified pigment cell-lineage specific responses to TH, and assessed roles for TH receptors. We show that TH promotes maturation of both cell types but in distinct ways. In melanophores, TH drives terminal differentiation, limiting final cell numbers. In xanthophores, TH promotes accumulation of orange carotenoids, making the cells visible. TH receptors act primarily to repress these programs when TH is limiting. Our findings show how a single endocrine factor integrates very different cellular activities during the generation of adult form.

2.2 INTRODUCTION

Mechanisms that synchronize developmental signals and integrate them across cell types and organ systems remain poorly defined but are fundamentally important to both development and evolution of adult form (Atchley and Hall, 1991; Ebisuya and Briscoe, 2018). A powerful system for eluci-

dating how organisms coordinate fate specification and differentiation with morphogenesis is the array of cell types that arise from embryonic neural crest (NC), a key innovation of vertebrates (Gans and Northcutt, 1983). NC cells disperse throughout the body, contributing peripheral neurons and glia, osteoblasts and chondrocytes, pigment cells and other derivatives. Differences in the patterning of these cells underlie much of vertebrate diversification.

Thyroid hormone (TH) coordinates post-embryonic development of NC and other derivatives through mechanisms that are incompletely characterized (Brown and Cai, 2007; Shi, 1999). During the abrupt metamorphosis of amphibians, TH drives outcomes as disparate as tail resorption and limb outgrowth (Shi, 1999). During the more protracted post-embryonic development of zebrafish—which has similarities to fetal and neonatal development of mammals (Parichy et al., 2009b)—TH coordinates modifications to several traits including pigmentation. Remarkably, TH has seemingly opposite effects on two classes of NC-derived pigment cells, curtailing the population of black melanophores yet promoting development of yellow/orange xanthophores; fish lacking TH have about twice the normal number of melanophores and lack visible xanthophores (Figure 2.1C) (McMenamin et al., 2014).

We asked how a single endocrine factor can have such different effects on cells sharing a common embryonic origin. Using transcriptomic analyses of individual cell states, we comprehensively define the context for TH activities by identifying populations and subpopulations of adult NC derivatives. We then assess the consequences of TH status for lineage maturation across pigment cell classes. Our analyses show that TH drives maturation of cells committed to melanophore and xanthophore fates through different mechanisms, involving cellular senescence and carotenoid-dependent repigmentation, respectively. These mechanisms reflect different developmental histories of these NC sublineages, and yield different cell-type abundances when TH is absent. Our findings provide new insights into post-embryonic NC lineages, contribute new resources for studying adult pigment cells and other NC-derived cell types, and illustrate how a circulating endocrine factor influences local cell behaviors to coordinate adult trait development.

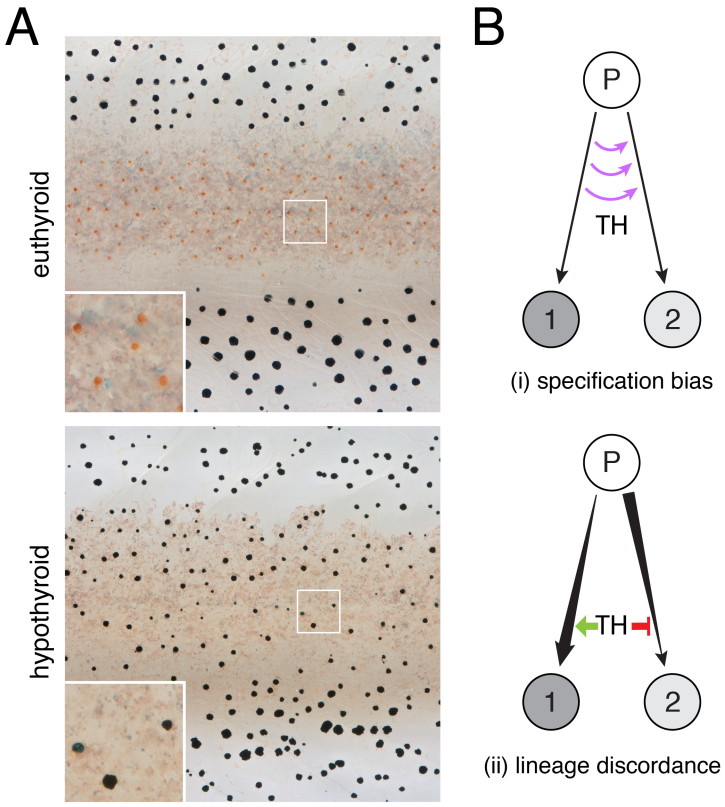

Figure 2.1: **TH dependent phenotypes and models for TH action.** Euthyroid and hypothyroid zebrafish [stage 10 SSL (Parichy et al., 2009b); ∼21 d post fertilization, dpf]. Insets, yellow/orange xanthophores of euthyroid fish and absence of these cells in hypothyroid fish. (B) Models for TH effects on alternative cell types derived from a common progenitor (P), by regulating cell fate specification (i) or lineage-specific amplification and restraint of committed cell-types, through differential effects on morphogenesis and differentiation (ii).

2.3 Results

2.3.1 Post-embryonic NC-derived subpopulations revealed by single cell RNA-sequencing

To explain the pigment cell imbalance of hypothyroid fish, we envisaged two models for TH activity during normal development (Figure 2.1B): (i) TH influences specification, directing multipotent cells away from one fate and towards the other; or (ii) TH has discordant effects on different lineages, driving the selective amplification of cells already committed to one fate while simulta-

neously restraining amplification of cells committed to the other fate.

To evaluate the contributions of these two models to the imbalance of pigment cells, we sought to capture the range of intermediate states through which these cells transit during normal and hypothyroid development. Accordingly, we sequenced transcriptomes of thousands of individual NC-derived cells isolated from trunks of euthyroid and hypothyroid fish (Figure 2.9 and Figure 2.10). Dimensionality reduction (Becht et al., 2018; Cao et al., 2019) followed by unsupervised clustering identified melanophores, xanthophores and a third class of NC-derived pigment cells, iridescent iridophores (Figure 2.2A and B). A cluster likely corresponding to multipotent pigment cell progenitors (Kelsh et al., 2017; Singh et al., 2016) was marked by genes encoding pigment cell transcription factors, mesenchymal NC markers, and factors associated with proliferation and migration but not pigment synthesis (Figure 2.11). Also present were neurons, Schwann cells and other glia, and presumptive progenitors not described previously. Clusters exhibited distinct expression of genes encoding ligands and receptors, cell adhesion molecules, and products likely to have diverged in function after genome duplication (Figure 2.12). To learn if NC-derived cells employ similar gene expression programs across life cycle phases, we compared cells isolated from embryonic–early larval ("EL") and middle larval–juvenile ("adult") stages, which revealed broad overlap of transcriptional profiles (Figure 2.13). Overall, our survey captured numerous NC-derived cell types, including abundant pigment cells and progenitors, and revealed substantial variation in gene expression programs among them.

2.3.2 Pigment cell sub-classes and gene expression dynamics across differentiation

To understand the gene expression context in which TH impacts each pigment cell type, we compared pigment cells and progenitors, the lineages of which have been described (Budi et al., 2011; Eom et al., 2015; Mahalwar et al., 2014; McMenamin et al., 2014; Singh et al., 2016) (Figure 2.3A). These analyses revealed subsets of melanophores and xanthophores (Figure 2.3B; 2.14), consistent with distinct morphogenetic and differentiative behaviors (Eom et al., 2015; Parichy et al., 2000b; Parichy and Spiewak, 2015), new markers of xanthophore and iridophore lineages (Figure 2.15 and

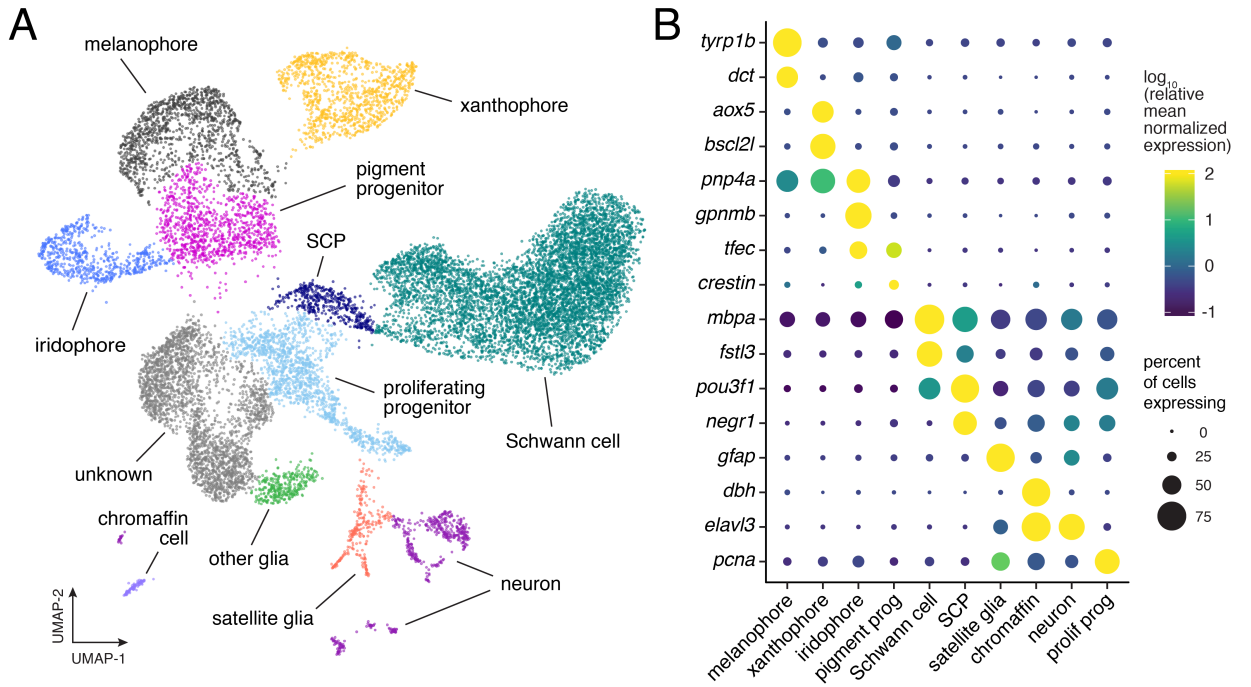

Figure 2.2: **Single cell transcriptomic identification of post-embryonic NC-derived cell types.** A) Cell-type assignments for clusters of cells (n=16,150) from euthyroid and hypothyroid fish. Cell types known to be of non-NC derivation were removed from analysis. B) Known cell-type marker genes and new candidate markers (for cluster-specific genes, see Table 2.2).

Figure 2.16), and cell-type specific expression of some previously identified markers [e.g., *tyrp1b*, *aox5*, *tfec* (Lister et al., 2011; McMenamin et al., 2014)] (Figure 2.3C). Expression of other genes was broader than might be expected from mutational or other analyses (Figure 2.17); e.g., *mitfa*, encoding a transcription factor required for melanophore fate specification (Lister et al., 1999) was expressed in melanophores and progenitors, but also xanthophores (Figure 2.3C).

To characterize transcriptional dynamics through lineage maturation, we pseudotemporally ordered cells (Qiu et al., 2017a,b; Trapnell et al., 2014), yielding a differentiation trajectory with each pigment cell type arising from a common progenitor (Figure 2.3D). This topology differed from lineage relationships (Figure 2.3A), but was consistent with similarity of EL and adult gene expression programs (Figure 2.13D). Branch expression analysis modeling (BEAM) (Qiu et al., 2017a) confirmed that genes known to function in specification (e.g., *mitfa* in melanophores) were

expressed early in pseudotime whereas genes associated with differentiation [e.g., *dct*, encoding a melanin synthesis enzyme (Kelsh et al., 2000)] were expressed late (Figure 2.3E; Figure 2.18A). These analyses revealed dynamics of hundreds of genes likely identifying discrete processes in lineage-specific maturation as well as broader trends. For example, transcripts per cell declined in melanophores but not iridophores, consistent with an expectation of reduced RNA abundance as melanophores—but not iridophores—exit the cell cycle with maturation (Figure 2.18B) (Budi et al., 2011; Darzynkiewicz et al., 1980; McMenamin et al., 2014; Spiewak et al., 2018).

2.3.3 TH-independence of pigment cell fate specification and absence of lineage-specific restraints on developmental progress

Resolution of pigment cell states through their development allowed us to test if TH functions in fate specification (Figure 2.1B-i). If so, excess melanophores and missing xanthophores of hypothyroid fish should reflect biases on specification of multipotent progenitors or transdifferentiation of initially specified cells. Such alterations should be evident in reduced-dimension transcriptomic space as strong skew in the apportionment of cells between branches or abnormal paths in the cellular trajectory, respectively. Yet, euthyroid and hypothyroid trajectories were topologically equivalent. Moreover, pigment cell progenitors were not depleted in hypothyroid fish as might occur were these cells being allocated inappropriately as melanophores (Figure 2.4A–D).

Through a second model—lineage discordance—TH could have opposite effects on cells already committed to particular fates, selectively amplifying one cell type while simultaneously repressing amplification of the other (Figure 2.1B-ii). For example, TH could promote differentiation of xanthoblasts to xanthophores, but prevent differentiation of melanoblasts to melanophores. Alternatively, TH could be a survival factor in the xanthophore lineage but a pruning factor in the melanophore lineage. Terminal phenotypes of both hypothyroid and hyperthyroid mutant fish are consistent with such effects (McMenamin et al., 2014). If TH has discordant effects between lineages, we predicted that hypothyroid fish should exhibit a strong depletion of xanthophores from the end of their branch of the trajectory, whereas melanophores should be strongly over-represented

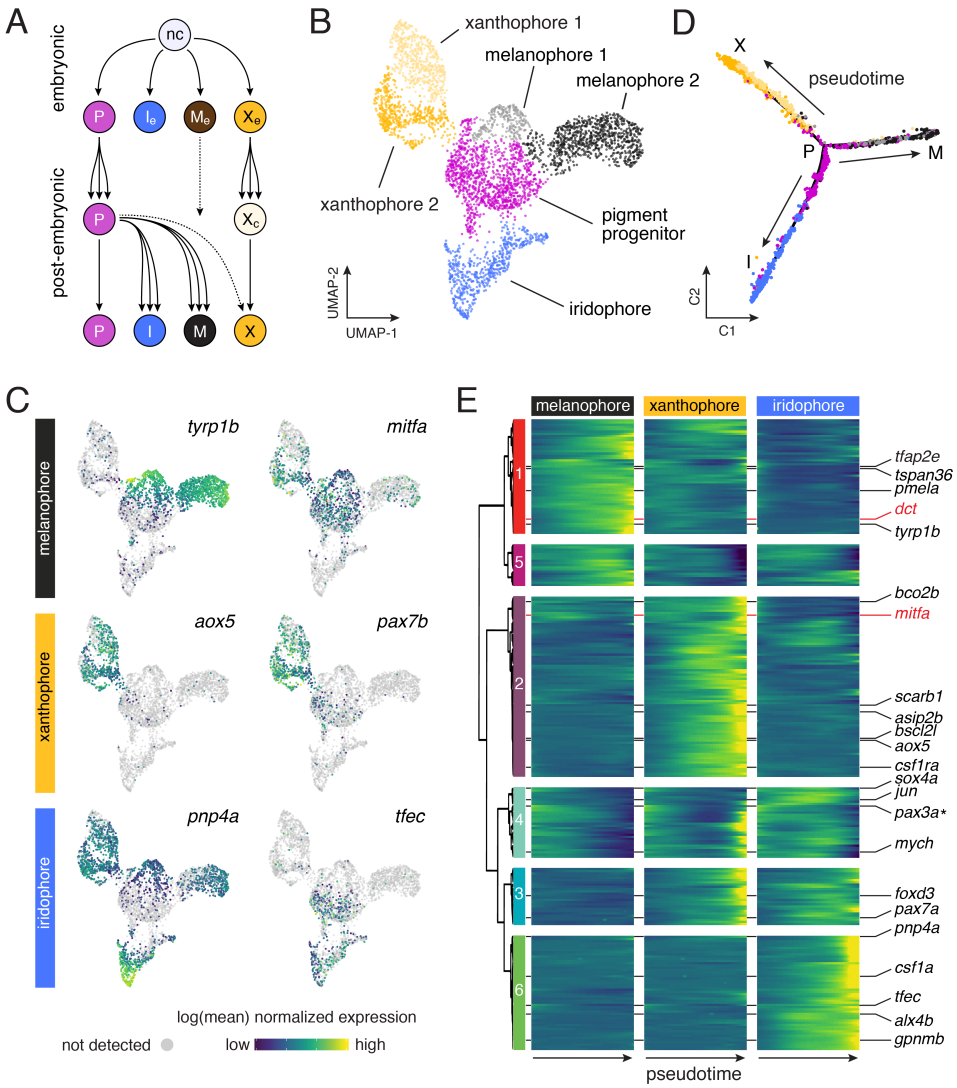

Figure 2.3: **Pigment cell subpopulations and dynamics of gene expression across pigment cell lineages.** A) Established lineage relationships of embryonic (e) and post-embryonic pigment cells. Multipotent pigment cell progenitors (P) in the peripheral nervous system generate adult iridophores (I), melanophores (M) and some xanthophores (X). A few embryonic melanophores (Me) persist whereas embryonic xanthophores (Xe) proliferate and lose their pigment to enter a cryptic phase (Xc), and then reacquire pigment late in pattern formation to form most adult xanthophores (Patterson et al., 2014). B) Sub-clusters of melanophores and xanthophores with distinct gene expression signatures. C) Pigment cell clusters defined by markers for each cell-type (Parichy and Spiewak, 2015). D-E) Pseudotemporal ordering (D) and BEAM (E) revealed dynamics of gene expression over pseudotime for each pigment cell branch (q <6.0E-11 for all genes; except pax3a (starred, q=0.03), expressed as anticipated during early pseudotime in each branch.

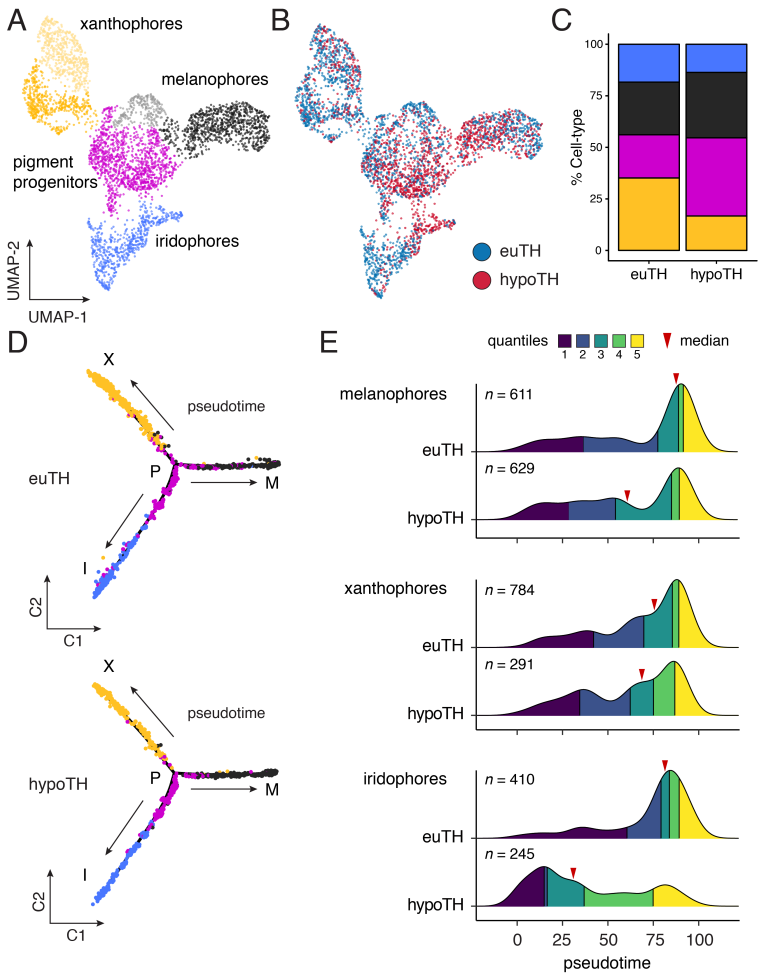

Figure 2.4: **Thyroid hormone biased pigment cell lineages towards later steps of pseudotime.** A) UMAP dimensionality reduction of euthyroid and hypothyroid pigment cells and pigment progenitors. Subclustering reveals two xanthophore and two melanophore clusters (indicated by different shades of yellow and grey, respectively). B) Pigment cells colored by TH status. Euthyroid and hypothyroid cells generally intermix with some biases apparent within melanophore and iridophore clusters. C) Percentages of each pigment cell class by TH-status. Colors are consistent with other pigment cell plots. Of cells captured, a higher proportion of pigment cells from euthyroid fish were xanthophores and iridophores compared to those from hypothyroid fish. D) Trajectories for euthyroid and hypothyroid pigment cells (plotted together, faceted by condition). Broad differences in trajectory topologies were not apparent between the two conditions. E) Distributions of each pigment cell-type across pseudotime by condition. For each trajectory branch (mel, xan, irid) hypoTH cells were biased towards early pseudotime (Wilcoxon signed-rank tests, mel: Z=-6.54, P $<$0.0001, xan: Z=-4.54, P $<$0.0001, irid: Z=-13.55, P $<$0.0001). Median is indicated by red arrowhead and different colors demarcate quartiles over pseudotime.

near the tip of their branch. Yet, empirical distributions of pigment cell states in hypothyroid fish were all biased towards earlier steps in pseudotime, sometimes severely (Figure 2.4E). Indeed, prior analyses showed that addition of exogenous TH to hypothyroid cells ex vivo can promote differentiation of unpigmented melanoblasts to melanophores (McMenamin et al., 2014), contrary to the idea that TH specifically blocks melanophore development. Together these findings allow us to reject a model in which TH regulation of pigment cell abundance in the adult fish depends on discordant effects across lineages.

2.3.4 TH promotes a melanophore maturation program

Having rejected both of our initial models (Figure 2.1B), we considered a third possibility, that TH promotes the maturation of both lineages, but in distinct ways. For melanophores, inspection of transcriptomic states and cellular phenotypes supported a role for TH in promoting maturation of this lineage. Genes expressed during terminal differentiation of melanophores from euthyroid fish (e.g., *tfap2a*, *tyrp1b*) were expressed at lower levels in melanophores of hypothyroid fish, suggesting an impediment to maturation in the absence of TH (Figure 2.5A).

To test further test the idea that TH promotes the maturation of melanophores, we examined additional cellular phenotypes. Melanophores of juvenile euthyroid fish tended to be uniformly well-melanized and stellate whereas melanophores of juvenile hypothyroid fish were variably melanized and dendritic (Figure 2.5B), reminiscent of earlier stages of melanophore development in wild-type (Eom et al., 2015; Parichy et al., 2003). Quantification of melanin content within individual cells confirmed that melanophores of euthyroid fish are more heavily melanized than those of hypothyroid fish (Figure 2.5C). Prior analyses indicated that melanophores of euthyroid fish fail to divide whereas those of hypothyroid fish continue to do so (McMenamin et al., 2014). These findings raised the possibility that melanophores of euthyroid fish might exhibit signs of cellular senescence or other indications of proliferative cessation not observed in melanophores of hypothyroid fish. Human nevus melanocytes, and melanophores of teleost melanoma models, exhibit senescent or senescent-like phenotypes and can be multinucleated (Leikam et al., 2015; Regneri et al., 2018).

Accordingly, we asked whether similar attributes were evident for zebrafish stripe melanophores. When plated ex vivo, some stripe melanophores exhibited senescence-associated β-galactosidase (SA-β-gal) activity (Figure 2.19A) although we were unable to score such staining reliably, precluding comparisons across TH conditions. SA-β-gal staining results from lysosomal β-gal activity and both β-gal activity and lysosome number increase in aging cells (Kurz et al., 2000; Lee et al., 2003). We therefore quantified lysosome-specific Lysotracker labeling (Figure 2.19B and F) of melanophores by fluorescence activated cell sorting tyrp1b:palm-mCherry+ melanophores. Lysosomal contents of melanophores from euthyroid fish were greater than melanophores from hypothyroid fish (Figure 2.19C). Measurements of forward scatter (FSC-A) also suggested that melanophores from juvenile euthyroid fish were larger than melanophores from hypothyroid fish (Figure 2.19D), though FSC-A can be influenced by cell-size independent factors as well (Tzur et al., 2011)).

Finally we examined multinucleation, a condition linked to increased cell survival and size (Orr-Weaver, 2015; Usui et al., 2018). In euthyroid fish, $\sim$20% of melanophores were binucleate near the onset of adult melanophore differentiation but $>$50% were binucleate by juvenile stages, confirming an overall increase in binucleation with somatic stage and melanophore age (Figure 2.19E). In stage-matched comparisons for TH status, 70% of melanophores from euthyroid fish were binucleated, whereas only $\sim$25% of melanophores from hypothyroid fish were in this state (Figure 2.5D and E). Collectively, our observations and those of McMenamin et al. (2014) suggest a model in which TH drives melanophores into a terminally differentiated state of increased melanization, larger size and lysosomal content, binucleation, and proliferative cessation.

2.3.5 TH promotes carotenoid-dependent xanthophore re-pigmentation during adult development

We next examined TH functions specific to the xanthophore lineage. Most adult xanthophores develop directly from EL xanthophores that lose their pigment and then reacquire it late in adult pattern formation (Figure 2.3A) (McMenamin et al., 2014). Because xanthophores of hypothyroid

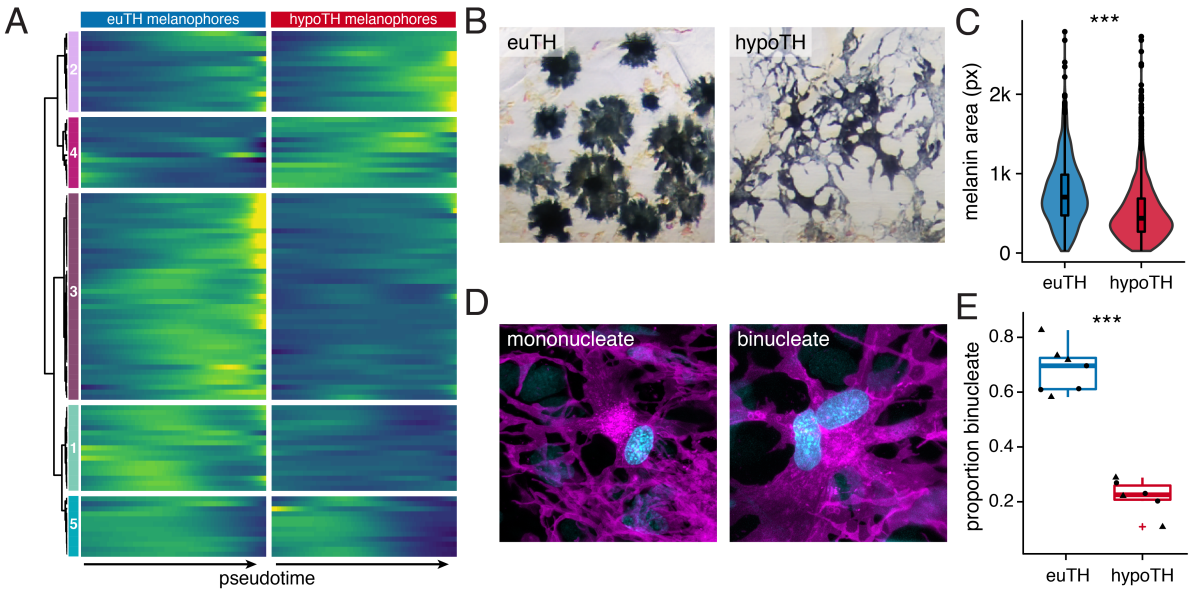

Figure 2.5: **TH promoted melanophore maturation by measures of transcriptomic state and cellular phenotype.** A) Gene expression differences between melanophores over pseudotime by TH-status (q <1E-7, genes expressed in >10% of melanophores). Heatmap is hierarchically clustered by row (method, Ward D2). The largest cluster (#3) contains 41% of the genes and represents loci expressed late in pseudotime of euthyroid melanophores but downregulated in hypothyroid melanophores [e.g. *tfap2a* and *tyrp1b*], identifying novel candidate genes for roles in melanophore maturation (Baxter et al., 2018). B) Euthyroid melanophores tended to be highly melanized and stellate whereas hypothyroid melanophores were variably melanized and often dendritic. C) Quantification of melanin contents per cell, as estimated by area of pixels (px) having melanin following contraction of melanin granules in response to epinephrine (e.g., 2.1A). Melanophores of euthyroid fish contained more melanin than those of hypothyroid fish ($F_{1,2710}=271.2$, $P<0.0001$), after controlling for individual variation among fish within TH conditions ($F_{10,2710}=8.5$, $P<0.0001$; sample sizes: n=1180 cells from 5 euthyroid fish, n=1542 cells from 5 hypothyroid fish). If planar areas of concentrated melanin granules are assumed spherical, then euthyroid melanophores had on average ∼1.7x the total melanin content of hypothyroid melanophores. D) Fully differentiated melanophores of zebrafish are often binucleate (Usui et al., 2018). Left panel shows a binucleate stripe melanophore in a euthyroid fish (12 SSL). Right panel shows a mononucleate melanophore in a hypothyroid fish at the same stage. Magenta, membrane labeling of melanophores by tyrp1b:palm-mCherry. Blue, nuclei revealed by tuba8l3:nEosFP. E) Euthyroid fish had proportionally more binucleate melanophores than hypothyroid fish ($P<0.0001$) after controlling for a higher incidence of binucleation in developmentally more advanced fish overall (11.5–13 SSL;$P<0.05$). Individual points indicate proportions of binucleate melanophores observed in dorsal stripes (circles) and ventral stripes (diamonds), which did not differ significantly ($P=0.8$; sample sizes: n=383 melanophores in 4 euthyroid fish, n=706 melanophores in 3 hypothyroid fish).

fish persist, albeit in a cryptic state (McMenamin et al., 2014), we predicted that TH effects should be less pervasive in these cells than in melanophores that develop *de novo* from a post-embryonic progenitor. Indeed, fewer genes were expressed differentially between TH backgrounds in xanthophore than melanophore lineages (3.6% vs. 9%; Figure 2.6A). Prominent among these were several loci implicated in, or plausibly associated with, yellow/orange carotenoid coloration (Figure 2.6B and C; Figure 2.20) (Toews et al., 2017). These differences in gene expression suggested a carotenoid pigmentation deficiency that we confirmed by HPLC, histology, and transmission electron microscopy (Figure 2.6D; Figure 2.21). Among carotenoid genes, scavenger receptor B1 (*scarb1*) encodes a high density lipoprotein receptor essential for carotenoid accumulation in birds and invertebrates (Kiefer et al., 2002; Toomey et al., 2017) and we found it to be required in zebrafish for carotenoid deposition, though not cell persistence (Figure 2.22A and B). *scarb1* was expressed more highly in xanthophores of euthyroid than hypothyroid fish (q=1.1E-10) (Figure 2.6B and E; Figure 2.20) and exogenous TH was sufficient to rescue both expression and yellow/orange coloration (Figure 2.6F; Figure 2.22C). Together these findings demonstrate an essential role for TH in carotenoid pigmentation and suggest that concerted TH modulation of a suite of carotenoid pathway genes is required for cryptic xanthophores to re-pigment during adult pattern formation.

The distinct phases of xanthophore embryonic/early larval and adult pigmentation, and the TH-dependence of the latter, led us to ask whether mechanisms underlying coloration might be stage-specific. In contrast to the defect of adult xanthophore pigmentation in scarb1 mutants, we found that 5 dpf larval xanthophores were indistinguishable from wild-type (Figure 2.23A). Conversely, mutants lacking xanthophore pigmentation at 5 dpf have normal adult xanthophores (Odenthal et al., 1996; Lister, 2019). Because two pigment classes—carotenoids and pteridines—can contribute to xanthophore coloration, we hypothesized that visible colors at different stages depend on different pathways. Carotenoids were undetectable in euthyroid 5 dpf larvae, and carotenoid related genes were expressed at lower levels in EL xanthophores than adult xanthophores (Figure 2.23B and C). By contrast, pteridine pathway genes tended to be expressed similarly across stages regardless of TH status, and were even moderately upregulated in hypothyroid xanthophores (Figure 2.6)C, Figure 2.23C); pteridine autofluorescence and pterinosomes were also indistinguishable

between euthyroid and hypothyroid fish (Figure 2.23D; Figure 2.21B) despite the overt difference in xanthophore color with TH status [Figure 2.1A; (McMenamin et al., 2014)]. Together, these observations imply that TH induces new, carotenoid-based pigmentation, allowing transiently cryptic xanthophores to reacquire coloration during adult pattern development. TH therefore drives maturation of both xanthophores and melanophores yet has markedly different roles in each lineage, promoting re-pigmentation of the former and proliferative senescence of the latter.

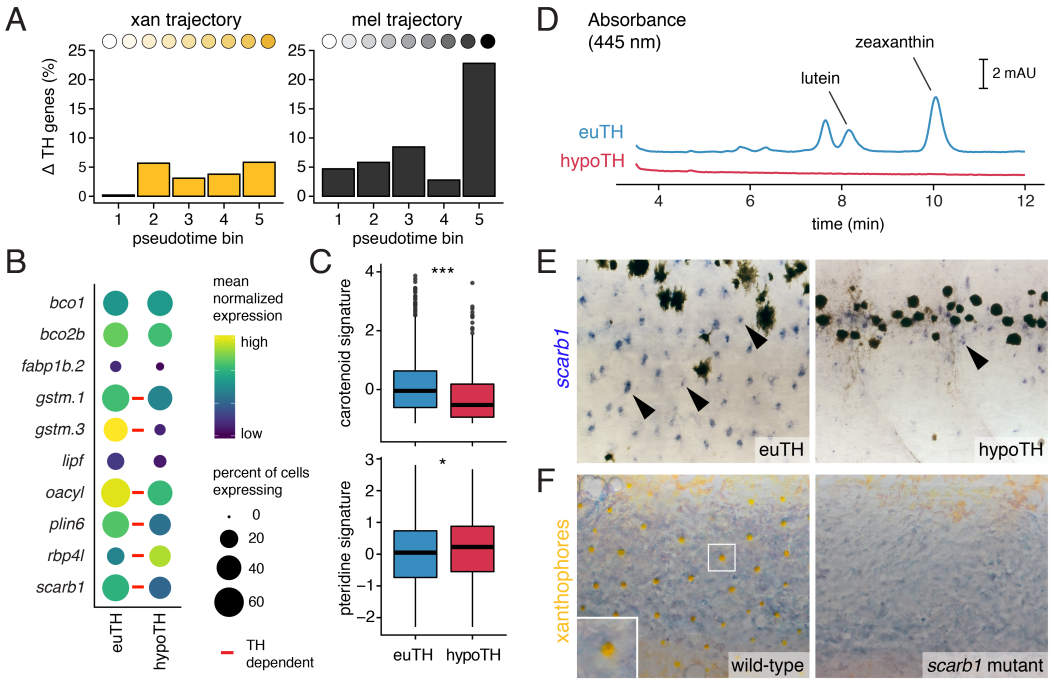

Figure 2.6: **TH promotes xanthophore maturation via scarb1-dependent carotenoid uptake.** A) Proportions of differentially expressed genes in euthyroid and hypothyroid cells across pseudotime bins. Xanthophores expressed fewer TH-dependent genes than melanophores (expressed gene cutoff = 2% of bin expressing, DEGs are genes with q <0.05 and fold change >1.5X). Of 160 xanthophore DEGs and 519 melanophore DEGs, only 58 were found to be overlapping. B) TH-dependent expression of genes related to carotenoid pigmentation in xanthophores. Red bars: q <0.05, $\log_2$ fold-change $\geq$ 2.0. C) Carotenoid pathway gene expression score was higher in xanthophore lineage cells of euthyroid fish compared to hypothyroid fish (P=1.5E-15, Wilcoxon). By contrast, pteridine pathway gene expression was marginally lower in cells from euthyroid fish (P=0.01). Box-and-whisker plots represent scores across groups (center line, median; box limits, upper and lower quartiles; whiskers, 1.5x interquartile range; points, outliers). D) Carotenoids were detected by HPLC in skin containing xanthophores of euthyroid but not hypothyroid fish (11 SSL). E) *scarb1* expression in euthyroid and hypothyroid zebrafish (10 SSL). F) scarb1 mutants lacked mature, yellow xanthophores (12 SSL).

2.3.6 Adult pigment cell maturation programs are gated by TH receptors

Finally, to understand how TH effects are transduced in pigment cell lineages, we evaluated roles for TH nuclear receptors (TRs) that classically repress gene expression when unliganded but activate target genes when ligand (T3) is present (Brent, 2012; Buchholz et al., 2003; Hörlein et al., 1995). Genes encoding each of the three zebrafish TRs (*thraa*, *thrab*, *thrb*) were expressed by melanophores and xanthophores, yet presumptive null alleles for each unexpectedly had pigment cell complements and patterns that resembled the wild type (Figure 2.7A; Figure 2.24A–D).

Given the absence of grossly apparent phenotypes for TR mutants, we hypothesized that instead of acting to promote maturation when T3 is present, TRs may function primarily to repress maturation when T3 is limiting. If so, we predicted that xanthophore development in hypothyroid fish should be rescued by mutation of TR. We therefore generated fish lacking TH and TRs. Loss of thrab, on its own or in conjunction with loss of thraa, partially restored the deposition of carotenoids in interstripe xanthophoes; mutation of all three receptors fully rescued the number of carotenoid-containing xanthophores (Figure 2.7B–D; Figure 2.24E). TR receptor mutations likewise reduced the total numbers of melanophores in hypothyroid fish to levels indistinguishable from euthyroid fish (Figure 2.7D).

These findings suggest that repression by unliganded TRs contributes to pigment-associated phenotypes in hypothyroid fish, implying a function for TRs in repressing the repigmentation of xanthophores and terminal differentiation of melanophores until late stages in adult pigment pattern development. Nevertheless, roles for TRs are likely to be complex and outcomes of derepression dependent on context. For example, the simplest model of TR gating would predict that loss of TRs in euthyroid fish should result in the precocious maturation of pigment cells. Yet, we found no evidence for early pigmentation of xanthophores in euthyroid fish homozygous for thrab mutation (Figure 2.24F), suggesting essential roles for other factors present only at later stages (Patterson and Parichy, 2013).

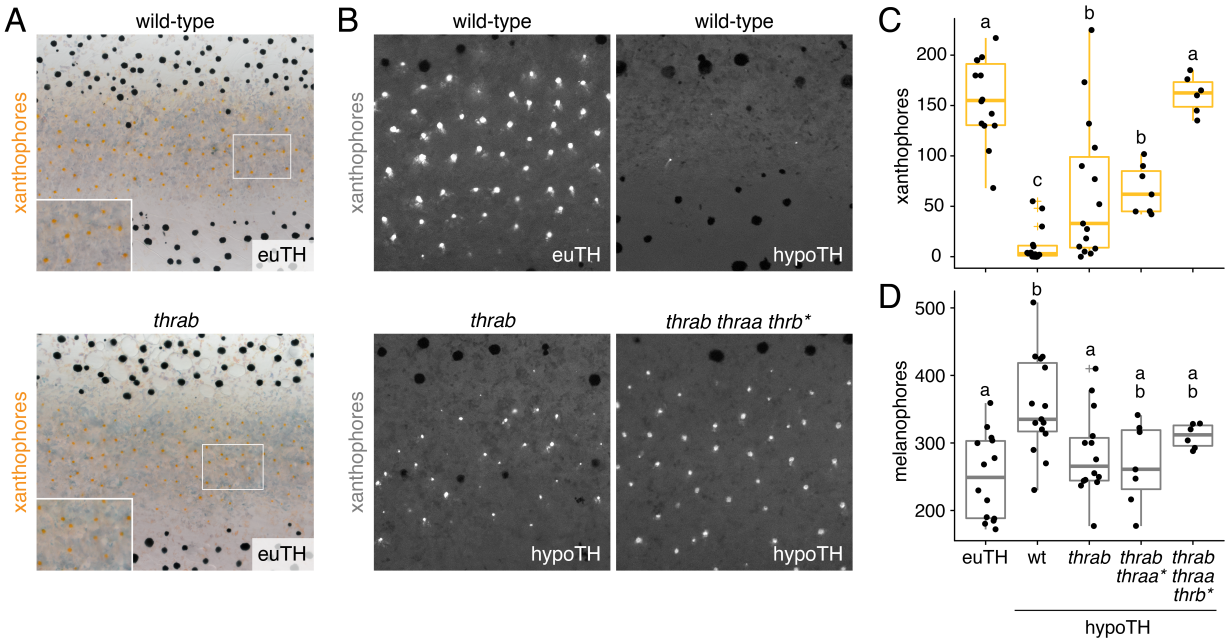

Figure 2.7: **TH receptors repress developmental progression of pigment cell lineages.** A) In euthyroid fish, homozygous TR mutants singly and in combination resembled wild-type; shown is thrab. B) Euthyroid fish wild-type for TRs exhibited numerous autofluorescing, carotenoid-containing xanthophores (upper left), whereas hypothyroid fish wild-type for TRs lacked nearly all of these cells (upper right). By contrast, hypothyroid fish mutant for TRs developed substantial complements of these cells. Shown here are representative individuals homozygous for thrab mutation (lower left) and homozygous thrab individuals with somatically induced mutations for *thraa* (*) as well as doubly *thraa* and *thrab* individuals with somatically induced mutations for *thrb* (*thrb**; lower right). Fish are 11.5 SSL. C, D) Homozygous thrab mutation partially rescued numbers of pigmented xanthophores and more fully rescued numbers of melanophores in hypothyroid fish. Somatic mutagenesis of *thraa* in fish homozygous mutant for thrab mutants (*thrab thraa**) did not significantly enhance the rescue of xanthophore maturation or melanophore numbers. By contrast somatic mutagenesis of thrb in fish doubly homozygous mutant for thraa and thrab (*thrab thraa thrb**) rescued xanthophore maturation to wild-type levels in the absence of TH. Numbers of visible xanthophores and melanophores were not distinguishable between euthyroid fish wild-type or homozygous mutant for TR mutations either singly or in combination ($P>0.1$), and are shown combined here. Box plots as in Figure 2.6C with different letters above data indicating significant differences in *post hoc* comparisons (Tukey HSD, $P<0.05$).

2.4 Discussion

Our study provides insights into how TH coordinates local cellular events during the development of adult form. The stripes of adult zebrafish comprise three major classes of pigment cells that

develop at specific stages and from distinct NC sublineages. Perturbations that affect the times of appearance, states of differentiation or morphogenetic behaviors of these cells can dramatically alter pattern by affecting total numbers of cells and the cascade of interactions normally required for spatial organization (Parichy and Spiewak, 2015; Patterson et al., 2014; Watanabe and Kondo, 2015). Fish lacking TH have gross defects in pigment cell numbers and pattern with two-fold the normal complement of melanophores and the simultaneous absence of visible xanthophores (McMenamin et al., 2014). We show that this phenotype arises not because TH normally biases cell fate specification, or has discordant effects on a particular cellular behavior that amplifies one cell type while repressing the other. Rather, our findings—combining discovery-based analyses of single-cell transcriptomic states with experiments to test specific cellular hypotheses—suggest a model whereby TH promotes maturation of both melanophores and xanthophores in distinct ways that reflect the developmental histories of these cells (Figure 2.8). Our study provides a glimpse into the diversity of cell states among post-embryonic NC-derivatives and illustrates how a single endocrine factor coordinates diverse cellular behaviors in a complex developmental process.

By sampling individual cell transcriptomes across NC-derived lineages, our study complements prior investigations of lineage relationships, morphogenetic behaviors, genetic requirements, and spatial and cell-type specific gene expression profiles (Eom et al., 2015; Irion et al., 2016; Johnson et al., 1995; Kelsh et al., 2017; McMenamin et al., 2014; Parichy and Spiewak, 2015; Singh et al., 2014, 2016). Multipotent progenitors that give rise to adult melanophores, some xanthophores, and iridophores are established in the embryo and reside within peripheral nerves as development progresses (Budi et al., 2008, 2011; Dooley et al., 2013a; Singh et al., 2016; Camargo-Sosa et al., 2019). As the adult pattern forms, some of these cells migrate to the hypodermis where they differentiate and integrate into dark stripes or light interstripes. The peripheral-nerve association of pigment cell progenitors in zebrafish is reminiscent of nerve-associated Schwann cell precursors that contribute to melanocytes of mammals and birds (Adameyko et al., 2009). Our collected cell-types, which include immature and mature glia, differentiating pigment cells, and presumptive progenitors of different types identify new candidate genes for promoting—and recognizing—distinct states of differentiation and morphogenetic activities, and will enable efforts to define how multi-

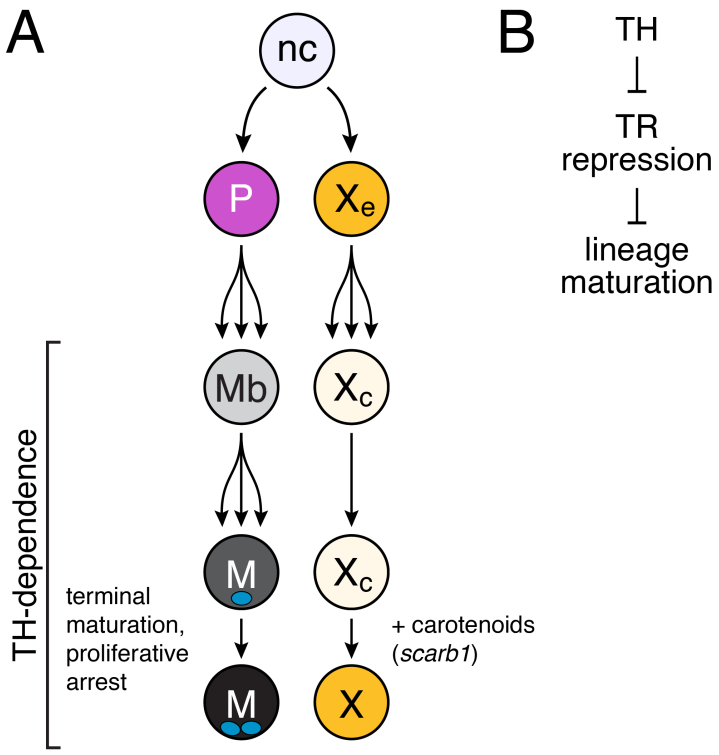

Figure 2.8: **Model of TH dependence in zebrafish pigment cell lineages.** A) Post-embryonic progenitor-derived, specified adult melanoblasts (Mb) that expand their population and differentiate to a proliferatively arrested (McMenamin et al., 2014), senescent and binucleate state, and EL-derived cryptic xanthophores that redifferentiate as carotenoid-containing yellow/orange adult xanthophores. Disparate cell-type specific outcomes in fish lacking TH reflect differences in events required for maturation between sublineages. B) TH-dependent lineage maturation involves a double negative gate, with essential repressive effects of unliganded TR.

potent NC progenitors are maintained and recruited into particular lineages. That corresponding populations of embryonic and adult populations had largely overlapping transcriptomic states (Figure 2.10D) additionally highlights the intriguing problem of how specific pathways are deployed reiteratively across life cycle phases to achieve specific morphogenetic outcomes.

Our identification of a role for TH in the adult melanophore lineage illuminates how these cells develop normally and mechanisms that likely contribute to the supernumerary melanophores of hypothyroid fish. Melanoblasts derived from peripheral-nerve associated progenitors are prolifera-

tive during adult pigment pattern formation yet this activity largely ceases as the cells differentiate (Budi et al., 2011; McMenamin et al., 2014). Several lines of evidence suggest that TH promotes melanophore maturation to a senescent state: in the presence of TH, melanophores became terminally binucleate and exhibited both senescence-associated β-galactosidase activity and lysosomal content. TH also promotes the melanization of melanoblasts ex vivo and the proliferative arrest of melanophores in vivo (McMenamin et al., 2014). Our findings are broadly consistent with a role for TH in balancing proliferation and differentiation (Brent, 2012) and may be of clinical relevance, as human melanoma is associated with hypothyroidism and recurrent TH pathway mutations (Ellerhorst et al., 2003; Shah et al., 2006; Sisley et al., 1993). We suggest a model in which TH normally curtails expansion of the adult melanophore population by ensuring that cells enter a senescent state in a timely manner; in hypothyroid fish, the inappropriate retention of immature melanophores allows continued population growth during these post-embryonic stages. Effects of TH on melanophores may be direct, as these cells expressed TRs, or indirect and mediated by stromal or other cells with which melanophores interact (Lang et al., 2009). Indeed, iridophores regulate melanophore behavior during stripe establishment (Frohnhöfer et al., 2013; Patterson and Parichy, 2013) and we observed striking differences in iridophore maturation dependent on TH status (Figure 2.4E).

TH promoted the terminal differentiation of xanthophores, but in a manner distinct from melanophores. We found far fewer TH-dependent genes in xanthophores than melanophores, likely reflecting the different developmental histories of these cells. Unlike adult melanophores that arise from a transit-amplifying progenitor, most adult xanthophores develop directly from EL xanthophores that lose their pigment and then regain color late in adult pattern formation (McMenamin et al., 2014; Patterson et al., 2014) when TH levels are ramping up (Chang et al., 2012). The yellow-orange color of xanthophores can arise from pteridine pigments, carotenoid pigments, or both (Granneman et al., 2017; Bagnara and Matsumoto, 2006; Ziegler, 2003; Odenthal et al., 1996; Lister, 2019). We showed that TH positively regulates carotenoid-associated genes and carotenoid deposition, allowing cryptic xanthophores to reacquire visible pigmentation. TH did not similarly influence pteridine pathway genes. These observations suggest that TH mediates a transition from

pteridine-dependent pigmentation at embryonic/early larval stages to carotenoid-dependent pigmentation of the same cells in the adult. Consistent with the notion of TH-mediated pigment-type switching, TH-dependent *scarb1* was required for carotenoid accumulation during adult pattern formation, yet mutants lacked an embryonic xanthophore phenotype. Conversely, mutants with pteridine and color deficiencies in embryonic/early larval xanthophores have normally pigmented adult xanthophores (Odenthal et al., 1996; Lister, 2019). In xanthophores, then, TH drives a state of terminal differentiation from a developmental program that is relatively more advanced than that of progenitor-derived melanophores. That cryptic xanthophores appear poised to re-differentiate likely explains the smaller proportion of genes that were TH-dependent in these cells as compared to melanophores. Cryptic and fully differentiated xanthophores also differ from one another in their interactions with melanophores (Eom et al., 2015), and it will be interesting to determine whether genes contributing to these behaviors are under TH control as well.

Finally, our study provides clues to likely roles for TRs during adult pigment pattern formation. TR mutants lacked overt pigmentation defects yet allowed for partial rescues of both melanophore and xanthophore defects in hypothyroid fish, suggesting that unliganded TRs normally repress maturation of these lineages. Loss of TRs similarly allows the survival of congenitally hypothyroid mice (Flamant et al., 2002; Flamant and Samarut, 2003). TRs may therefore prevent the inappropriate activation of gene expression programs required for lineage maturation when TH levels are low, as is thought to occur during amphibian metamorphosis (Choi et al., 2015; Shi, 2013). Nevertheless, the failure of xanthophores to develop precociously in euthyroid fish mutant for thrab suggests additional requirements for TRs, or functional redundancies among their loci.

Taken together, our findings shed light on how globally available signals can control fine-grained patterning of cells within complex adult tissues.

2.5 METHODS

Staging, rearing and stocks

Staging followed (Parichy et al., 2009a) and fish were maintained at 28.5°C under 14:10 light:dark cycles. All thyroid-ablated (Mtz-treated) and control (DMSO-treated) *Tg(tg:nVenus-v2a-nfnB)* fish were kept under TH-free conditions and were fed only Artemia, rotifers enriched with TH-free Algamac (Aquafauna), and bloodworms. Fish stocks used were: wild-type AB^{wp} or its derivative WT(ABb) (Eom et al., 2015); *Tg(tg:nVenus-v2a-nfnB)*$^{wp.rt8}$, *Tg(aox5:palmEGFP)*$^{wp.rt22}$, *Tg(tyrp1b:palm-mCherry)*$^{wp.rt11}$ (McMenamin et al., 2014); *csf1ra*^{j4blue} (Parichy et al., 1999); *Tg(-28.5Sox10:Cre)*^{zf384} (Kague et al., 2012); *Tg(-3.5ubi:loxP-EGFP-loxP-mCherry)*^{cz1701} (Mosimann et al., 2011); *tuba8l3:nEosFP*$^{vp.rt17}$, *thrab*$^{vp.r31c1}$, *thraa*$^{vp.r32c1}$, *thrb*$^{vp.r33c1}$, *scarb1*$^{vp.r32c1}$ and *tyr*$^{vp.r34c1}$ (this study). Mutants and transgenic lines were maintained in the WT(ABb) genetic background. Fish were anesthetized prior to imaging with MS222 and euthanized by overdose of MS222. All procedures involving live animals followed federal, state and local guidelines for humane treatment and protocols approved by Institutional Animal Care and Use Committees of University of Virginia and University of Washington.

Nitroreductase-mediated cell ablation

To ablate thyroid follicles of *Tg(tg:nVenus-2a-nfnB)*, we incubated 4 day post-fertilization (dpf) larvae for 8 h in 10 mM Mtz with 1% DMSO in E3 media, with control larvae incubated in 1% DMSO in E3 media. For all thyroid ablations, treated individuals were assessed for loss of nuclear-localizing Venus (nVenus) the following day. Ablated thyroid glands fail to regenerate (McMenamin et al., 2014) and absence of regeneration in this study was confirmed by continued absence of nVenus expression.

Mutant and transgenic line production

For CRISPR/Cas9 mutagenesis, 1-cell stage embryos were injected with 200 ng/μl sgRNAs and 500 ng/μl Cas9 protein (PNA Bio) using standard procedures (Shah et al., 2015). Guides were

tested for mutagenicity by Sanger sequencing and injected fish were reared through adult stages at which time they were crossed to *Tg(tg:nVenus-v2a-nfnB)* to generate heterozygous F1s from which single allele strains were recovered. CRISPR gRNA targets (excluding protospacer adjacent motif) are included in Table 2.4. Mutant alleles of *scarb1* and TR loci are provided in 2.22 and 2.24, respectively. The melanin free $tyr^{vp.r34c1}$ allele generated for analyses of melanophore lysosomal content exhibits a 4 nucleotide deletion beginning at position 212 that leads to novel amino acids and a premature stop codon (H71QEWTIESDGL*).

For F0 thrb mutagenesis analysis in the thraa; thrab mutant background, chemically synthesized Alt-R CRISPR-Cas9 sgRNAs targeting the thrb site and Cas9 protein (Alt-R S.p. Cas9 nuclease, v.3) were obtained from Integrated DNA Technologies (IDT). RNPs were prepared as recommended and 1 nl was injected into the cytoplasm of one-cell stage embryos.

To label nuclei of adult melanophores, BAC CH73-199E17 containing the *puma* gene *tuba8l3* (Larson et al., 2010) was recombineered to contain nuclear-localizing photoconvertible fluorophore EosFP using standard methods (Sharan et al., 2009; Suster et al., 2011).

Imaging

Images were acquired on: Zeiss AxioObserver inverted microscopes equipped with Axiocam HR or Axiocam 506 color cameras; a Zeiss AxioObserver inverted microscope equipped with CSU-X1 laser spinning disk (Yokogawa) and Orca Flash 4.0 camera (Hamamatsu Photonics); or a Zeiss LSM 880 scanning laser confocal microscope with Fast Airyscan and GaAsP detectors. Images were corrected for color balance and adjusted for display levels as necessary with conditions within analyses treated identically.

Cell counts

Melanophores and xanthophores were counted within regions defined dorsally and ventrally by the margins of the primary stripes, anteriorly by the anterior margin of the dorsal fin, and posteriorly by five myotomes from the start. Only hypodermal melanophores were included in analysis; dorsal

melanophores and those in scales were excluded. Mature xanthophores were counted by the presence of autofluorescent carotenoid with associated yellow pigment. Cell counts were made using ImageJ. Individual genotypes of fish assessed were confirmed using PCR or Sanger sequencing.

In situ hybridization

In situ hybridization (ISH) probes and tissue were prepared as described (Quigley et al., 2004). Probes were hybridized for 24 hr at 66°C. Post-hybridization washes were performed using a BioLane HTI 16Vx (Intavis Bioanalytical Instruments), with the following parameters: 2x SSCT 3 x 5 min, 11 x 10 min at 66°C; 0.2x SSCT 10 x 10 min; blocking solution [5% normal goat serum (Invitrogen), 2 mg/mL BSA (RPI) in PBST] for 24 hr at 4°C; anti-Dig-AP, Fab fragments (1:5000 in blocking solution, Millipore-Sigma) for 24 hr at 4°C; PBST 59 x 20 min. AP staining was performed as described (Quigley et al., 2004).

Pigment analyses

Xanthophore pigments were examined by imaging autofluorescence in eGFP and DAPI spectral ranges for carotenoids and pteridines respectively. For imaging pteridines, fish were euthanized and treated with dilute ammonia to induce autofluorescence (Odenthal et al., 1996).

For analyses of carotenoid contents by HPLC we pooled three skin samples from each genotype and condition (Mtz-treated or control) into two separate samples. We homogenized the tissue in a glass dounce homogenizer with 1 ml of 0.9% NaCl and quantified the protein content of each sample with a bicinchoninic acid (BCA) assay (23250, Thermo). We then extracted carotenoids by combining the homogenates with 1 ml methanol, 2 ml distilled water, and 2 ml of hexane:tert-methyl butyl ether (1:1 vol:vol), separated the fractions by centrifuging, collected the upper solvent fraction, and dried it under a stream of nitrogen. We saponified these extracts with 0.2 M NaOH in methanol at room temperature for four hours following the protocol described in (Toomey and McGraw, 2007). We extracted the saponified carotenoids from this solution with 2 ml of hexane:tert-methyl butyl ether (1:1 vol:vol) and dried the solvent fraction under a stream of nitrogen. We

resuspended the saponified extracts in 120 μl of methanol:acetonitrile 1:1 (vol:vol) and injected 100 μl of this suspension into an Agilent 1100 series HPLC fitted with a YMC carotenoid 5.0 μm column (4.6 mm x 250 mm, YMC). We separated the pigments with a gradient mobile phase of acetonitrile:methanol:dichloromethane (44:44:12) (vol:vol:vol) through 11 minutes, a ramp up to acetonitrile:methanol:dichloromethane (35:35:30) for 11-21 minutes and isocratic conditions through 35 minutes. The column was warmed to 30°C, and mobile phase was pumped at a rate of 1.2 ml min-1 throughout the run. We monitored the samples with a photodiode array detector at 400, 445, and 480 nm, and carotenoids were identified and quantified by comparison to authentic standards (a gift of DSM Nutritional Products, Heerlen, The Netherlands). Analyses of 5 dpf wild-type and *csf1ra* mutants used only larval heads where xanthophores are abundant in the wild type; other procedures were the same as for later stages.

Immunohistochemistry and Oil-red-O staining

Skins of Tg(aox5:palmEGFP) euthyroid and hypothyroid zebrafish (8.6–10.4 SSL) were dissociated and plated at low density in L-15 medium (serum free) on collagen-coated, glass bottom dishes (Mattek) for 5 h. Cells were then fixed with freshly prepared 4% PFA for 15 m, rinsed with PBST (0.1%), blocked (5% goat serum, 1% BSA, 1X PBS), then incubated at 4°C overnight with rabbit anti-GFP primary antibody (ThermoFisher). Stained cells were rinsed 3X with 1X PBS and fixed again with 4% PFA for 30 minutes. Cells were then rinsed twice with ddH2O, washed with 60% isopropanol for 5 min, and then dried completely. Cells were incubated with filtered, Oil Red O solution (5 mM in 60% isopropanol) for 10 min, and rinsed 4X with ddH20 before imaging (Koopman et al., 2001). All GFP+ cells were imaged across two plates per condition and were scored for presence or absence of red staining.

Melanophore maturation assays

For assaying senescence of melanophores *ex vivo*, skins from euthyroid and hypothyroid fish (n=3 each, 11 SSL) were dissociated and plated on glass-bottom, collagen coated dishes (MatTek) in L-

15 medium (Gibco) and incubated overnight at 28°C. Cells were then rinsed with dPBS, fixed and stained using a Senescence β-Galactosidase Staining Kit (Cell Signaling Technologies, cat.#9860) according to manufacturer's instructions (Ceol et al., 2011; Dimri et al., 1995). Staining was carried out for 48 h at pH 6 prior to imaging.

To assay senescence as measured by lysosomal content (Kurz et al., 2000; Lee et al., 2006) of melanophores by FACS skins from euthyroid and hypothyroid *Tg(tyrp1b:palm-mCherry; tuba8l3:nEOS)*, *tyr* fish lacking melanin (n=12 each) were dissociated and resuspended 1% BSA / 5% FBS / dPBS. Cells were incubated for 1 h with Lysotracker (75 nM) (ThermoFisher, L12492) and Vybrant DyeCycle Violet stain (5 μM) (ThermoFisher, V35003) shaking at 500 rpm, 28°C. Without washing, cells were FAC sorted. Single transgene controls and wild type cells were used to adjust voltage and gating. Prior to analysis of fluorescence levels, single cells were isolated by sequentially gating cells according to their SSC-A vs. FSC-A, FSC-H vs FSC-W and SSC-H vs SSC-W profiles according to standard flow cytometry practices. Intact live cells were then isolated by excluding cells with low levels of DyeCycle violet staining (DAPI-A). As expected these cells express a wide range of our *tuba8l3:nlsEosFP* transgene as determined by levels of green fluorescence (FITC-A). Melanophores were isolated by identifying cells with high fluorescence in the FITC-A and mCherry-A channels which describe expression of the *tuba8l3:nlsEosFP* and *tyrp1b:palm-mCherry* transgenes. Lastly, lysosomal content of melanophores was determined by the median fluorescence intensity of our lysosomal marker, Lysotracker Deep Red (APC-A) (Figure 2.5E). The data were collected on a FACS ARIA using FACSDiva version 8 software (BD Biosciences). Data were analyzed using FlowJo v10.

Melanin content was measured from brightfield images in Fiji. All image quantifications were performed using the base processing and analysis functions in ImageJ. Images were aligned and centered on the horizontal myoseptum and cropped to 2500 x 1500 pixels around dorsal and ventral stripes. Images were segmented based on red channel intensity using "Auto Local Threshold" with parameters "method=Sauvola radius=50". To account for close or overlapping melanophores, particles were further segmented using watershed segmentation. Particles larger than 25 pixels and not touching an edge were used for subsequent analyses.

Transmission electron microscopy

Fish were euthanized then fixed in sodium cacodylate buffered 4% glutaraldehyde overnight at 4°C. Trunk regions were dissected then tissue stained in 2% osmium tetroxide for 30 minutes, washed, and then stained in 1% uranyl acetate overnight at 4°C. Samples were dehydrated with a graded ethanol series then infiltrated with a 1:1 propylene oxide:Durcupan resin for 2 hours followed by fresh Durcupan resin overnight and flat embedded prior to polymerization. Blocks were thin sectioned on a Leica EM UC7 and sections imaged on a JEOL 1230 transmission electron microscope.

Tissue dissociations and FACS

Trunks or skins of staged, post-embryonic zebrafish (7.2–11.0 SSL) were dissected (n=8 per replicate) and enzymatically dissociated with Liberase (Sigma-Aldrich cat. 5401119001, 0.25 mg/mL in dPBS) at 25°C for 15 min followed by manual trituration with a flame polished glass pipette for 5 min. Cell suspensions were then filtered through a 70 μm Nylon cell strainer to obtain a single cell suspension. Liberated cells were re-suspended in 1% BSA / 5% FBS in dPBS and DAPI (0.1 μg/mL, 15 min) before FACS purification. All plastic and glass surfaces of cell contact were coated with 1% BSA in dPBS before to use. Prior to sorting for fluorescence levels, single cells were isolated by sequentially gating cells according to their SSC-A vs. FSC-A, FSC-H vs FSC-W and SSC-H vs SSC-W profiles according to standard flow cytometry practices. Cells with high levels of DAPI staining were excluded as dead or damaged. Cells from wild-type and *Tg(ubi:switch)* zebrafish without Cre were used as negative control to determine gates for detection of mCherry and GFP fluorescence, then cells from *Tg(sox10:Cre; ubi:switch)* zebrafish were purified according to these gates. NC-derived cells cells were isolated by identifying cells with high fluorescence in the mCherry-A channel which describes expression of the ubi:loxP-EGFP-loxP-mCherry transgene after permanent conversion to ubi:mCherry after exposure to Sox10:Cre (see Figure 2.9C). All samples were kept on ice except during Liberase incubation, and sorted chilled.

RT-PCR

Skin tissue from stage-matched fish was dissociated as above and melanophores and xanthophores were FAC sorted for the presence aox5:palmeGFP or tyrp1b:palm-mCherry, respectively. RNA was extracted from pools of 1000 cells using the RNAqueous-Micro kit (Thermo Fisher, cat. AM1912). Full length cDNA was synthesized with Superscript III reverse transcriptase (Thermo Fisher, cat. #18080093). Amplifications were 40 cycles with Q5 DNA polymerase (NEB, M0492), 38 cycles at 94°C, 30 s; 67°C, 20 s; 72°C, 20 s. For primer sequences (*actb1*, *thraa*, *thrab*, *thrb*), see Table 2.4.

Single cell collection, library construction and sequencing

Whole-trunks or skins were collected from stage-matched *Tg(tg:nVenus-2a-nfnB)* euthyroid and hypothyroid siblings, dissociated, and sox10:Cre:mCherry+ cells isolated by FACS. We replicated the experiment three times. For each replicate, we collected cells from euthyroid and hypothyroid fish at 7.2 SSL, 8.6 SSL, and 9.6 SSL (mid-larval, 6–10 fish per stage, per replicate) and sorted equal numbers of mCherry+ cells from each group into a single sample. Cells were pelleted and resuspended in 0.04% ultrapure BSA (ThermoFisher Scientific). Representing a terminal stage of pigment pattern development, we also collected mCherry+ cells from one sample within each replicate of 11 SSL (juvenile, 5 fish per condition) euthyroid and hypothyroid fish. To capture cells representing the EL pigment pattern, we collected mCherry+ cells from 5 dpf larvae (50 fish). In each experiment, we ran parallel euthyroid and hypothyroid samples (fish were siblings). For each sample, we targeted 2000–4000 cells for capture using the Chromium platform (10X Genomics) with one lane per sample. Single-cell mRNA libraries were prepared using the single-cell 3' solution V2 kit (10X Genomics). Quality control and quantification assays were performed using a Qubit fluorometer (Thermo Fisher) and a D1000 Screentape Assay (Agilent). Libraries were sequenced on an Illumina NextSeq 500 using 75-cycle, high output kits (read 1: 26 cycles, i7 Index: 8 cycles, read 2: 57 cycles). Each sample was sequenced to an average depth of 150 million total reads. This resulted in an average read depth of $\sim$40,000 reads/cell after read-depth

normalization.

scRNA-Seq data processing

We found that for many genes, annotated 3' UTRs in the Ensembl 93 zebrafish reference transcriptome were shorter than true UTR lengths observed empirically in pileups of reads mapped to the genome. This led to genic reads being counted as intergenic. To correct for this bias in aligning reads to the transcriptome, we extended all 3' UTR annotations by 500 bp. In rare cases, UTR extension resulted in overlap with a neighboring gene and in these instances we manually truncated the extension to avoid such overlap. We built a custom zebrafish STAR genome index using gene annotations from Ensembl GRCz11 with extended 3' UTRs plus manually annotated entries for mCherry transcript, filtered for protein-coding genes (with Cell Ranger mkgtf and mkref options). Final cellular barcodes and UMIs were determined using Cell Ranger 2.0.2 (10X Genomics) and cells were filtered to include only high-quality cells. Cell Ranger defaults for selecting cell-associated barcodes versus barcodes associated with empty partitions were used. All samples were aggregated (using 10X Cell Ranger pipeline "cellranger aggr" option), with intermediary depth normalization to generate a gene-barcode matrix containing $\sim$25,000 barcoded cells and gene expression counts.

UMAP visualization and clustering

We used Uniform Manifold Approximation and Projection (UMAP) (McInnes et al., 2018) to project cells in two or three dimensions and performed louvain clustering (Blondel et al., 2008) using the reduceDimension and clusterCells functions in Monocle (v.2.99.1) using default parameters (except for, reduceDimension: reduction_method=UMAP, metric=cosine, n_neighbors=30, mid_dist=0.5; clusterCells: res=1e-3, k=15). We assigned clusters to cell types based on the detection of published marker genes. Cells isolated from euthyroid and hypothyroid fish were combined to maintain consistency of analysis and for comparisons between groups. Batch correction methods were not used between the two groups or across samples because we did not observe

sample-specific separation or clustering in UMAP space. Cells with more than 15,000 UMIs were discarded as possible doublets. All genes were given as input to Principal Components Analysis (PCA). The top 30 principal components (high-loading, based on the associated scree plot) were then used as input to UMAP for generating either 2D or 3D projections of the data. For, subclustering of pigment cell clusters (melanophores, iridophores, xanthophores, and pigment progenitors) we subsetted the data set and again applied UMAP dimensionality reduction and louvain clustering.

Differential expression analysis to determine cell-type markers

To identify genes expressed cell-type specifically, we used the principalGraphTest function in Monocle3 (v.2.99.1) with default parameters (Cao et al., 2019). This function uses a spatial correlation analysis, the Moran's I test, to assess spatially restricted gene expression patterns in low dimensional space. We selected markers by optimizing for high specificity, expression levels and effect sizes within clusters (For extended list of cell-type specific genes, see Table 2.2).

Trajectory analysis

The top 800 highly dispersed genes within euthyroid pigment cells (melanophores, xanthophores, iridophores, and pigment progenitors) were chosen as feature genes to resolve pseudotemporal trajectories using the setOrderingFilter, reduceDimension, and orderCells functions in Monocle (v2.9.0) using default parameters with the exception of setting max_components = 3 and num_dim = 10 to generate the trajectory in 3D with the top 10 PCs (high-loading based on scree plot) during dimensionality reduction.

Branched Expression Analysis Modeling (BEAM)

After running trajectory analysis on pigment cells, we used the BEAM function in Monocle (v.2.9.0) with default settings (except, branch_point = 3) to determine differentially expressed genes between trajectory branches. To generate the BEAM heatmap for the three pigment cell trajectory

branches, we used the plot_multiple_branches_heatmap function with default settings (except assigning branch 1, 5, and 6 to iridophores, melanophores, and xanthophores, respectively; and num_clusters = 6). Genes were selected by significance levels for the three-branch BEAM analysis with additional significant genes added from the melanophore and iridophore two-branch analysis for more even distribution of genes across lineages (q<6.0E-11 for all genes, except for *pax3a* (starred, q=0.03) which is a positive indicator of early pseudotime for all lineages).

Differential expression analysis across pseudotime

To determine differentially expressed genes over pseudotime that were TH-dependent, we filtered the data set for genes expressed in at least 5 cells and performed differential expression analysis using a full model of sm.ns(Pseudotime, df=3)*condition and a reduced model of sm.ns(Pseudotime, df=3).

Development and analysis of pathway signature scores

Gene sets for signature scores were selected using gene ontology (terms and gene sets from zfin.org; cell-cycle, unfolded protein response, AP-1 transcription factor complex members) or manual curation based on literature when required (carotenoid, pteridine, melanin) (see Table 2.3). Signature scores were calculated by generating z-scores (using scale( )) of the the mean of expression values (log transformed, size factor normalized) from genes in a given set.

Statistics

Parametric, non-parametric and multiple logistic regression analyses were performed using JMP 14.0 (SAS Institute, Cary, NC) or R [version 3.5.0] (R Core Team, 2017). For parametric analyses, residuals were assessed for normality and homoscedasticity to meet model assumptions and no transformations were found to be warranted.

2.6 Data availability

The accession number for the scRNA-seq data reported in this chapter is GSE131136.

2.7 Project acknowledgments

For assistance we thank D. Jackson, D. Huang, E. Bain, D.S. Eom, D. Raible, A. Fulbright, A. Leith, A. Schwindling, T. Linbo, D. White, B. McCluskey, and E. Parker. Funding: Supported by NIH R35 GM122471 (DMP); NIH T32 GM007067 (LMS); NIH P30 EY001730 (Core Grant for Vision Research); NIH DP2 HD088158 (CT); Paul G. Allen Frontiers Group - Allen Discovery Center grant (CT); W.M. Keck Foundation Grant (CT); Alfred P. Sloan Foundation Research Fellowship (CT); NIH EY024958, EY025196, and EY026672 (JCC).

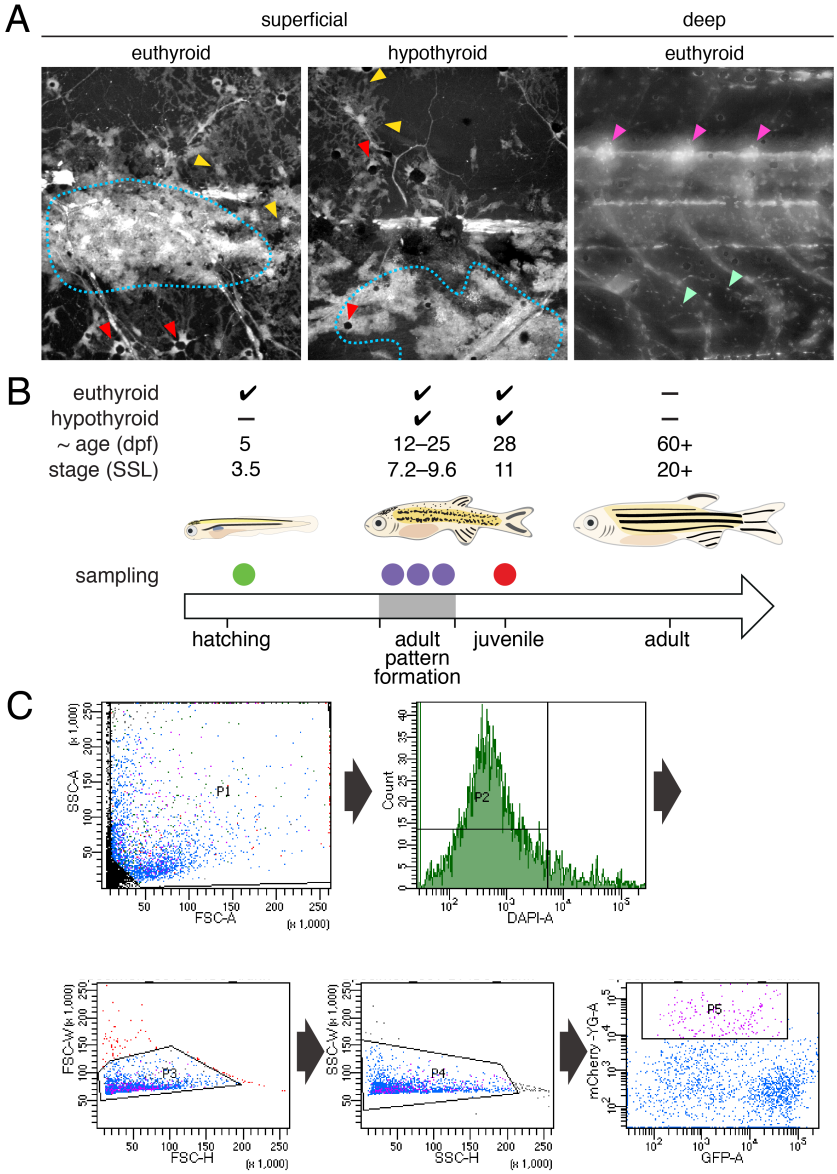

Figure 2.9: **Experimental design and isolation of NC-derived cells from post-embryonic zebrafish.** A) Fish transgenic for sox10:cre and ubi:loxP-EGFP-loxP-mCherry permanently and robustly expressed mCherry in NC-derived cells of both euthyroid and hypothyroid fish (Kague et al., 2012; Mosimann et al., 2011). At superficial layers, mCherry+ xanthophores (yellow arrowheads), melanophores (red arrowheads), and iridophores (blue dotted line) were apparent. At deeper layers, mCherry+ cells were found in dorsal root ganglia (magenta arrowheads) and other locations (e.g., mint arrowheads), potentially representing glia, neurons, progenitors and other cell types. mCherry+ cells of non-NC origin were evident as well (see Extended data Fig. 2). Stage shown is 9.8 (mm) standardized standard length (SSL) (Parichy et al., 2009b). (*legend continued on next page*)

Figure 2.9: (*continued*) B) Single-cell RNA-Seq (scRNA-Seq) experimental design. To ensure that progenitors, cells at intermediate states of specification and commitment, and fully differentiated cells were captured, euthyroid and hypothyroid fish were collected at a range of stages encompassing adult pattern formation (7.2–9.8 SSL) and from juvenile fish (11 SSL) in which the first two adult stripes had fully formed (Parichy et al., 2009b). To compare transcriptomic signatures of NC-derived cells from embryonic–early larval and middle larval–juvenile stages, cells were additionally collected from euthyroid larvae at 5 dpf (3.5 SSL). C) Cells were FACS-isolated by detection of mCherry vs. GFP fluorescence. D) Representative FAC sort for NC-derived cells from post-embryonic skins and trunks. Single cells were isolated by sequentially gating cells according to their SSC-A vs. FSC-A, FSC-H vs. FSC-W, and SSC-H vs. SSC-W profiles according to standard flow cytometry practices. Cells with high levels of DAPI staining were excluded as dead or damaged. NC-derived cells were isolated by identifying cells with high fluorescence in the mCherry-A channel which describes expression of the ubi:loxP-EGFP-loxP-mCherry transgene after permanent conversion to ubi:mCherry after exposure to sox10:Cre (see 2.9A)).

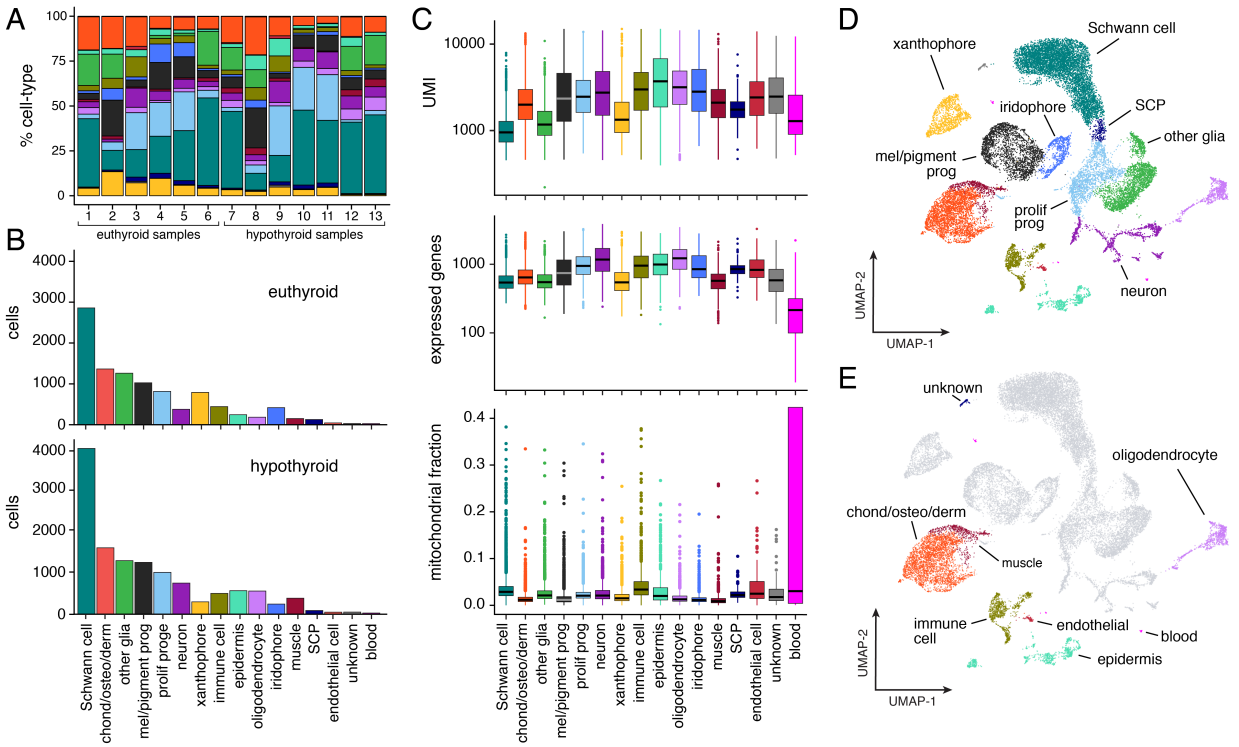

Figure 2.10: **Population characteristics for full scRNA-Seq dataset from post-embryonic zebrafish.** A) Percentages of cell types across samples (for details, see Table 2.1). All cell types are represented in each sample in similar overall proportions. Colors correspond to cell types in (B–E). B) Counts of cells by type captured from euthyroid and hypothyroid fish at post-embryonic stages ($\geq$7.2 SSL). C) Counts of unique molecular identifiers (UMI) and unique genes expressed, as well as fractions of mitochondrial reads by cell-type (shown are medians with boxes spanning interquartile ranges; vertical lines indicate farthest observations of data with outlier samples shown individually). Increased fractions of mitochondrially encoded genes may indicate broken cell (Ilicic et al., 2016); consistent with this idea, Schwann cells—many of which are expected to be damaged owing to their concentrically layered morphology—exhibited one of the largest overall proportions of UMIs derived from mitochondrial genes. D) Two-dimensional UMAP representation of all post-embryonic cells ($\geq$7.2 SSL) captured in scRNA-Seq that passed quality thresholds (22,613 cells, 13 combined samples). E) Same cells as in D, with presumptive NC-derivatives shown in grey and presumptive non-NC derived cells highlighted by type.

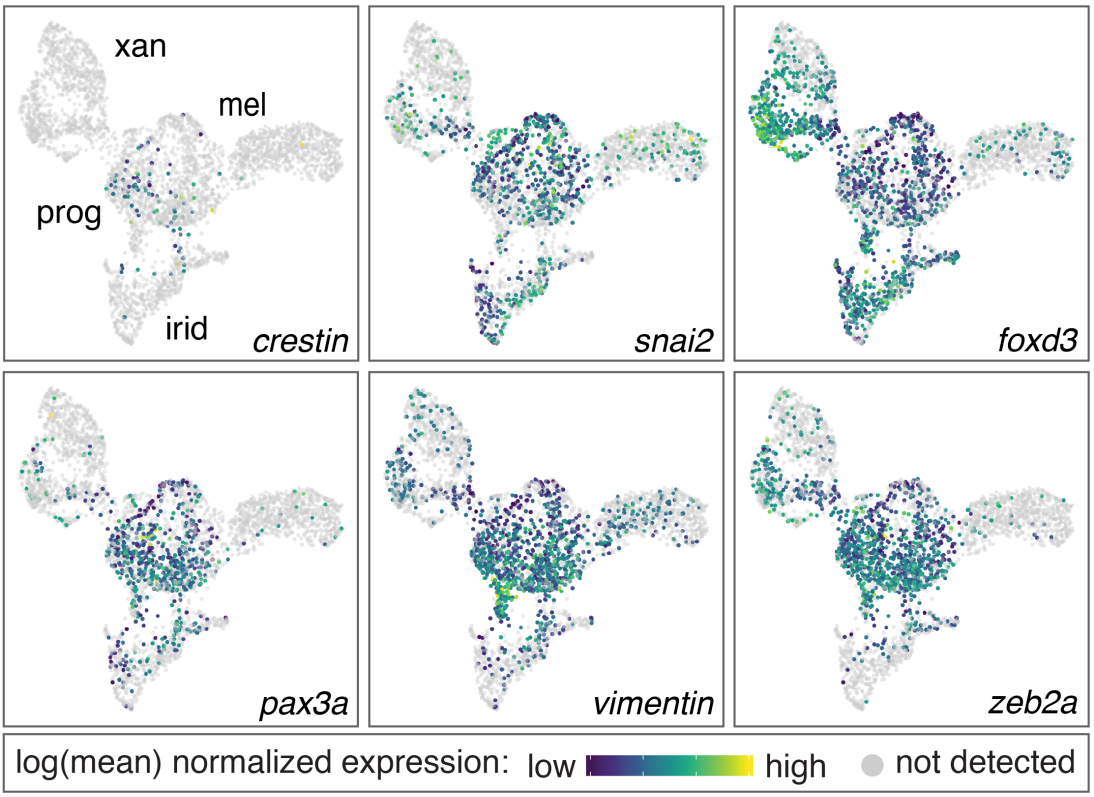

Figure 2.11: **Genes enriched in pigment progenitor clusters include known markers of embryonic NC cells.** Genes enriched in the pigment progenitor cluster compared to differentiated pigment cells included loci expressed in embryonic, migratory NC cells of zebrafish and other species (*crestin*, snai2, *foxd3*, *pax3a*, *vim*, *zeb2a*) (Kaufman et al., 2016; Kelsh et al., 2000; Luo et al., 2001; Minchin and Hughes, 2008; Thisse et al., 1995; Van de Putte et al., 2003; Ziller et al., 1983). Color indicates relative expression of each gene within individual cells (xan, xanthophores; mel, melanophores; irid, iridophores; prog, pigment progenitors).

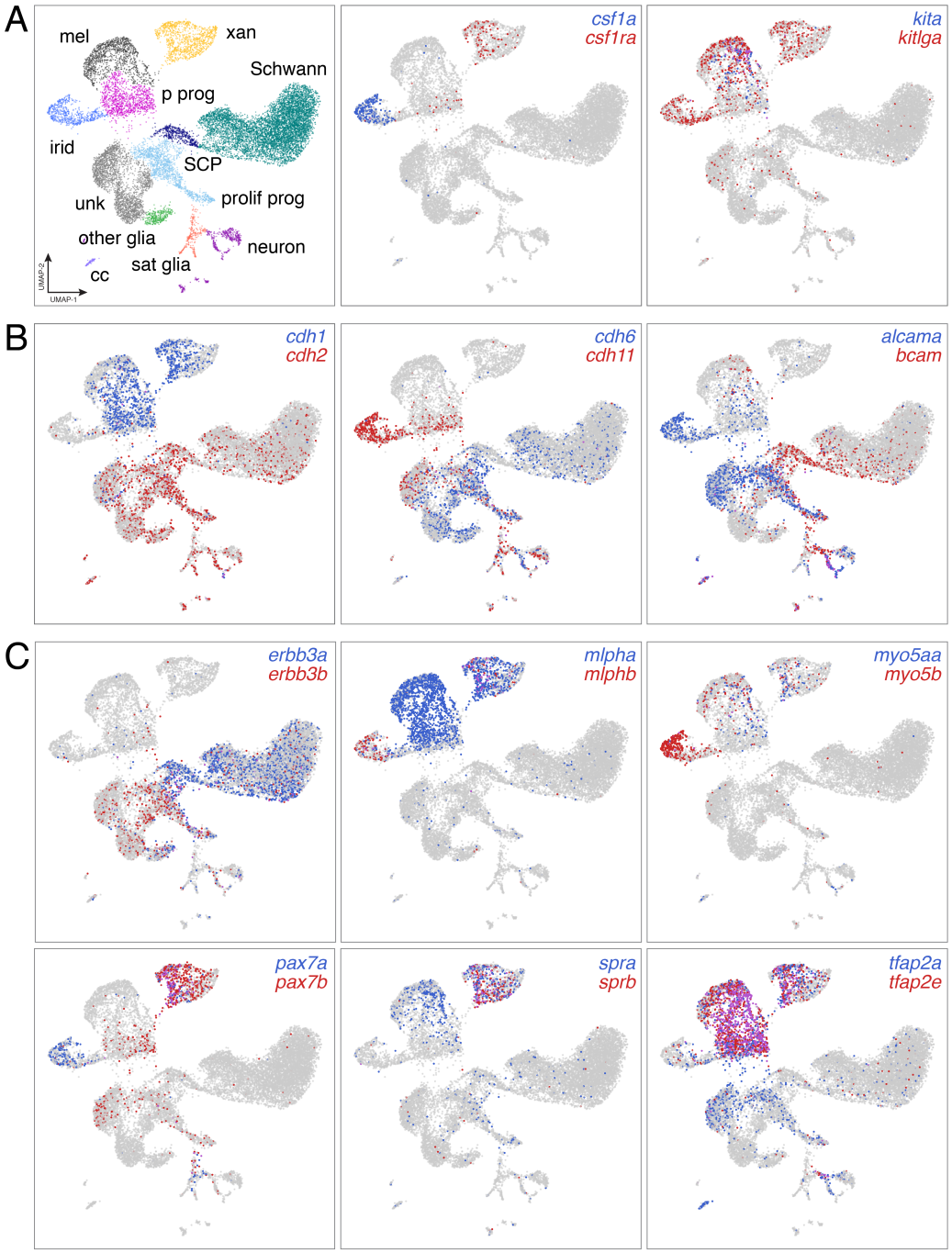

Figure 2.12: **Distinct domains of gene expression across diverse NC derivatives.** (*legend continued on next page*)

Figure 2.12: (*continued*) **Distinct domains of gene expression across diverse NC derivatives.** A) UMAP representation of major NC derivatives (left) with coordinate expression of two exemplar ligand–receptor gene pairs (middle and right). Xanthophores are known to express and require type III receptor tyrosine kinase (RTK) gene colony stimulating factor 1 receptor a (*csf1ra*) and to depend for their development on *csf1a* expressed by nearby iridophores (Parichy et al., 2000b; Patterson and Parichy, 2013). Melanophores require the type III RTK gene *kita* (Parichy et al., 1999) and ligand encoded by *kitlga*, expressed by skin (Hultman et al., 2007; Patterson and Parichy, 2013), but also pigment cells and progenitors revealed here by scRNA-Seq. B) Pairs of cell adhesion molecules with distinct expression domains suggest differing morphogenetic requirements between pigment cell and other lineages (*cdh1* vs. *cdh2*), and for specific cell types [e.g., *cdh11* of iridophores, which form epithelium-like mats within adult interstripes (Singh et al., 2014)]. C) In teleosts, an ancient clade-specific genome duplication resulted in extra genes, allowing for subfunctionalization and retention of some paralogs (Braasch et al., 2009, 2015). scRNA-Seq revealed different degrees to which paralog expression has been partitioned across NC derived cell types. For example, proliferating progenitors and unknown (unk) cells were more likely to express receptor tyrosine kinase gene *erbb3b*, required for development of glia and adult melanophores (Budi et al., 2008), whereas Schwann cells and Schwann cell progenitors (SCP) were more likely to express *erbb3a*. Likewise, xanthophores express and require transcription factor genes *pax7a* and *pax7b* (Nord et al., 2016), but iridophores were also marked by *pax7a* expression, suggesting the possibility of functional significance to this cell type exclusive of *pax7b* activities (A–C, expression thresholds=1.)

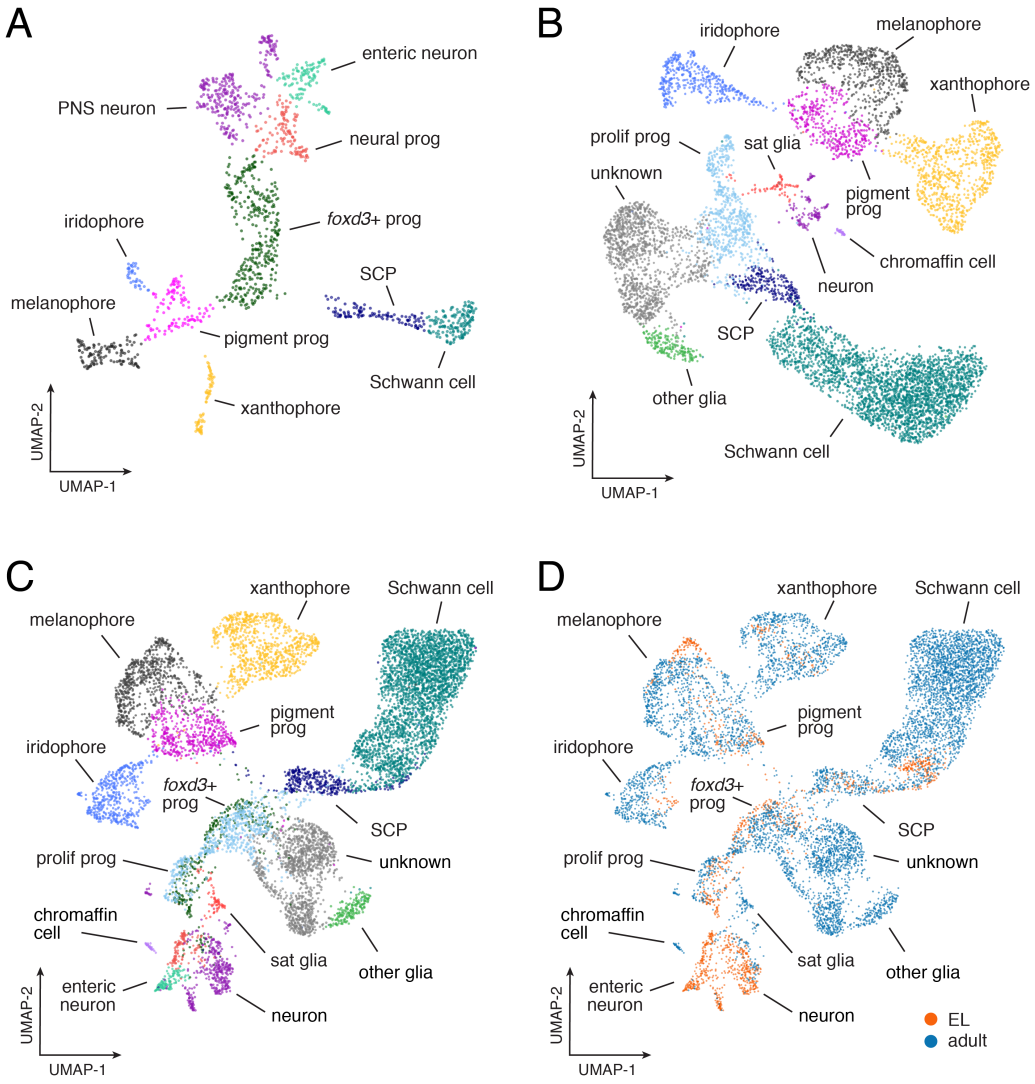

Figure 2.13: **Similarities and differences between EL and adult gene expression programs.** A) UMAP representation of EL NC-derived cells (n=1,466) isolated from euthyroid 5 dpf fish (3.5 SSL; prog, progenitor; SCP, Schwann cell precursors; PNS, non-enteric peripheral nervous system). B) Adult NC-derived cells (n=7,611) isolated from euthyroid middle larva–juvenile ($\geq$7.2 SSL) fish (sat, satellite). C) Combined EL and adult. D) Comparison of EL (orange) and adult (blue) cell distributions revealed broadly overlapping domains of xanthophores in UMAP space, consistent with known derivation of most adult xanthophores from EL xanthophores (McMenamin et al., 2014) [and see Main text].

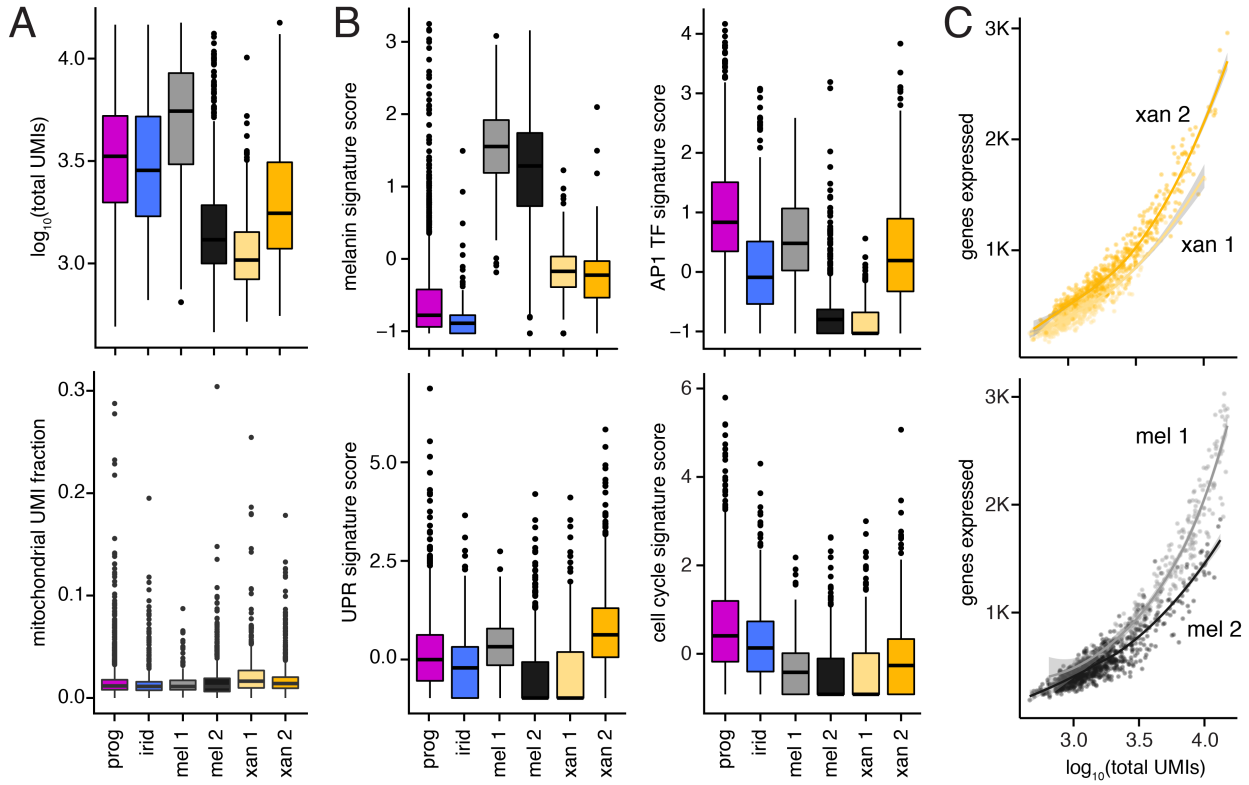

Figure 2.14: **Differences between melanophore and xanthophore sub-populations revealed distinct levels and types of transcriptional activity.** A) Median transcript numbers (unique molecular identifiers, UMIs; upper plot) differed across pigment cell subpopulations. Reduced total RNA content is associated with a G0 cell state (i.e., quiescence, replicative senescence, and/or terminal differentiation) (Coller et al., 2006; Darzynkiewicz et al., 1980); low median UMI counts in sub-clusters of melanophores and xanthophores (mel 2, xan 1) suggest alternative states within these differentiated cell populations. Mitochondrial read fraction (lower plot) was low and consistent across sub-clusters, suggesting that low median UMI counts (upper plot) were unlikely to reflect damage specifically incurred by particular cell types (Ilicic et al., 2016). B) Both melanophore subclusters highly express genes associated with melanin synthesis, indicating that they are both represent true melanophores. However, cell clusters with lower median UMIs (mel 2, xan 1) exhibited gene expression trends indicative of curtailed transcriptional and translational activity, including reduced expression of AP-1 transcriptional complex members (AP1 TF signature score), and genes involved in unfolded protein response (UPR signature score), and proliferation (cell-cycle signature score) (Chinenov and Kerppola, 2001; Patil and Walter, 2001; Riabowol et al., 1992) (for details of genes in signature scores, see Table 2.3). C) Melanophores and xanthophores in subclusters with lower total UMI counts expressed fewer unique genes compared to cells in the other subcluster regardless of equivalent UMI counts, consistent with a more restricted gene expression profile of cells in a terminally differentiated state (shaded areas indicate standard error bounds).

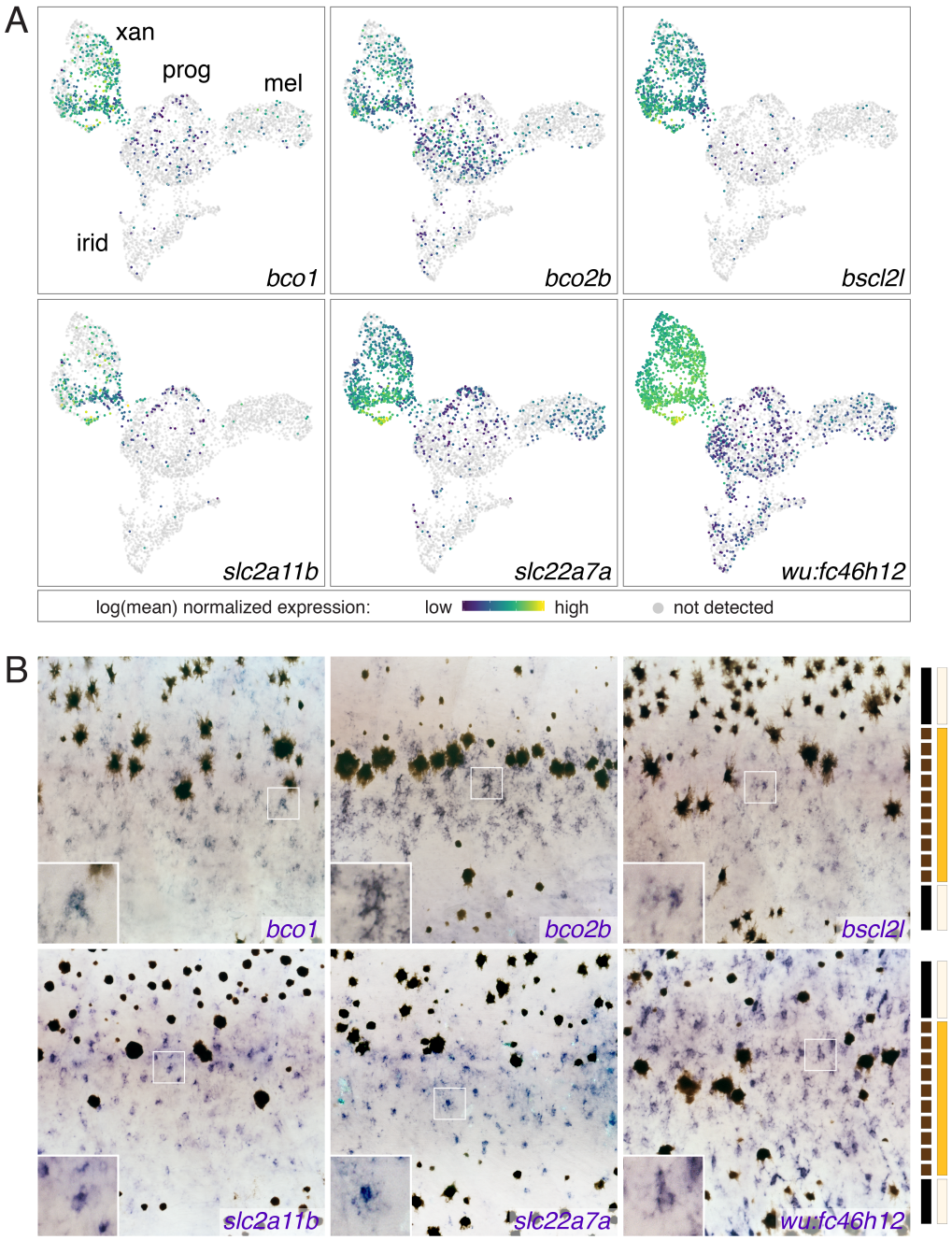

Figure 2.15: **Xanthophore cluster-specific expression identifies novel xanthophore markers.** A) UMAP plots of pigment cells colored by expression of xanthophore cluster-enriched genes (*bco1*, *bco2b*, *bscl2l*, *slc2a11b*, *slc22a7a*, *wu:fc46h12*). B) Expression in xanthophores (e.g., red arrowheads) of genes shown in A, as revealed by whole-mount in situ hybridization patterns corresponding to those of known xanthophore lineage markers and localization of differentiated and cryptic xanthophores (Hamada et al., 2014; Lang et al., 2009; McMenamin et al., 2014; Parichy et al., 2000b).

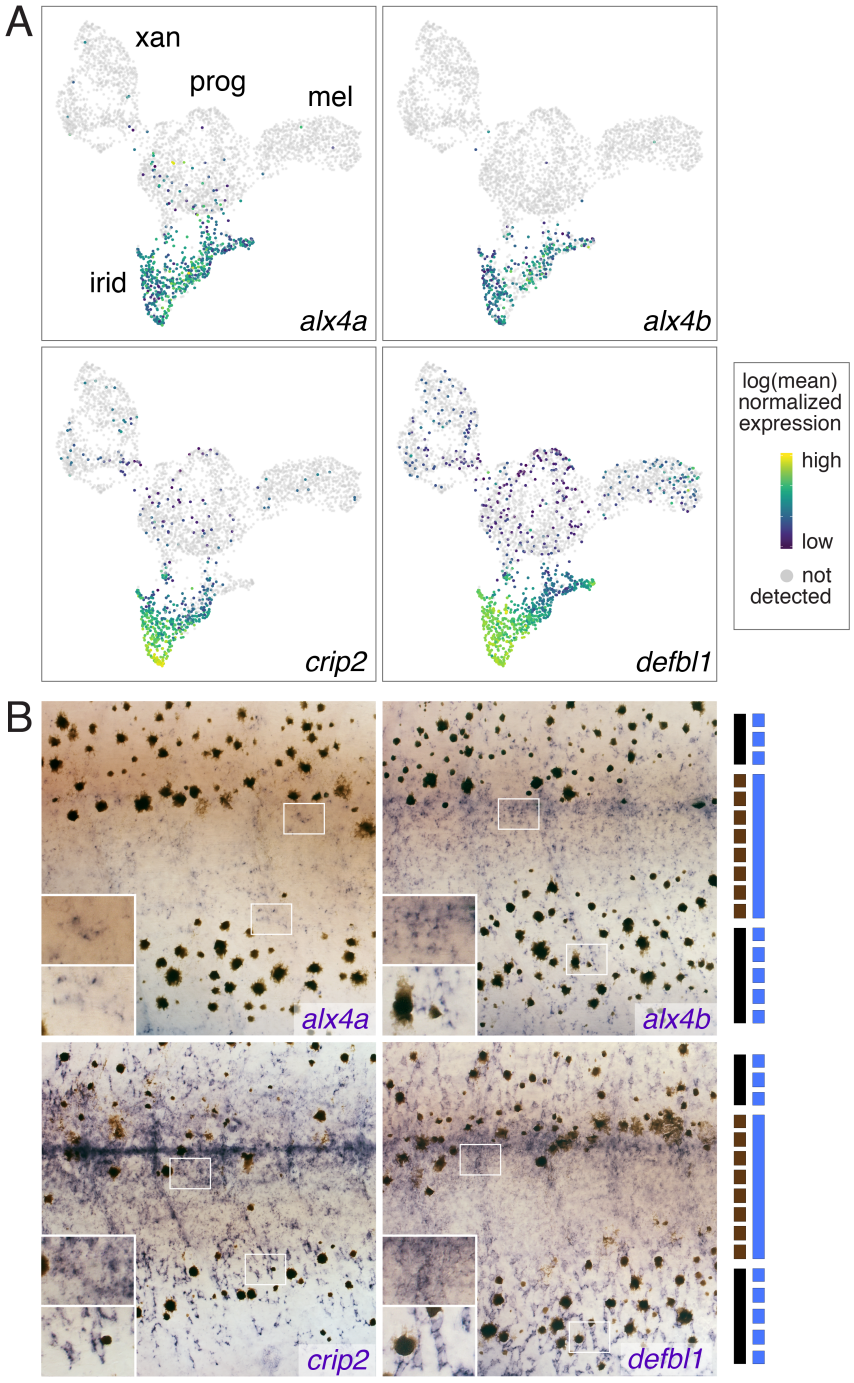

Figure 2.16: **Iridophore cluster-specific expression identifies novel iridophore markers.** A) UMAP plots of pigment cells colored by expression of iridophore cluster-specific genes (*alx4a*, *alx4b*, *crip2*, *defbl1*). B) Whole-mount in situ hybridization of genes in A reveals patterns corresponding to previously described iridophore markers and locations (Lang et al., 2009; Patterson and Parichy, 2013; Spiewak et al., 2018). Insets, higher magnification views of blue-stained iridophores.

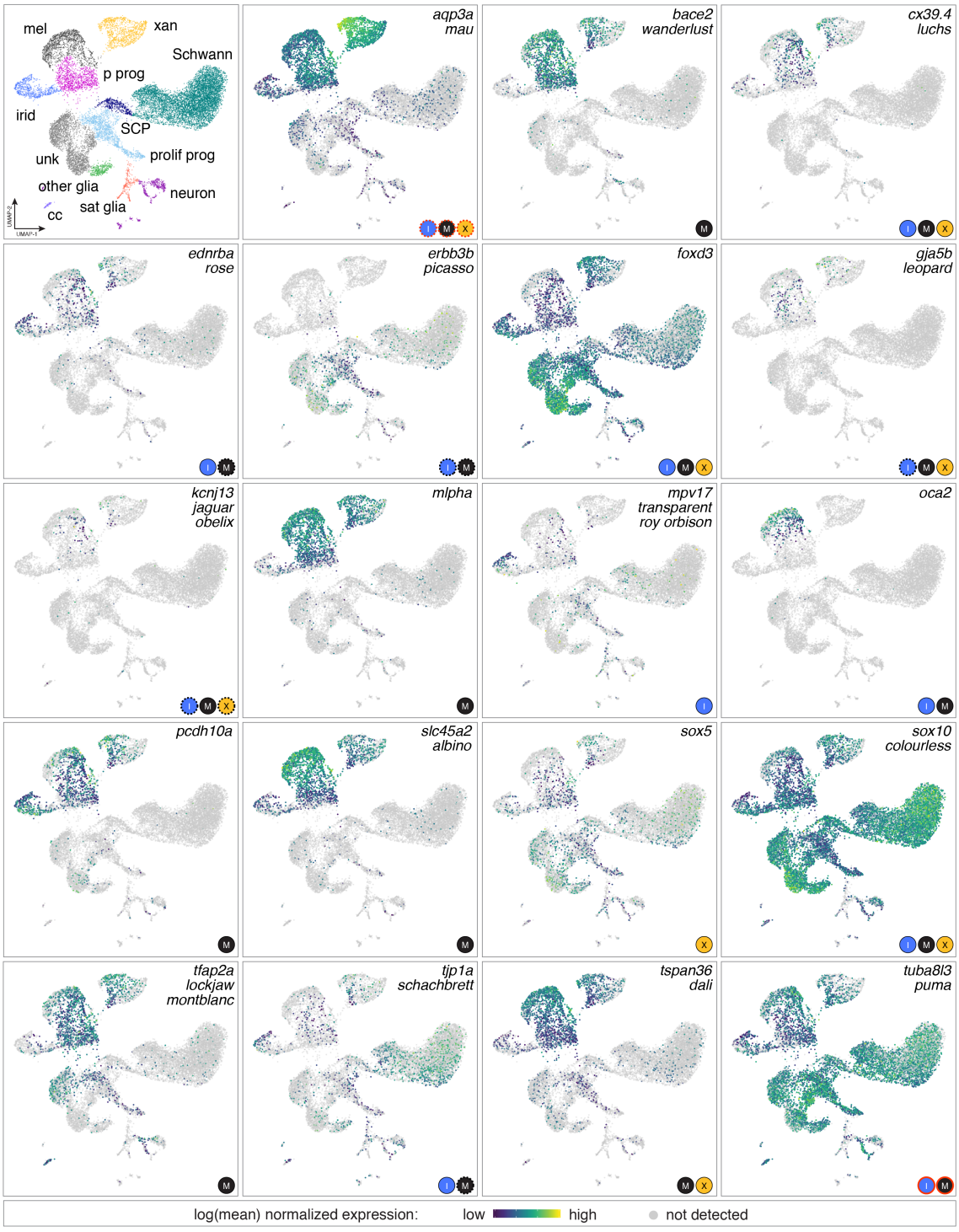

Figure 2.17: **Genes identified as zebrafish pigmentation mutants often had expression domains beyond affected cell types.** (*legend on next page*)

Figure 2.17: (*continued*) **Genes identified as zebrafish pigmentation mutants often had expression domains beyond affected cell types.** Mutations affecting a variety of pigmentary traits have been recovered or induced and affect pigment deposition, specification or morphogenesis of one or more pigment cell classes, and pattern at EL, adult or both stages (Arduini et al., 2009; Barrallo-Gimeno et al., 2004; Beirl et al., 2014; Budi et al., 2008; D'Agati et al., 2017; Dooley et al., 2013b; Dutton et al., 2001; Eskova et al., 2017; Fadeev et al., 2015; Inoue et al., 2014; Irion et al., 2014; Iwashita et al., 2006; Knight et al., 2003; Krauss et al., 2013; Larson et al., 2010; Nagao et al., 2018; Parichy et al., 2000a; Sheets et al., 2007; Watanabe et al., 2006; Williams et al., 2018; Zhang et al., 2018). Shown are expression domains observed for affected genes in scRNA-Seq analyses of adult NC-derived cells (euthyroid and hypothyroid). Gene names are listed at upper right of each box, with corresponding mutant names indicated below for those loci identified in forward genetic screens (for mutants isolated independently in different screens more than one name is indicated). Logos at lower right of each panel are cell types reported to be affected. In some instances only EL phenotypes have been reported (e.g., *pcdh10a*). Red outlines around cell type logos indicates neomorphic alleles (*aqp3a*, *tuba8l3a*); dashed lines indicate effects that are known to be non-autonomous to the affected cell types (e.g., *erbb3b*). In many instances scRNA-Seq expression domains identified a more diverse array of cell types than would be expected from gross mutant phenotypes alone. For example, *slc45a2* is required for melanization of melanophores but detected at lower levels in xanthophores and iridophores, whereas *mlpha* is required for melanosome dispersion but also expressed in xanthophores. Such instances raise the possibility of cell-type specific expression that is not functionally significant (e.g., if other pathway members are not themselves expression), unanticipated functions that result in only subtle loss-of-function phenotypes not yet identified, or amelioration of functional deficiencies by cell-type specific mechanisms of genetic compensation. Conversely, genes not expressed in affected cell types suggest or support prior inferences of non-autonomous functions, or requirements in a common progenitor (*erbb3b*, *oca2*). Genes for some well-studied mutants [e.g., *ltk*/sparse (Johnson et al., 1995; Parichy et al., 1999)] were expressed at levels too low to be detected by scRNA-Seq.

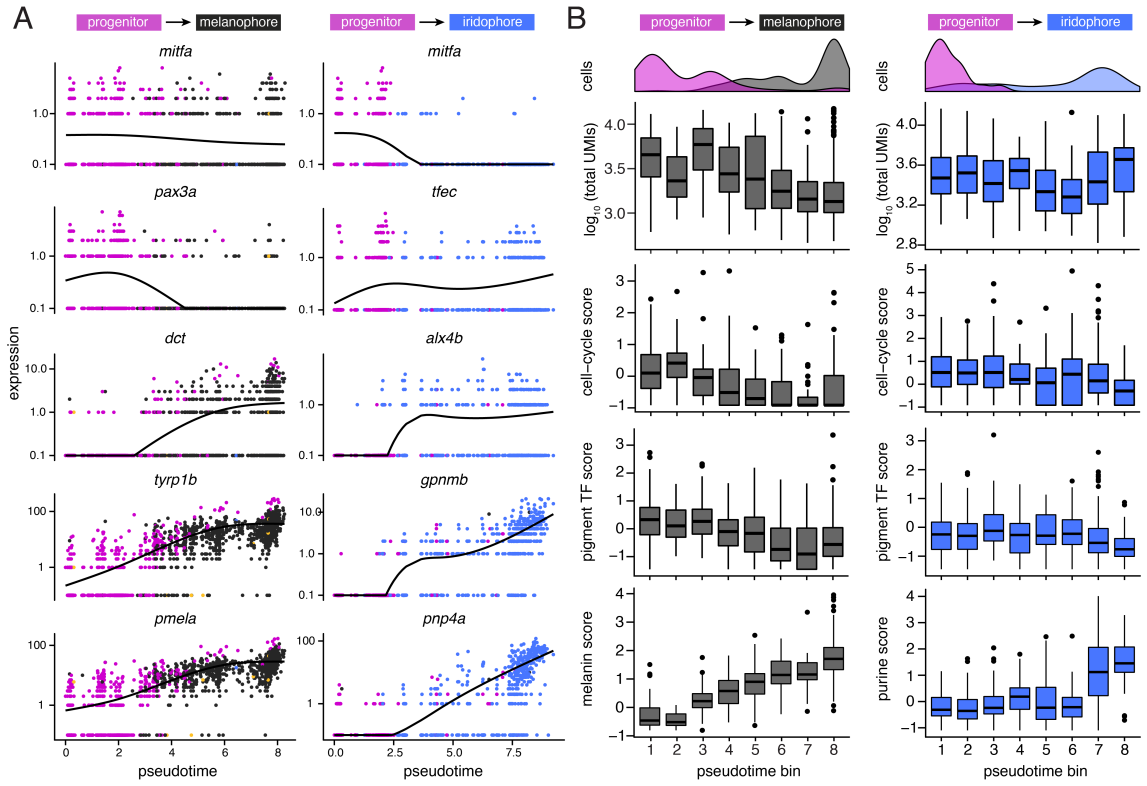

Figure 2.18: **Dynamics of gene expression over pseudotime recapitulated distinct melanophore and iridophore differentiation programs.** A) Expression of genes over pseudotime reflect predicted kinetics for melanophores and iridophores. Solid lines indicate smoothed expression curves for all cells in the branch. *mitfa* expression declined only marginally with melanophore differentiation yet decreased markedly with a transition from progenitor to iridophore as expected (Curran et al., 2010). *pax3a* was expressed in pigment progenitors (magenta) and decreased across pseudotime in melanophores, whereas expression of *tfec*, a transcription factor expressed in iridophores (Lister et al., 2011), increased over pseudotime. Melanin synthesis enzyme genes, *dct* and *tyrp1b*, as well as *pmel*, encoding a melanosome-associated transmembrane protein, all increased over pseudotime in melanophores. In iridophores, *gpnmb* and *pnp4a* showed elevated expression late in pseudotime, as expected (Curran et al., 2010; Higdon et al., 2013). B) Trends of total transcript UMI counts, scores of expressed cell-cycle (e.g. *ccnd1*, *pcna*), pigment cell transcription factors (e.g. *mitfa*, *tfec*, *pax7b*, *tfap2a*), and pigment synthesis-related genes (e.g. *impdh1b*, *gart*, and *atic* for purine processing in iridophores; *tyrp1b*, *pmela*, and *tyr* for melanin synthesis in melanophores) in bins across pseudotime for melanophore and iridophore trajectory branches (for all score-associated genes, see 2.3). Histograms indicate cell-type specific densities across pseudotime for each branch. For melanophores, total transcript number per cell decreased over pseudotime and expression levels of melanin synthesis genes increased. In iridophores, mRNA levels stayed relatively constant whereas expression of purine synthesis genes increased. The expression score for cell-cycle genes was greater for iridophores than melanophores at the terminal step of pseudotime ($P < 0.0002$; Wilcoxon; pseudotime bin 8; n=91 iridophores, 319 melanophores), consistent with iridophores continuing to proliferate even after differentiation, and melanophores normally failing to do so (Budi et al., 2011; Darzynkiewicz et al., 1980; McMenamin et al., 2014; Spiewak et al., 2018).

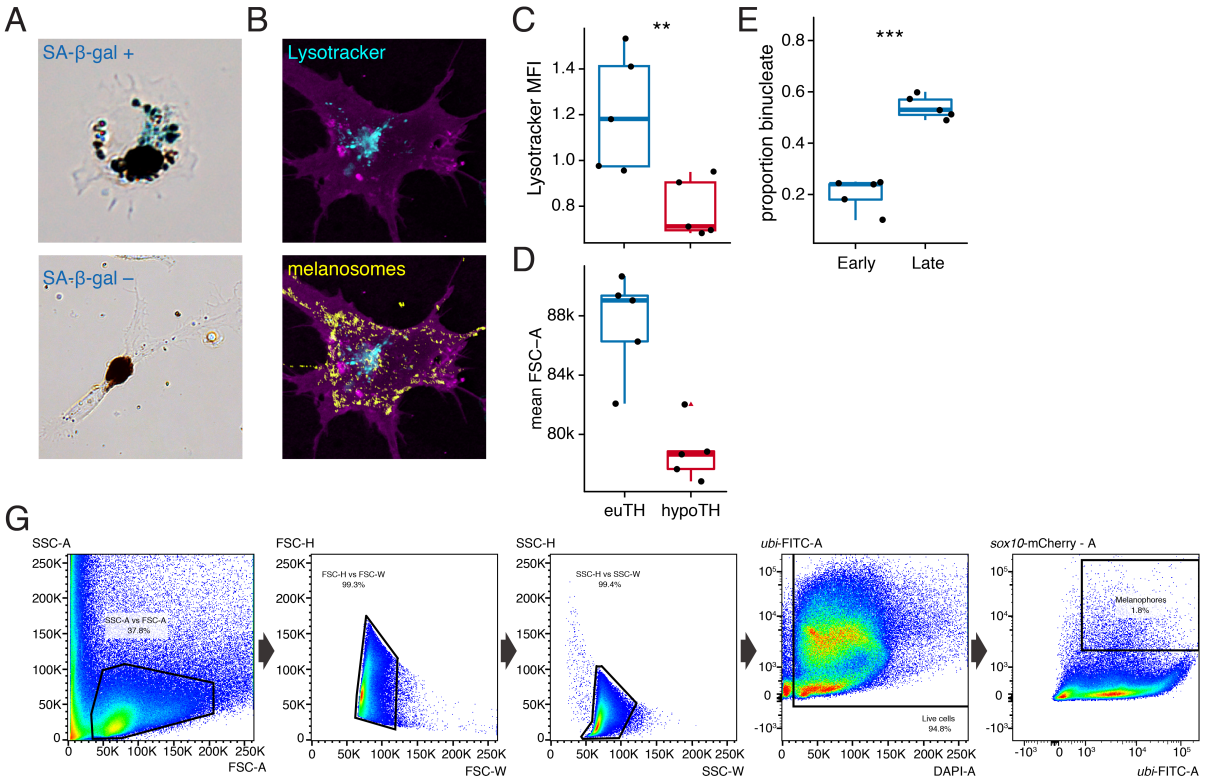

Figure 2.19: **Metrics of melanophore maturation in response to TH.** A) Melanophores plated ex vivo from fish at terminal stages of stripe development had diverse morphologies and some exhibited senescence-associated β-galactosidase staining (SA-β-gal; blue precipitate, upper panel), though relative intensities of staining were difficult to score, precluding a quantitative assessment. Xanthophores plated *ex vivo* did not exhibit SA-β-gal staining. B) Lysosomes were revealed in tyrp1b:palm-mCherry+ (magenta) melanophores by Lysotracker dye (cyan), which did not stain melanosomes (yellow) despite some similarities between these organelles (Raposo et al., 2007). Melanosomes were visualized in bright field and an inverted and pseudocolored overlay is shown here. C) Lysosomal content revealed significantly greater normalized mean fluorescence intensity (MFI) of Lysotracker dye in melanophores from euthyroid fish as compared to hypothyroid fish (euthyroid, 20,423 melanophores from 10 fish; hypothyroid, 87,252 melanophores from 10 fish; $P<0.01$, Wilcoxon). D) FSC-A values were higher for euthyroid compared to hypothyroid cells overall [$P<0.001$; cells are the same as in C)], consistent with an overall difference in cell size. E) Euthyroid fish at a later stage of pattern formation exhibit a higher proportion of binucleate melanophores compared to those at earlier stages (early, 7.2 SSL: n=153 in 5 fish; late, 11 SSL: n=477 melanophores in 5 fish; $P<0.001$). F) Sequential FACS gating strategy (left to right) used in determining Lysotracker normalized MFI. For details, see Materials and Methods. (SSC, side scatter; FSC, forward scatter; W, width; H, height; A, area).

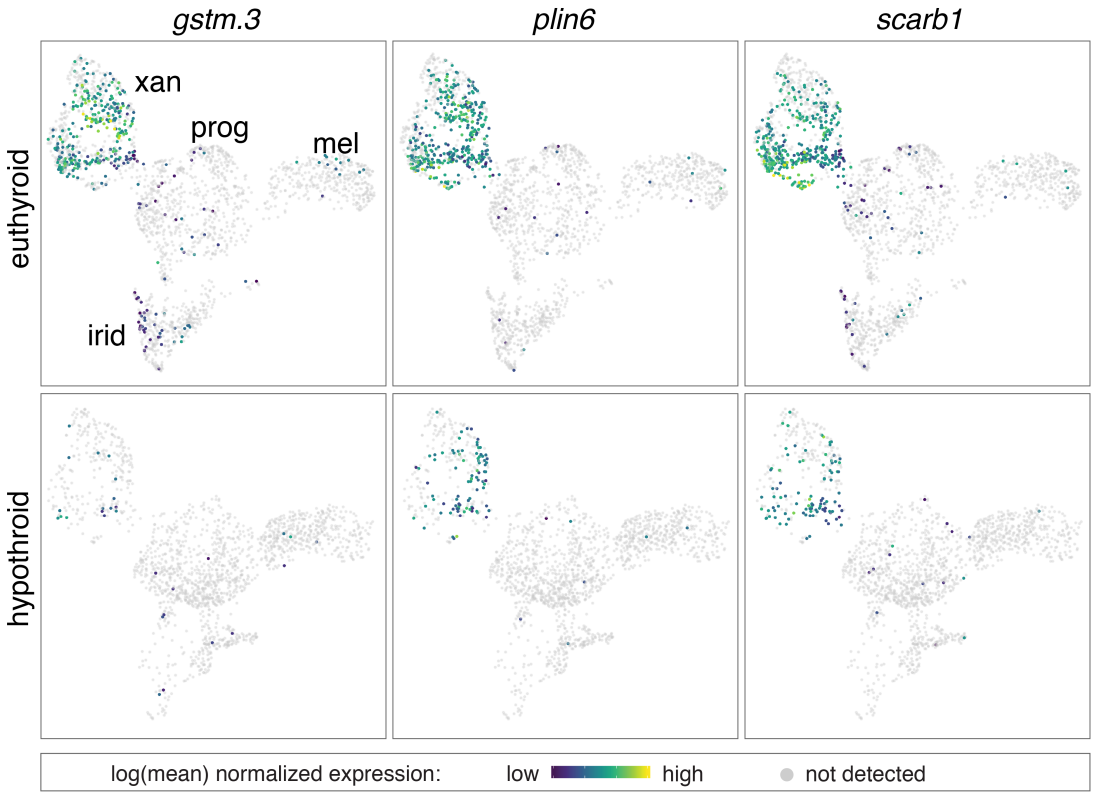

Figure 2.20: **Expression of multiple carotenoid-related genes in xanthophores are affected by TH.** UMAP plots of pigment cell clusters colored by expression of TH-dependent genes in xanthophores: *gstm.3* (q=6.9E-99, $\log_2$ FC = 4.3), *plin6* (q=1.9E-13, $\log_2$ FC=1.3), *scarb1* (q=3.5E-11, $\log_2$ FC=1.2).

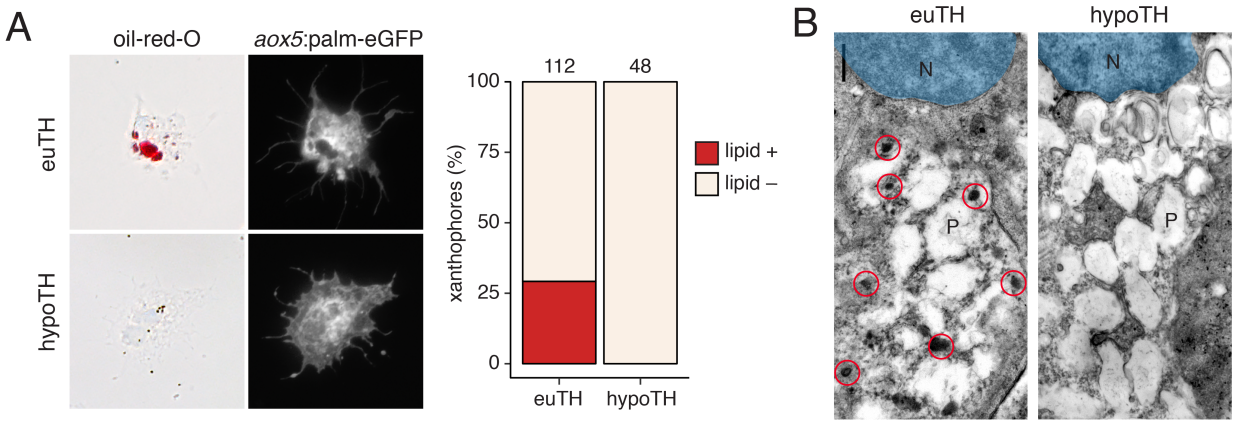

Figure 2.21: **TH promotes development of lipid-filled carotenoid droplets in xanthophores.** A) Carotenoid pigments are normally localized to lipid droplets, the presence of which can be revealed by Oil-red-O staining. Here, a proportion of *aox5*:palmEGFP+ xanthophores stained *ex vivo* from euthyroid fish (n=112 cells) contained lipid (red), whereas xanthophores from hypothyroid fish (n=48 cells) were never observed to have such lipid contents. B) Ultrastructurally, carotenoids and lipids are detectable as electron-dense carotenoid vesicles (red circles) (Djurdjevič et al., 2015; Granneman et al., 2017; Obika, 1993), which were observed in xanthophores from euthyroid but not hypothyroid fish. N, nucleus. P, pterinosome—the pteridine-containing organelle of xanthophores (Bagnara et al., 1968; Hirata et al., 2003; Matsumoto, 1965; Obika, 1993).

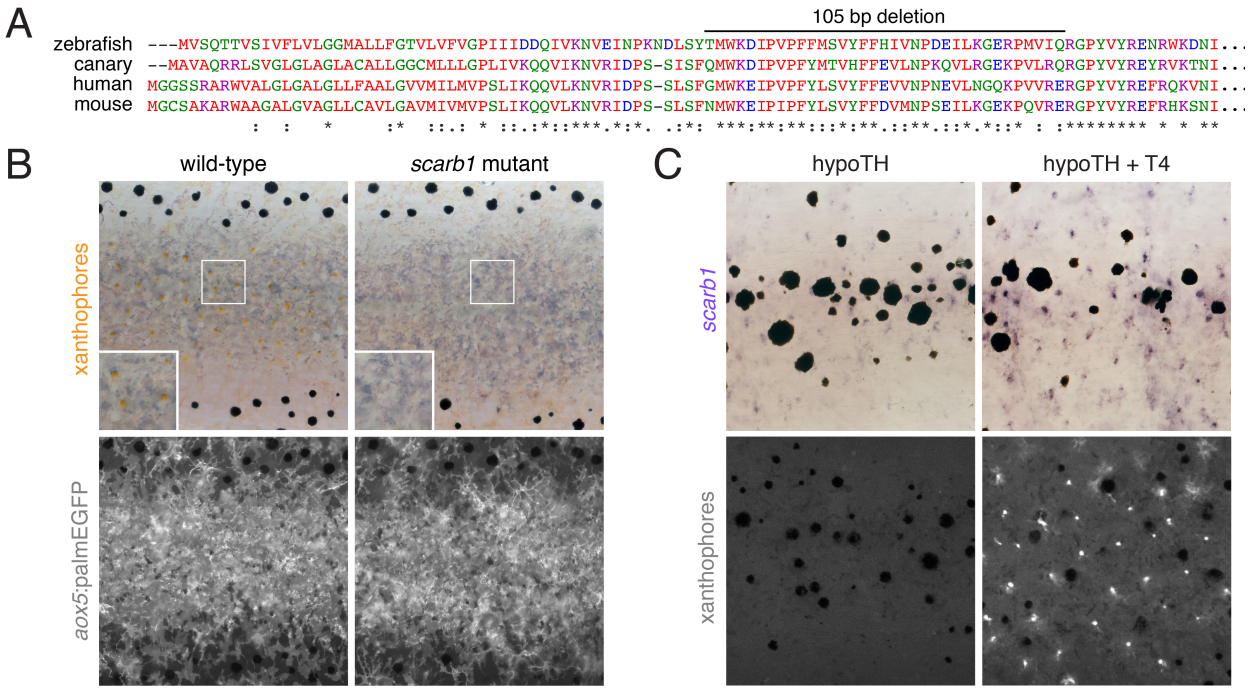

Figure 2.22: ***scarb1* is specifically involved in xanthophore maturation and is induced by TH.** A) Scarb1 protein alignment. Zebrafish *scarb1* mutants had a 105 bp, in-frame deletion in a conserved region of the protein. B) *scarb1* mutants lacked mature, interstripe xanthophores but had normal stripes and aox5:palmEGFP expression, suggesting that patterning and unpigmented xanthophores were normal. C) In hypothyroid fish treated with exogenous TH (T4), *scarb1* expression was rescued within ∼1d (upper) and carotenoid autofluorescence of xanthophores was recovered within ∼2d (lower).

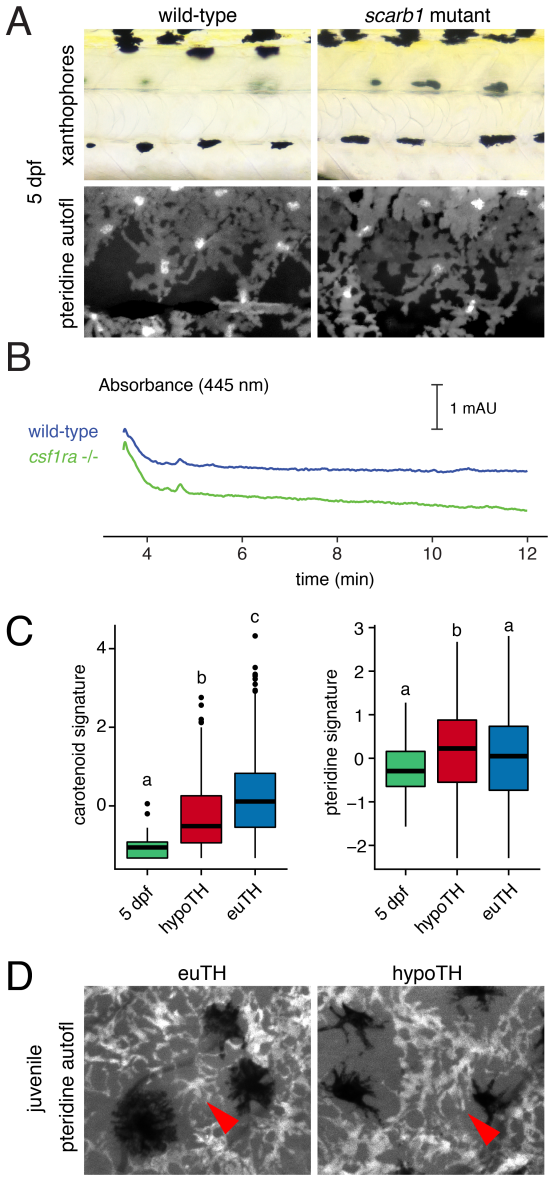

Figure 2.23: **Xanthophores switch yellow pigmentation programs during the larval-to-adult transition.** A) At 5 dpf, *scarb1* mutants had yellow larval xanthophores with wild-type levels of pteridines. B) Carotenoids were not detectable in EL zebrafish (5 dpf, wild-type; compare to Figure 2.3D); *csf1ra* mutants, which lack xanthophores, had HPLC profiles indistinguishable from wild-type. C) Carotenoid and pteridine pathway signature scores for xanthophores in euthyroid EL and euthyroid and hypothyroid adult scRNA-Seq data sets. Box plots as in Figure 2.3 with different letters above data indicating significant differences in post hoc comparisons (carotenoid - P<2e-16, pteridine - P=0.01, Tukey HSD). Pteridine signatures between EL, hypothyroid, and euthyroid xanthophores were more similar than carotenoid signatures. D) Ammonia-induced pteridine fluorescence was present in adult xanthophores of both euthyroid and hypothyroid fish (red arrowheads).

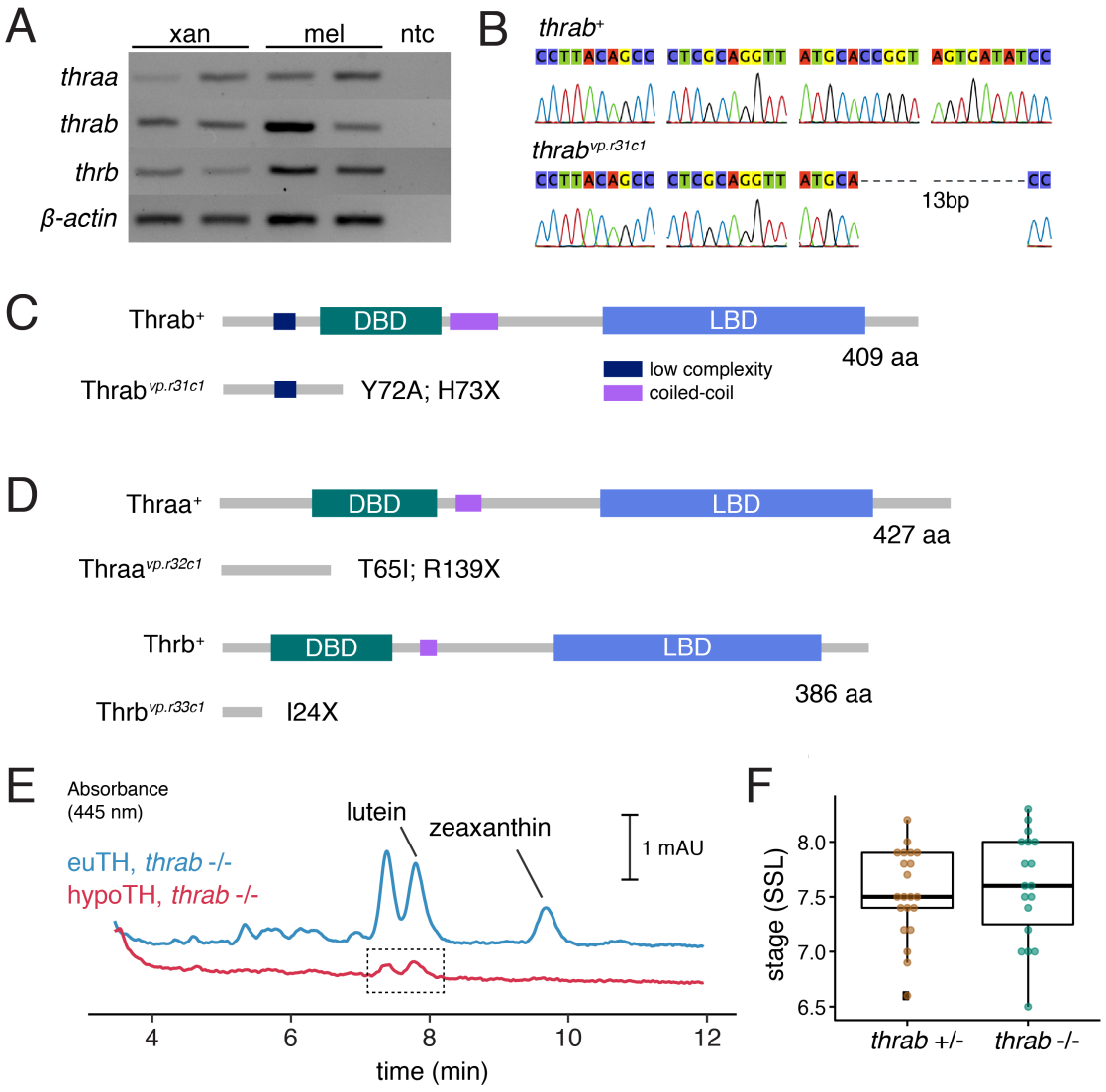

Figure 2.24: **Zebrafish TR gene expression and mutants.** A) RT-PCR for *thraa*, *thrab*, and *thrb* in xanthophores and melanophores sorted by FACS for *aox5*:palmEGFP and *tyrp1b*:palm-mCherry, respectively. B) Sanger sequencing of CRISPR/Cas9-induced mutant allele of *thrab* revealed a 13 bp deletion. C) Schematic of Thrab wild-type and mutant proteins illustrating introduction of a novel amino acid followed by a premature stop codon at position 73. DBD, DNA binding domain; LBD, ligand binding domain. D) Additional CRISPR/Cas9 mutant alleles for thraa and thrb had phenotypes indistinguishable from wild-type or thrab (Figure 2.7A). E) HPLC revealed persisting carotenoids in hypothyroid fish mutant for thrab (boxed region), in contrast to the absence of detectable carotenoids in hypothyroid fish that were wild-type for *thrab* (Figure 2.6D). F) Stage of first xanthophore appearance did not differ significantly (P=0.7) between euthyroid fish that were heterozygous or homozygous wild-type for *thrab* mutation.

Sample	Condition	Stage (SSL)	Tissue	Cell number
1	Euthyroid	11.0	trunk	2168
2	Euthyroid	7.2-10.4	skin	3008
3	Euthyroid	7.2-10.4	trunk	944
4	Euthyroid	7.2-10.4	trunk	808
5	Euthyroid	7.2-10.4	trunk	807
6	Euthyroid	7.2-10.4	trunk	2384
7	Hypothyroid	11.0	trunk	2135
8	Hypothyroid	7.2-10.4	skin	3033
9	Hypothyroid	7.2-10.4	trunk	1073
10	Hypothyroid	7.2-10.4	trunk	941
11	Hypothyroid	7.2-10.4	trunk	774
12	Hypothyroid	7.2-10.4	trunk	1888
13	Hypothyroid	7.2-10.4	trunk	2650
14	5 dpf, Euthyroid	3.8	tail	2154

Table 2.1: **Single cell RNA-seq sample information.**

Cell Type	Ensembl ID	Gene symbol	Gene full name	specificity	q-value
Chromaffin	ENSDARG00000111997	npffr1	neuropeptide FF receptor 1	0.95897224	0
Chromaffin	ENSDARG00000074387	alkal1	NA	0.95377069	0
Chromaffin	ENSDARG00000030621	th	tyrosine hydroxylase	0.95259157	0
Chromaffin	ENSDARG00000016141	slc6a2	solute carrier family 6 (neurotransmitter transporter), member 2	0.93590093	0
Chromaffin	ENSDARG00000079980	si:ch211-202h22.9	si:ch211-202h22.9	0.92395012	0
Chromaffin	ENSDARG00000069446	dbh	dopamine beta-hydroxylase (dopamine beta-monooxygenase)	0.92316361	0
Chromaffin	ENSDARG00000100991	chrna3	cholinergic receptor, nicotinic, alpha 3	0.92197315	0
Chromaffin	ENSDARG00000093021	FAM163A	NA	0.92193989	0
Chromaffin	ENSDARG00000101522	FO907089.1	NA	0.91817851	0
Chromaffin	ENSDARG00000086214	ntrk3b	neurotrophic tyrosine kinase, receptor, type 3b	0.90425109	0
Chromaffin	ENSDARG00000074064	rem2	RAS (RAD and GEM)-like GTP binding 2	0.90098837	0
Chromaffin	ENSDARG00000070954	hmx2	H6 family homeobox 2	0.89260753	0
Chromaffin	ENSDARG00000007406	phox2a	paired-like homeobox 2a	0.89011727	0
Chromaffin	ENSDARG00000091029	phox2bb	paired-like homeobox 2bb	0.85875676	0
Chromaffin	ENSDARG00000008305	hand2	heart and neural crest derivatives expressed 2	0.84964429	0
Chromaffin	ENSDARG00000100971	fxyd6	FXYD domain containing ion transport regulator 6	0.84910372	0
Chromaffin	ENSDARG00000058969	cntnap2a	contactin associated protein-like 2a	0.83962364	0
Chromaffin	ENSDARG00000028306	prph	peripherin	0.83452825	0
Chromaffin	ENSDARG00000078768	abhd15a	abhydrolase domain containing 15a	0.83315201	0
Chromaffin	ENSDARG00000004023	isl1	ISL LIM homeobox 1	0.82789557	0
Chromaffin	ENSDARG00000056262	slc35g2a	solute carrier family 35, member G2a	0.82723813	0
Chromaffin	ENSDARG00000070491	hpcal4	hippocalcin like 4	0.82648652	0
Chromaffin	ENSDARG00000009026	ank2a	ankyrin 2a, neuronal	0.82386789	0
Chromaffin	ENSDARG00000035338	tppp2	tubulin polymerization-promoting protein family member 2	0.82335315	0
Chromaffin	ENSDARG00000008829	chga	chromogranin A	0.8217436	0
Chromaffin	ENSDARG00000051875	islr2	immunoglobulin superfamily containing leucine-rich repeat 2	0.81683987	0
Chromaffin	ENSDARG00000060434	map1b	microtubule-associated protein 1B	0.81586177	0
Chromaffin	ENSDARG00000054794	plcxd3	phosphatidylinositol-specific phospholipase C, X domain containing 3	0.81308486	0
Chromaffin	ENSDARG00000034522	rab6ba	RAB6B, member RAS oncogene family a	0.80432446	0
Chromaffin	ENSDARG00000043932	stmn4l	stathmin-like 4, like	0.79603511	0
Iridophore	ENSDARG00000113438	CR318624.2	NA	0.94897571	0
Iridophore	ENSDARG00000076959	si:ch211-38m6.6	si:ch211-38m6.6	0.94812122	0
Iridophore	ENSDARG00000075436	sytl2b	synaptotagmin-like 2b	0.94548424	0
Iridophore	ENSDARG00000074442	alx4b	ALX homeobox 4b	0.93855792	0
Iridophore	ENSDARG00000008306	rdh5	retinol dehydrogenase 5 (11-cis/9-cis)	0.93646542	0
Iridophore	ENSDARG00000053709	si:ch73-89b15.3	si:ch73-89b15.3	0.93085472	0
Iridophore	ENSDARG00000017246	prx	periaxin	0.92610848	0
Iridophore	ENSDARG00000057706	si:ch211-137i24.10	si:ch211-137i24.10	0.92523905	0
Iridophore	ENSDARG00000058492	si:dkey-30c15.17	si:dkey-30c15.17	0.92403985	0
Iridophore	ENSDARG00000055172	si:ch211-256m1.8	si:ch211-256m1.8	0.92144116	0
Iridophore	ENSDARG00000006112	myof	myoferlin	0.91938104	0
Iridophore	ENSDARG00000004392	hdr	hematopoietic death receptor	0.91913569	0
Iridophore	ENSDARG00000062688	gpnmb	glycoprotein (transmembrane) nmb	0.90926329	0
Iridophore	ENSDARG00000069495	tmem179b	transmembrane protein 179B	0.90298323	0
Iridophore	ENSDARG00000074528	unm_sa821	un-named sa821	0.899869	0
Iridophore	ENSDARG00000003991	fhl2b	four and a half LIM domains 2b	0.89594157	0
Iridophore	ENSDARG00000091792	akap12a	A kinase (PRKA) anchor protein 12a	0.89460613	0
Iridophore	ENSDARG00000079252	fam117ab	family with sequence similarity 117, member Ab	0.89038864	0
Iridophore	ENSDARG00000075343	csf1a	colony stimulating factor 1a (macrophage)	0.88816858	0
Iridophore	ENSDARG00000089441	si:ch211-105c13.3	si:ch211-105c13.3	0.88353331	0
Iridophore	ENSDARG00000088332	alx4a	ALX homeobox 4a	0.8617735	0
Iridophore	ENSDARG00000092240	si:ch211-243a20.3	si:ch211-243a20.3	0.85669823	0
Iridophore	ENSDARG00000070597	prelp	proline/arginine-rich end leucine-rich repeat protein	0.85583845	0
Iridophore	ENSDARG00000060345	apoda.1	apolipoprotein Da, duplicate 1	0.83779058	0
Iridophore	ENSDARG00000042018	fhl2a	four and a half LIM domains 2a	0.83196996	0
Iridophore	ENSDARG00000032862	ugt5g1	UDP glucuronosyltransferase 5 family, polypeptide G1	0.824965	0
Iridophore	ENSDARG00000075629	si:dkey-197i20.6	si:dkey-197i20.6	0.81448093	0
Iridophore	ENSDARG00000097804	lypc	ly6 domain containing, pigment cell	0.80211732	0
Iridophore	ENSDARG00000104495	pltp	phospholipid transfer protein	0.80148387	0
Iridophore	ENSDARG00000073978	crabp2a	cellular retinoic acid binding protein 2, a	0.79161518	0
Melanophore	ENSDARG00000061303	oca2	oculocutaneous albinism II	0.8894009	0
Melanophore	ENSDARG00000006008	dct	dopachrome tautomerase	0.822667	0
Melanophore	ENSDARG00000100917	slc30a8	solute carrier family 30 (zinc transporter), member 8	0.81746529	0
Melanophore	ENSDARG00000029204	tyrp1a	tyrosinase-related protein 1a	0.81525607	0
Melanophore	ENSDARG00000020143	pah	phenylalanine hydroxylase	0.78883537	0
Melanophore	ENSDARG00000044767	tspan10	NA	0.77565963	0
Melanophore	ENSDARG00000011076	zgc:91968	zgc:91968	0.76069011	0
Melanophore	ENSDARG00000005823	slc39a10	solute carrier family 39 (zinc transporter), member 10	0.75703493	0
Melanophore	ENSDARG00000056151	tyrp1b	tyrosinase-related protein 1b	0.73879632	0
Melanophore	ENSDARG00000091298	pmela	premelanosome protein a	0.71799603	0

Table 2.2: **Genes enriched in specific cell types from post-embryonic NC derivatives.**

Cell Type	Ensembl ID	Gene symbol	Gene full name	specificity	q-value
Melanophore	ENSDARG00000034757	zdhhc2	zinc finger, DHHC-type containing 2	0.68867369	0
Melanophore	ENSDARG00000053269	slc2a15b	solute carrier family 2 (facilitated glucose transporter), member 15b	0.6870176	0
Melanophore	ENSDARG00000061692	yjefn3	YjeF N-terminal domain containing 3	0.66755425	0
Melanophore	ENSDARG00000044501	viml	vimentin like	0.66517815	0
Melanophore	ENSDARG00000042428	gstt1a	glutathione S-transferase theta 1a	0.65673072	0
Melanophore	ENSDARG00000002593	slc45a2	solute carrier family 45, member 2	0.6549489	0
Melanophore	ENSDARG00000042214	tmem243a	transmembrane protein 243, mitochondrial a	0.65237771	0
Melanophore	ENSDARG00000011961	csrp2	cysteine and glycine-rich protein 2	0.64913712	0
Melanophore	ENSDARG00000040190	qdpra	quinoid dihydropteridine reductase a	0.64540256	0
Melanophore	ENSDARG00000070991	mlpha	melanophilin a	0.64465774	0
Melanophore	ENSDARG00000101586	si:ch73-389b16.1	si:ch73-389b16.1	0.64270727	0
Melanophore	ENSDARG00000032746	tnfsf10l3	tumor necrosis factor (ligand) superfamily, member 10 like 3	0.64225545	0
Melanophore	ENSDARG00000034572	gpr143	G protein-coupled receptor 143	0.63251402	0
Melanophore	ENSDARG00000077653	rabl6b	RAB, member RAS oncogene family-like 6b	0.63211849	0
Melanophore	ENSDARG00000008861	tfap2e	transcription factor AP-2 epsilon	0.62734578	0
Melanophore	ENSDARG00000024540	tspan36	tetraspanin 36	0.62183585	0
Melanophore	ENSDARG00000059391	gyg1b	glycogenin 1b	0.62139127	0
Melanophore	ENSDARG00000043342	gpx3	glutathione peroxidase 3	0.61965635	0
Melanophore	ENSDARG00000036427	slc3a2a	solute carrier family 3 (amino acid transporter heavy chain), member 2a	0.61500081	0
Melanophore	ENSDARG00000077082	agtrap	angiotensin II receptor-associated protein	0.61278219	0
Neuron	ENSDARG00000031598	calb1	calbindin 1	0.90259113	0
Neuron	ENSDARG00000027419	gad1b	glutamate decarboxylase 1b	0.87627534	0
Neuron	ENSDARG00000020794	neurod6b	neuronal differentiation 6b	0.86662989	0
Neuron	ENSDARG00000059775	slc32a1	solute carrier family 32 (GABA vesicular transporter), member 1	0.850583	0
Neuron	ENSDARG00000023445	atp2b3b	ATPase, Ca++ transporting, plasma membrane 3b	0.8485164	0
Neuron	ENSDARG00000053499	isl2b	ISL LIM homeobox 2b	0.84416402	0
Neuron	ENSDARG00000104139	atp1a3b	ATPase, Na+/K+ transporting, alpha 3b polypeptide	0.83707865	0
Neuron	ENSDARG00000015537	gad2	glutamate decarboxylase 2	0.83094575	0
Neuron	ENSDARG00000025728	grin1b	glutamate receptor, ionotropic, N-methyl D-aspartate 1b	0.82255582	0
Neuron	ENSDARG00000003994	syt9a	synaptotagmin IXa	0.79730575	0
Neuron	ENSDARG00000062056	elmod1	ELMO/CED-12 domain containing 1	0.79533868	0
Neuron	ENSDARG00000014018	lhx1a	LIM homeobox 1a	0.79456466	0
Neuron	ENSDARG00000056108	ndufa4	NADH dehydrogenase (ubiquinone) 1 alpha subcomplex, 4	0.77627839	0
Neuron	ENSDARG00000100244	ebf3a	early B-cell factor 3a	0.77299945	0
Neuron	ENSDARG00000069329	drgx	dorsal root ganglia homeobox	0.76615136	0
Neuron	ENSDARG00000019566	neurod1	neuronal differentiation 1	0.75352318	0
Neuron	ENSDARG00000093677	si:ch211-56a11.2	si:ch211-56a11.2	0.74024446	0
Neuron	ENSDARG00000027740	adcyap1b	adenylate cyclase activating polypeptide 1b	0.73785425	0
Neuron	ENSDARG00000091756	insm1a	insulinoma-associated 1a	0.73099946	0
Neuron	ENSDARG00000102501	hoxa5a	homeobox A5a	0.72889053	0
Neuron	ENSDARG00000053301	insm1b	insulinoma-associated 1b	0.71818801	0
Neuron	ENSDARG00000023600	sh3gl2a	NA	0.70663992	0
Neuron	ENSDARG00000087784	si:dkeyp-110a12.4	si:dkeyp-110a12.4	0.70586304	0
Neuron	ENSDARG00000020609	snap25a	synaptosomal-associated protein, 25a	0.69014244	0
Neuron	ENSDARG00000031587	flvcr1	feline leukemia virus subgroup C cellular receptor 1	0.68576977	0
Neuron	ENSDARG00000109715	sncgb	synuclein, gamma b (breast cancer-specific protein 1)	0.68236016	0
Neuron	ENSDARG00000056175	scrt2	scratch family zinc finger 2	0.6815874	0
Neuron	ENSDARG00000101387	CAMK2N1	NA	0.67837591	0
Neuron	ENSDARG00000076833	atp1b1b	ATPase, Na+/K+ transporting, beta 1b polypeptide	0.67735802	0
Neuron	ENSDARG00000077256	nat8l	N-acetyltransferase 8-like	0.67629678	0
Other Glia	ENSDARG00000043806	postna	periostin, osteoblast specific factor a	0.65474159	0
Other Glia	ENSDARG00000102956	mmp17b	matrix metallopeptidase 17b	0.6533764	0
Other Glia	ENSDARG00000034470	aldoab	aldolase a, fructose-bisphosphate, b	0.64538653	0
Other Glia	ENSDARG00000099144	igfbp3	insulin-like growth factor binding protein 3	0.62772002	0
Other Glia	ENSDARG00000017624	krt4	keratin 4	0.62608124	0
Other Glia	ENSDARG00000045066	entpd1	ectonucleoside triphosphate diphosphohydrolase 1	0.62454937	0
Other Glia	ENSDARG00000019986	grhprb	glyoxylate reductase/hydroxypyruvate reductase b	0.6177344	0
Other Glia	ENSDARG00000021172	cyp2ad2	cytochrome P450, family 2, subfamily AD, polypeptide 2	0.61543698	0
Other Glia	ENSDARG00000070498	phyhiplb	phytanoyl-CoA 2-hydroxylase interacting protein-like b	0.61482743	0
Other Glia	ENSDARG00000095901	col18a1b	NA	0.61088541	0
Other Glia	ENSDARG00000077257	timd4	T-cell immunoglobulin and mucin domain containing 4	0.60986288	0
Other Glia	ENSDARG00000074908	col6a1	collagen, type VI, alpha 1	0.60604933	0
Other Glia	ENSDARG00000037960	lrrc17	leucine rich repeat containing 17	0.60582267	0
Other Glia	ENSDARG00000018787	efna1b	ephrin-A1b	0.60437906	0
Other Glia	ENSDARG00000068912	zgc:153012	zgc:153012	0.6037038	0
Other Glia	ENSDARG00000011602	si:dkeyp-117h8.2	si:dkeyp-117h8.2	0.60309644	0
Other Glia	ENSDARG00000030753	prrg4	proline rich Gla (G-carboxyglutamic acid) 4 (transmembrane)	0.59936571	0
Other Glia	ENSDARG00000061579	myo1cb	myosin Ic, paralog b	0.59924142	0
Other Glia	ENSDARG00000028027	trim63a	tripartite motif containing 63a	0.59747405	0
Other Glia	ENSDARG00000103277	cyp24a1	cytochrome P450, family 24, subfamily A, polypeptide 1	0.59642658	0

Table 2.2: (continued) **Genes enriched in specific cell types from post-embryonic NC derivatives.**

Cell Type	Ensembl ID	Gene symbol	Gene full name	specificity	q-value
Other Glia	ENSDARG00000002391	tlcd1	TLC domain containing 1	0.59573869	0
Other Glia	ENSDARG00000025670	fstl3	follistatin-like 3 (secreted glycoprotein)	0.59256916	0
Other Glia	ENSDARG00000087403	si:ch211-214p13.3	si:ch211-214p13.3	0.59129146	0
Other Glia	ENSDARG00000071460	si:ch211-234p6.5	si:ch211-234p6.5	0.59107895	0
Other Glia	ENSDARG00000039626	nrgna	neurogranin (protein kinase C substrate, RC3) a	0.59096638	0
Other Glia	ENSDARG00000089418	si:dkey-164f24.2	si:dkey-164f24.2	0.59056617	0
Other Glia	ENSDARG00000058064	cx31.7	connexin 31.7	0.59009453	0
Other Glia	ENSDARG00000006427	fabp2	fatty acid binding protein 2, intestinal	0.58966605	0
Other Glia	ENSDARG00000042826	egr2b	early growth response 2b	0.58948273	0
Other Glia	ENSDARG00000089477	si:ch211-132g1.3	si:ch211-132g1.3	0.58870328	0
Pigment Progenitor	ENSDARG00000008861	tfap2e	transcription factor AP-2 epsilon	0.65128354	0
Pigment Progenitor	ENSDARG00000003732	mitfa	microphthalmia-associated transcription factor a	0.64610622	0
Pigment Progenitor	ENSDARG00000043342	gpx3	glutathione peroxidase 3	0.635656	0
Pigment Progenitor	ENSDARG00000041715	bco2b	beta-carotene oxygenase 2b	0.6232253	0
Pigment Progenitor	ENSDARG00000103476	trpm1b	transient receptor potential cation channel, subfamily M, member 1b	0.61809699	0
Pigment Progenitor	ENSDARG00000101461	emp3b	epithelial membrane protein 3b	0.61414402	0
Pigment Progenitor	ENSDARG00000034757	zdhhc2	zinc finger, DHHC-type containing 2	0.6088735	0
Pigment Progenitor	ENSDARG00000097964	arhgef33	Rho guanine nucleotide exchange factor (GEF) 33	0.60881792	0
Pigment Progenitor	ENSDARG00000070991	mlpha	melanophilin a	0.60315309	0
Pigment Progenitor	ENSDARG00000019274	rasd1	RAS, dexamethasone-induced 1	0.60056485	0
Pigment Progenitor	ENSDARG00000024540	tspan36	tetraspanin 36	0.60048064	0
Pigment Progenitor	ENSDARG00000101586	si:ch73-389b16.1	si:ch73-389b16.1	0.59587772	0
Pigment Progenitor	ENSDARG00000077653	rabl6b	RAB, member RAS oncogene family-like 6b	0.59495466	0
Pigment Progenitor	ENSDARG00000002593	slc45a2	solute carrier family 45, member 2	0.59218457	0
Pigment Progenitor	ENSDARG00000000690	sypl2b	synaptophysin-like 2b	0.58777314	0
Pigment Progenitor	ENSDARG00000030530	slc22a2	solute carrier family 22 (organic cation transporter), member 2	0.58704398	0
Pigment Progenitor	ENSDARG00000099729	pcdh10a	protocadherin 10a	0.58249872	0
Pigment Progenitor	ENSDARG00000059680	fscn1a	fascin actin-bundling protein 1a	0.58240095	0
Pigment Progenitor	ENSDARG00000059279	tfap2a	transcription factor AP-2 alpha	0.58037208	0
Pigment Progenitor	ENSDARG00000003808	aqp3a	aquaporin 3a	0.57684186	0
Pigment Progenitor	ENSDARG00000078619	pnp5a	purine nucleoside phosphorylase 5a	0.57672879	0
Pigment Progenitor	ENSDARG00000034572	gpr143	G protein-coupled receptor 143	0.57607861	0
Pigment Progenitor	ENSDARG00000015765	iah1	isoamyl acetate-hydrolyzing esterase 1 homolog (S. cerevisiae)	0.57518057	0
Pigment Progenitor	ENSDARG00000011076	zgc:91968	zgc:91968	0.57047996	0
Pigment Progenitor	ENSDARG00000040039	pttg1ipb	pituitary tumor-transforming 1 interacting protein b	0.56952809	0
Pigment Progenitor	ENSDARG00000042428	gstt1a	glutathione S-transferase theta 1a	0.56941345	0
Pigment Progenitor	ENSDARG00000094695	si:dkey-204f11.64	si:dkey-204f11.64	0.56760252	0
Pigment Progenitor	ENSDARG00000091298	pmela	premelanosome protein a	0.56718631	0
Pigment Progenitor	ENSDARG00000102051	mtbl	metallothionein-B-like	0.56615582	0
Pigment Progenitor	ENSDARG00000033539	paics	phosphoribosylaminoimidazole carboxylase, phosphoribosylaminoimidazole succinoca	0.56163276	0
Proliferating Progenitor	ENSDARG00000103754	aspm	abnormal spindle microtubule assembly	0.7841195	0
Proliferating Progenitor	ENSDARG00000086112	si:ch211-266i6.3	si:ch211-266i6.3	0.77947464	0
Proliferating Progenitor	ENSDARG00000015460	racgap1	Rac GTPase activating protein 1	0.77764404	0
Proliferating Progenitor	ENSDARG00000058471	plk1	polo-like kinase 1 (Drosophila)	0.76921726	0
Proliferating Progenitor	ENSDARG00000070656	si:ch211-69g19.2	si:ch211-69g19.2	0.76582775	0
Proliferating Progenitor	ENSDARG00000045167	dlgap5	discs, large (Drosophila) homolog-associated protein 5	0.76340738	0
Proliferating Progenitor	ENSDARG00000007221	pbk	PDZ binding kinase	0.76025861	0
Proliferating Progenitor	ENSDARG00000070109	ncapg	non-SMC condensin I complex, subunit G	0.76006347	0
Proliferating Progenitor	ENSDARG00000078654	tpx2	TPX2, microtubule-associated, homolog (Xenopus laevis)	0.75833202	0
Proliferating Progenitor	ENSDARG00000002403	nusap1	nucleolar and spindle associated protein 1	0.75826654	0
Proliferating Progenitor	ENSDARG00000043137	cdca8	cell division cycle associated 8	0.75488189	0
Proliferating Progenitor	ENSDARG00000087554	cdk1	cyclin-dependent kinase 1	0.75272842	0
Proliferating Progenitor	ENSDARG00000071410	cks2	CDC28 protein kinase regulatory subunit 2	0.75175022	0
Proliferating Progenitor	ENSDARG00000093622	spc24	SPC24, NDC80 kinetochore complex component, homolog (S. cerevisiae)	0.74722227	0
Proliferating Progenitor	ENSDARG00000004713	mad2l1	MAD2 mitotic arrest deficient-like 1 (yeast)	0.74494934	0
Proliferating Progenitor	ENSDARG00000055133	cenpf	centromere protein F	0.74367397	0
Proliferating Progenitor	ENSDARG00000024488	top2a	topoisomerase (DNA) II alpha	0.74365926	0
Proliferating Progenitor	ENSDARG00000078433	spc25	SPC25, NDC80 kinetochore complex component, homolog (S. cerevisiae)	0.74112762	0
Proliferating Progenitor	ENSDARG00000074379	knstrn	kinetochore-localized astrin/SPAG5 binding protein	0.73739834	0
Proliferating Progenitor	ENSDARG00000001558	kifc1	kinesin family member C1	0.73730285	0
Proliferating Progenitor	ENSDARG00000091150	mki67	marker of proliferation Ki-67	0.73441966	0
Proliferating Progenitor	ENSDARG00000038066	kpna2	karyopherin alpha 2 (RAG cohort 1, importin alpha 1)	0.73326466	0
Proliferating Progenitor	ENSDARG00000011094	ccna2	cyclin A2	0.73294073	0
Proliferating Progenitor	ENSDARG00000077822	si:dkey-6i22.5	si:dkey-6i22.5	0.7313248	0
Proliferating Progenitor	ENSDARG00000017744	smc2	structural maintenance of chromosomes 2	0.73033759	0
Proliferating Progenitor	ENSDARG00000099194	CABZ01058261.1	NA	0.72895837	0
Proliferating Progenitor	ENSDARG00000075421	pttg1	pituitary tumor-transforming 1	0.72444132	0
Proliferating Progenitor	ENSDARG00000037640	aurkb	aurora kinase B	0.7244289	0
Proliferating Progenitor	ENSDARG00000005058	ncapd2	non-SMC condensin I complex, subunit D2	0.71937818	0
Proliferating Progenitor	ENSDARG00000055753	suv39h1b	suppressor of variegation 3-9 homolog 1b	0.71732733	0

Table 2.2: (continued) **Genes enriched in specific cell types from post-embryonic NC derivatives.**

Cell Type	Ensembl ID	Gene symbol	Gene full name	specificity	q-value
Satellite Glia	ENSDARG00000052997	sema4e	semaphorin 4e	0.93352533	0
Satellite Glia	ENSDARG00000018459	msrb2	methionine sulfoxide reductase B2	0.92860838	0
Satellite Glia	ENSDARG00000010770	sox19a	SRY (sex determining region Y)-box 19a	0.90396465	0
Satellite Glia	ENSDARG00000089892	cd44b	CD44 molecule (Indian blood group) b	0.89848475	0
Satellite Glia	ENSDARG00000051730	slc7a10b	solute carrier family 7 (neutral amino acid transporter light chain, asc system), membe	0.88187886	0
Satellite Glia	ENSDARG00000059053	slc13a4	solute carrier family 13 (sodium/sulfate symporter), member 4	0.87897503	0
Satellite Glia	ENSDARG00000102858	sc:d189	sc:d189	0.87727036	0
Satellite Glia	ENSDARG00000088247	si:ch1073-303k11.2	si:ch1073-303k11.2	0.87279725	0
Satellite Glia	ENSDARG00000053262	atp1b4	ATPase, Na+/K+ transporting, beta 4 polypeptide	0.86782884	0
Satellite Glia	ENSDARG00000087981	slc6a11b	solute carrier family 6 (neurotransmitter transporter), member 11b	0.86725009	0
Satellite Glia	ENSDARG00000043322	gsx2	GS homeobox 2	0.86304184	0
Satellite Glia	ENSDARG00000103316	si:ch211-212k18.5	si:ch211-212k18.5	0.85407111	0
Satellite Glia	ENSDARG00000079191	zgc:172122	zgc:172122	0.8421098	0
Satellite Glia	ENSDARG00000053569	sox3	SRY (sex determining region Y)-box 3	0.83088162	0
Satellite Glia	ENSDARG00000018534	slc6a9	solute carrier family 6 (neurotransmitter transporter, glycine), member 9	0.82889962	0
Satellite Glia	ENSDARG00000102453	slc1a2b	solute carrier family 1 (glial high affinity glutamate transporter), member 2b	0.82752843	0
Satellite Glia	ENSDARG00000078411	hspb15	heat shock protein, alpha-crystallin-related, b15	0.82256777	0
Satellite Glia	ENSDARG00000035694	stm	starmaker	0.82160663	0
Satellite Glia	ENSDARG00000056732	her4.1	hairy-related 4, tandem duplicate 1	0.82128924	0
Satellite Glia	ENSDARG00000104949	slc27a1b	solute carrier family 27 (fatty acid transporter), member 1b	0.82117913	0
Satellite Glia	ENSDARG00000010710	msi1	musashi RNA-binding protein 1	0.81637636	0
Satellite Glia	ENSDARG00000045926	crabp1a	cellular retinoic acid binding protein 1a	0.80880521	0
Satellite Glia	ENSDARG00000060397	hhip	hedgehog interacting protein	0.80444041	0
Satellite Glia	ENSDARG00000035904	crabp1b	cellular retinoic acid binding protein 1b	0.80187732	0
Satellite Glia	ENSDARG00000056729	her4.2	hairy-related 4, tandem duplicate 2	0.79868044	0
Satellite Glia	ENSDARG00000071497	zic3	zic family member 3 heterotaxy 1 (odd-paired homolog, Drosophila)	0.79370611	0
Satellite Glia	ENSDARG00000018423	sulf2a	sulfatase 2a	0.78045386	0
Satellite Glia	ENSDARG00000004782	fgfr3	fibroblast growth factor receptor 3	0.77663405	0
Satellite Glia	ENSDARG00000094426	her4.2	hairy-related 4, tandem duplicate 2	0.7751191	0
Satellite Glia	ENSDARG00000015554	zic2a	zic family member 2 (odd-paired homolog, Drosophila), a	0.77378612	0
Schwann Cell	ENSDARG00000058064	cx31.7	connexin 31.7	0.64584726	0
Schwann Cell	ENSDARG00000025670	fstl3	follistatin-like 3 (secreted glycoprotein)	0.62605784	0
Schwann Cell	ENSDARG00000018787	efna1b	ephrin-A1b	0.6136353	0
Schwann Cell	ENSDARG00000019986	grhprb	glyoxylate reductase/hydroxypyruvate reductase b	0.61159659	0
Schwann Cell	ENSDARG00000087403	si:ch211-214p13.3	si:ch211-214p13.3	0.61006878	0
Schwann Cell	ENSDARG00000030753	prrg4	proline rich Gla (G-carboxyglutamic acid) 4 (transmembrane)	0.60945568	0
Schwann Cell	ENSDARG00000099960	elovl1a	ELOVL fatty acid elongase 1a	0.60652588	0
Schwann Cell	ENSDARG00000035553	cx27.5	connexin 27.5	0.60575438	0
Schwann Cell	ENSDARG00000006427	fabp2	fatty acid binding protein 2, intestinal	0.60487737	0
Schwann Cell	ENSDARG00000068912	zgc:153012	zgc:153012	0.60108925	0
Schwann Cell	ENSDARG00000089477	si:ch211-132g1.3	si:ch211-132g1.3	0.59877635	0
Schwann Cell	ENSDARG00000061579	myo1cb	myosin Ic, paralog b	0.59837334	0
Schwann Cell	ENSDARG00000042357	cldnk	claudin k	0.59777419	0
Schwann Cell	ENSDARG00000039626	nrgna	neurogranin (protein kinase C substrate, RC3) a	0.59682734	0
Schwann Cell	ENSDARG00000042826	egr2b	early growth response 2b	0.59622466	0
Schwann Cell	ENSDARG00000011602	si:dkeyp-117h8.2	si:dkeyp-117h8.2	0.59533736	0
Schwann Cell	ENSDARG00000077257	timd4	T-cell immunoglobulin and mucin domain containing 4	0.59317159	0
Schwann Cell	ENSDARG00000021433	asmtl	acetylserotonin O-methyltransferase-like	0.59263708	0
Schwann Cell	ENSDARG00000002391	tlcd1	TLC domain containing 1	0.59221728	0
Schwann Cell	ENSDARG00000079497	tcima	NA	0.58691009	0
Schwann Cell	ENSDARG00000071460	si:ch211-234p6.5	si:ch211-234p6.5	0.58467647	0
Schwann Cell	ENSDARG00000109276	CABZ01068367.1	NA	0.58374962	0
Schwann Cell	ENSDARG00000028027	trim63a	tripartite motif containing 63a	0.58301944	0
Schwann Cell	ENSDARG00000089418	si:dkey-164f24.2	si:dkey-164f24.2	0.5817082	0
Schwann Cell	ENSDARG00000061576	gldn	gliomedin	0.57786226	0
Schwann Cell	ENSDARG00000030265	scdb	stearoyl-CoA desaturase b	0.57605611	0
Schwann Cell	ENSDARG00000089828	si:rp71-19m20.1	si:rp71-19m20.1	0.5749729	0
Schwann Cell	ENSDARG00000043446	efhd1	EF-hand domain family, member D1	0.57283902	0
Schwann Cell	ENSDARG00000102995	rbm24a	RNA binding motif protein 24a	0.57120129	0
Schwann Cell	ENSDARG00000089838	si:dkey-262k9.4	si:dkey-262k9.4	0.57070181	0
Schwann Cell Precursor	ENSDARG00000021607	negr1	neuronal growth regulator 1	0.6469044	0
Schwann Cell Precursor	ENSDARG00000010878	cdkn1ca	cyclin-dependent kinase inhibitor 1Ca	0.61570424	0
Schwann Cell Precursor	ENSDARG00000000588	grasp	GRP1 (general receptor for phosphoinositides 1)-associated scaffold protein	0.61260682	0
Schwann Cell Precursor	ENSDARG00000061576	gldn	gliomedin	0.59733524	0
Schwann Cell Precursor	ENSDARG00000035553	cx27.5	connexin 27.5	0.59653106	0
Schwann Cell Precursor	ENSDARG00000044569	cldn19	claudin 19	0.59189615	0
Schwann Cell Precursor	ENSDARG00000009823	pou3f1	POU class 3 homeobox 1	0.58547345	0
Schwann Cell Precursor	ENSDARG00000071460	si:ch211-234p6.5	si:ch211-234p6.5	0.5854214	0
Schwann Cell Precursor	ENSDARG00000042826	egr2b	early growth response 2b	0.58401716	0
Schwann Cell Precursor	ENSDARG00000055043	depdc7a	NA	0.58114581	0

Table 2.2: (continued) **Genes enriched in specific cell types from post-embryonic NC derivatives.**

Cell Type	Ensembl ID	Gene symbol	Gene full name	specificity	q-value
Schwann Cell Precursor	ENSDARG00000089838	si:dkey-262k9.4	si:dkey-262k9.4	0.58106186	0
Schwann Cell Precursor	ENSDARG00000078898	pcdh7a	protocadherin 7a	0.57992739	0
Schwann Cell Precursor	ENSDARG00000021433	asmtl	acetylserotonin O-methyltransferase-like	0.57910051	0
Schwann Cell Precursor	ENSDARG00000102995	rbm24a	RNA binding motif protein 24a	0.57622931	0
Schwann Cell Precursor	ENSDARG00000010018	qki2	QKI, KH domain containing, RNA binding 2	0.57312543	0
Schwann Cell Precursor	ENSDARG00000061579	myo1cb	myosin Ic, paralog b	0.56881738	0
Schwann Cell Precursor	ENSDARG00000099960	elovl1a	ELOVL fatty acid elongase 1a	0.56762093	0
Schwann Cell Precursor	ENSDARG00000042357	cldnk	claudin k	0.56703008	0
Schwann Cell Precursor	ENSDARG00000037997	tubb5	tubulin, beta 5	0.56504991	0
Schwann Cell Precursor	ENSDARG00000089828	si:rp71-19m20.1	si:rp71-19m20.1	0.56346315	0
Schwann Cell Precursor	ENSDARG00000044532	nr4a2b	nuclear receptor subfamily 4, group A, member 2b	0.56213736	0
Schwann Cell Precursor	ENSDARG00000038941	ppp1r1c	protein phosphatase 1, regulatory (inhibitor) subunit 1C	0.5614549	0
Schwann Cell Precursor	ENSDARG00000006427	fabp2	fatty acid binding protein 2, intestinal	0.55554862	0
Schwann Cell Precursor	ENSDARG00000087403	si:ch211-214p13.3	si:ch211-214p13.3	0.55456243	0
Schwann Cell Precursor	ENSDARG00000038068	ddx5	DEAD (Asp-Glu-Ala-Asp) box helicase 5	0.55421675	0
Schwann Cell Precursor	ENSDARG00000062711	gal3st1a	galactose-3-O-sulfotransferase 1a	0.55393777	0
Schwann Cell Precursor	ENSDARG00000036036	mdka	midkine a	0.55361112	0
Schwann Cell Precursor	ENSDARG00000079497	tcima	NA	0.55305613	0
Schwann Cell Precursor	ENSDARG00000076532	si:ch211-222l21.1	si:ch211-222l21.1	0.55094541	0
Schwann Cell Precursor	ENSDARG00000009640	psmb1	proteasome subunit beta 1	0.55011024	0
Unknown	ENSDARG00000035309	entpd3	ectonucleoside triphosphate diphosphohydrolase 3	0.62803362	0
Unknown	ENSDARG00000103277	cyp24a1	cytochrome P450, family 24, subfamily A, polypeptide 1	0.61057788	0
Unknown	ENSDARG00000089187	wfdc2	WAP four-disulfide core domain 2	0.59109067	0
Unknown	ENSDARG00000017624	krt4	keratin 4	0.58758662	0
Unknown	ENSDARG00000034470	aldoab	aldolase a, fructose-bisphosphate, b	0.58231558	0
Unknown	ENSDARG00000102956	mmp17b	matrix metallopeptidase 17b	0.58107517	0
Unknown	ENSDARG00000037517	slc35c2	solute carrier family 35 (GDP-fucose transporter), member C2	0.58087857	0
Unknown	ENSDARG00000034588	scn4ab	sodium channel, voltage-gated, type IV, alpha, b	0.57365889	0
Unknown	ENSDARG00000074869	si:ch1073-291c23.2	si:ch1073-291c23.2	0.57325826	0
Unknown	ENSDARG00000043806	postna	periostin, osteoblast specific factor a	0.57181428	0
Unknown	ENSDARG00000045066	entpd1	ectonucleoside triphosphate diphosphohydrolase 1	0.56851963	0
Unknown	ENSDARG00000074908	col6a1	collagen, type VI, alpha 1	0.5683325	0
Unknown	ENSDARG00000060222	scn1ba	sodium channel, voltage-gated, type I, beta a	0.56792212	0
Unknown	ENSDARG00000099144	igfbp3	insulin-like growth factor binding protein 3	0.5678859	0
Unknown	ENSDARG00000037960	lrrc17	leucine rich repeat containing 17	0.56462113	0
Unknown	ENSDARG00000022650	cyp2ad3	cytochrome P450, family 2, subfamily AD, polypeptide 3	0.56185923	0
Unknown	ENSDARG00000042953	cyp2n13	cytochrome P450, family 2, subfamily N, polypeptide 13	0.56095875	0
Unknown	ENSDARG00000078659	tmem176	transmembrane protein 176	0.55960479	0
Unknown	ENSDARG00000093549	selenop	NA	0.55818115	0
Unknown	ENSDARG00000035810	rgcc	regulator of cell cycle	0.55816848	0
Unknown	ENSDARG00000040503	sb:cb81	sb:cb81	0.55763695	0
Unknown	ENSDARG00000042978	cyp2p6	cytochrome P450, family 2, subfamily P, polypeptide 6	0.55704826	0
Unknown	ENSDARG00000021172	cyp2ad2	cytochrome P450, family 2, subfamily AD, polypeptide 2	0.55574818	0
Unknown	ENSDARG00000105223	pmp22a	peripheral myelin protein 22a	0.55155986	0
Unknown	ENSDARG00000026726	anxa1a	annexin A1a	0.55118617	0
Xanthophore	ENSDARG00000045601	cax1	cation/H+ exchanger protein 1	0.87830336	0
Xanthophore	ENSDARG00000076844	plin6	NA	0.87098594	0
Xanthophore	ENSDARG00000075191	oacyl	O-acyltransferase like	0.86307796	0
Xanthophore	ENSDARG00000025912	bscl2l	Bernardinelli-Seip congenital lipodystrophy 2, like	0.84722551	0
Xanthophore	ENSDARG00000071475	aox5	aldehyde oxidase 5	0.84619617	0
Xanthophore	ENSDARG00000069630	tat	tyrosine aminotransferase	0.81589839	0
Xanthophore	ENSDARG00000044684	rbp4l	retinol binding protein 4, like	0.81201115	0
Xanthophore	ENSDARG00000063288	slc2a11b	solute carrier family 2 (facilitated glucose transporter), member 11b	0.78306751	0
Xanthophore	ENSDARG00000114760	asip2b	NA	0.76429191	0
Xanthophore	ENSDARG00000103789	tmem130	transmembrane protein 130	0.76339458	0
Xanthophore	ENSDARG00000056028	slc22a7a	solute carrier family 22 (organic anion transporter), member 7a	0.74820994	0
Xanthophore	ENSDARG00000029894	slc2a15a	solute carrier family 2 (facilitated glucose transporter), member 15a	0.72815499	0
Xanthophore	ENSDARG00000100719	uraha	NA	0.72696685	0
Xanthophore	ENSDARG00000070818	pax7b	paired box 7b	0.72581566	0
Xanthophore	ENSDARG00000104256	bco1	beta-carotene oxygenase 1	0.72522349	0
Xanthophore	ENSDARG00000101557	scarb1	scavenger receptor class B, member 1	0.71616171	0
Xanthophore	ENSDARG00000088116	gstm.3	glutathione S-transferase mu tandem duplicate 3	0.71567888	0
Xanthophore	ENSDARG00000068876	zgc:153031	zgc:153031	0.70696638	0
Xanthophore	ENSDARG00000020328	plekha6	pleckstrin homology domain containing, family A member 6	0.70152274	0
Xanthophore	ENSDARG00000093957	si:dkey-251i10.2	si:dkey-251i10.2	0.69321935	0
Xanthophore	ENSDARG00000041715	bco2b	beta-carotene oxygenase 2b	0.67707495	0
Xanthophore	ENSDARG00000070453	gch1	GTP cyclohydrolase 1	0.67072658	0
Xanthophore	ENSDARG00000100446	si:ch211-286o17.1	si:ch211-286o17.1	0.66751572	0
Xanthophore	ENSDARG00000035018	thy1	Thy-1 cell surface antigen	0.66550227	0
Xanthophore	ENSDARG00000025595	agmo	alkylglycerol monooxygenase	0.65910338	0

Cell Type	Ensembl ID	Gene symbol	Gene full name	specificity	q-value
Xanthophore	ENSDARG00000032746	tnfsf10l3	tumor necrosis factor (ligand) superfamily, member 10 like 3	0.65695578	0
Xanthophore	ENSDARG00000042214	tmem243a	transmembrane protein 243, mitochondrial a	0.64411225	0
Xanthophore	ENSDARG00000015765	iah1	isoamyl acetate-hydrolyzing esterase 1 homolog (S. cerevisiae)	0.64283371	0
Xanthophore	ENSDARG00000114516	CABZ01021592.1	NA	0.64155916	0
Xanthophore	ENSDARG00000029905	phyhd1	phytanoyl-CoA dioxygenase domain containing 1	0.63740227	0

Table 2.2: (continued) **Genes enriched in specific cell types from post-embryonic NC derivatives.**

Signature score	Ensembl ID	Gene symbol
melanin	ENSDARG00000020143	pah
melanin	ENSDARG00000029204	tyrp1a
melanin	ENSDARG00000061303	oca2
melanin	ENSDARG00000056151	tyrp1b
melanin	ENSDARG00000006008	dct
melanin	ENSDARG00000034572	gpr143
melanin	ENSDARG00000099101	gch2
melanin	ENSDARG00000039077	tyr
melanin	ENSDARG00000024771	slc24a5
melanin	ENSDARG00000002593	slc45a2
melanin	ENSDARG00000091298	pmela
AP1 TF complex	ENSDARG00000104773	junbb
AP1 TF complex	ENSDARG00000038141	atf4b
AP1 TF complex	ENSDARG00000111939	atf4a
AP1 TF complex	ENSDARG00000044301	atf1
AP1 TF complex	ENSDARG00000055481	atf7b
AP1 TF complex	ENSDARG00000067850	jund
AP1 TF complex	ENSDARG00000074378	junba
AP1 TF complex	ENSDARG00000043531	jun
AP1 TF complex	ENSDARG00000012656	atf6
AP1 TF complex	ENSDARG00000007823	atf3
AP1 TF complex	ENSDARG00000031683	fosab
AP1 TF complex	ENSDARG00000040623	fosl2
AP1 TF complex	ENSDARG00000015355	fosl1a
AP1 TF complex	ENSDARG00000055751	fosb
AP1 TF complex	ENSDARG00000077785	atf5b
cell cycle	ENSDARG00000101637	ccnd1
cell cycle	ENSDARG00000035810	rgcc
cell cycle	ENSDARG00000037158	rcc1
cell cycle	ENSDARG00000028335	hmga1a
cell cycle	ENSDARG00000011510	rcc2
cell cycle	ENSDARG00000054155	pcna
cell cycle	ENSDARG00000101578	e2f4
UPR	ENSDARG00000063563	creb3l2
UPR	ENSDARG00000035622	xbp1
UPR	ENSDARG00000054746	uggt1
UPR	ENSDARG00000037647	rnf175
UPR	ENSDARG00000017740	sec63
UPR	ENSDARG00000012656	atf6
UPR	ENSDARG00000020926	creb3l3l
UPR	ENSDARG00000017842	syvn1
UPR	ENSDARG00000099439	serp1
UPR	ENSDARG00000028448	edem2
UPR	ENSDARG00000039008	zgc:85858

Table 2.3: **Signature score genes.**

UPR	ENSDARG00000060282	rnf121
UPR	ENSDARG00000008542	yod1
UPR	ENSDARG00000057577	mbtps2
UPR	ENSDARG00000020218	amfra
purine	ENSDARG00000029524	impdh1b
purine	ENSDARG00000017049	adsl
purine	ENSDARG00000011683	prtfdc1
purine	ENSDARG00000101089	gart
purine	ENSDARG00000016706	atic
purine	ENSDARG00000003750	pfas
purine	ENSDARG00000033539	paics
purine	ENSDARG00000004517	ppat
purine	ENSDARG00000008884	hprt1
purine	ENSDARG00000079848	gmps
purine	ENSDARG00000057575	pnp4a
purine	ENSDARG00000014866	hprt1l
NC migration	ENSDARG00000035598	coro1ca
NC migration	ENSDARG00000077467	sox10
NC migration	ENSDARG00000020847	atp6v0a1a
NC migration	ENSDARG00000054578	arl6ip1
NC migration	ENSDARG00000059680	fscn1a
NC migration	ENSDARG00000052150	pbx4
NC migration	ENSDARG00000078416	zeb2b
NC migration	ENSDARG00000057633	cxcr4a
NC migration	ENSDARG00000077004	aldh1l1
NC migration	ENSDARG00000021032	foxd3
NC migration	ENSDARG00000011163	sema3fa
NC migration	ENSDARG00000075211	chd7
NC migration	ENSDARG00000010192	pax3a
NC migration	ENSDARG00000060148	sh3pxd2aa
NC migration	ENSDARG00000031894	lef1
NC migration	ENSDARG00000038446	nrp2b
NC migration	ENSDARG00000011188	acvr2aa
NC migration	ENSDARG00000034293	hif1ab
NC migration	ENSDARG00000032617	fgfrl1a
NC migration	ENSDARG00000078106	ocrl
NC migration	ENSDARG00000021895	disc1
NC migration	ENSDARG00000103959	pak1
NC migration	ENSDARG00000062824	alx1
NC migration	ENSDARG00000011510	rcc2
NC migration	ENSDARG00000076317	plod3
NC migration	ENSDARG00000105206	hmgcrb
NC migration	ENSDARG00000102153	nrp1a
NC migration	ENSDARG00000100252	capzb
NC migration	ENSDARG00000100944	glrx2

Table 2.3: (continued) **Signature score genes.**

Description	Sequence	Notes
thrab_gRNA	AAGCTACCGGATATCACTAC	forward
thraa_gRNA	GTGTGCGGAGACAAGGCCAC	
thrb_gRNA	GTTTGTGGAGACAAAGCAAC	
tyr_gRNA_1	GGGCCGCAGTATCCTCACTC	
scarb1_gRNA-1	ggGATCTCTCCTACACCATG	gRNAs combined and induce a ~100bp indel
scarb1_gRNA-2	gGGCCCATGGTGATCCAGAG	
thrab_seq-F	TGAAAACCTTGGAGCAGCTC	for sanger sequencing
thrab_seq-R	CGGCCCCTTACTTTGATTGT	
thrab_geno-F	AGCTATCTGGAGAAGGATGAGC	126bp, can resolve -13bp deletion
thrab_geno-R	gaagaccaacCTTACAGCCC	
scarb1_seq-F	TGTGCCTGAGTGCTTTAAACT	530bp, for genotyping
scarb1_seq-R	CGTGCTGCCTTTCTTTGAGT	
tyr_seq-F	TCTTCAGCTCGTCTCTCCAG	643bp, for sanger sequencing
tyr_seq-R	AGCTTCCGGATCTCATGCTC	
thraa_rt-pcr_F	CCAAGATCATTACGCCTGCC	209bp, RT-PCR
thraa_rt-pcr_R	TTTCAGCTGCTCTCGACTGA	
thrab_rt-pcr_F	TGGATTTGGAGGCCTTCAGT	222bp, RT-PCR
thrab_rt-pcr_R	GTTTGACAGCCATCTCTCCG	
thrb_rt-pcr_F	AACCAGTGCCAAGAATGTCG	248bp, RT-PCR
thrb_rt-pcr_R	TGTTTCCAGTGGTTGCCTTG	
actb1_rt-pcr_F	ACTGGGATGACATGGAGAAGAT	155bp, RT-PCR
actb1_rt-pcr_R	GTGTTGAAGGTCTCGAACATGA	

Table 2.4: **sgRNA and Oligonucleotide sequences.**

Chapter 3: CLOSING REMARKS AND FUTURE DIRECTIONS

In this dissertation, I detail my efforts to resolve the heterogeneous cell types that give rise to a complex, highly organized pattern during zebrafish stripe formation. I also resolve specific mechanisms underlying distinct responses to a global signal in two related pigment cell classes, black melanophores and yellow xanthophores. In this final chapter, I reflect on the importance of experimental design and computational proficiency as single cell genomic technologies become increasingly accessible to developmental biologists. I also explore future avenues of research towards a comprehensive understanding of TH-dependent mechanisms of specification, differentiation and morphogenesis during the generation of adult form.

3.1 COMPUTATIONAL SKILLS FOR DEVELOPMENTAL BIOLOGISTS

As a co-advised graduate student, I experienced the duality of being the token developmental biologist in a computational single-cell genomics lab and the token computational biologist in a developmental genetics lab. Through this unique vantage point, I was immersed in both the development and implementation of new technologies for unraveling the complexities of developmental systems. As a computational novice with a background in experimental developmental biology, learning to code in an environment of expert computational biologists was at first overwhelming and frustrating, but ultimately enlightening and rewarding. This experience has allowed me to reflect on the relationship between technology and software development for biologists and the usage of those technologies by biologists. Technology development in single cell genomics is moving at an extremely rapid pace, and studying organismal development inherently takes a long time. Thus, there is a persistent lag in the adoption of these technologies by researchers whose questions would most benefit from using them.

While single cell genomic data sets certainly speed up the dissection of complex biological systems, there is a bottleneck at the level of designing functional follow-up experiments (a topic

that I will discuss in a later section). An additional bottleneck lies in the analysis of these ever-larger datasets by researchers without prior computational training. While it is important for tool developers to consider usability of tools by offering vignettes, detailed documentation, timely issue responses and in some cases, easy-to-use graphical user interfaces, it is also in the best interest of biologists using these tools to develop a core set of computational skills. One main reason for this is to avoid full reliance on specific decisions made by those writing the software, such that the analysis process becomes more transparent to the user. The default options are often "best guesses" by those writing the software, and without the ability to interrogate and manipulate components of the software, options that are best for a data set of interest may be essentially hidden to the nascent user. I am often asked how best to acquire the skills necessary for analyzing single-cell data sets. The conclusion I've come to is that developing a strong basis in R (or alternative programming languages, but most of the tools are R based) plus self-training in specific applications for sc-genomics is a good strategy, because specialized courses for single cell analysis are scarce and computational tools are constantly changing. For those who are early on in their graduate or undergraduate careers, it is critical to take advantage of the university courses and other resources available for learning computational biology. Additionally, one of the best, most motivating ways to learn is to have your own data set that you want to interrogate. Regardless of career stage and background, it is hard to deny the benefits of being able to both execute and analyze large-scale scRNA-seq data sets and the field of developmental biology will benefit from more researchers with this interdisciplinary training.

3.2 Designing follow-up experiments from ever-larger genomic datasets

As single cell RNA-sequencing continues to become cheaper and more accessible to researchers, high quality data sets from many systems are becoming publicly available. For many of these data sets, groups have only just scratched the surface of extracting biologically meaningful information. Additionally, researchers developing technologies will perform proof-of-principal experiments in systems with a wide interest base, essentially offering all the data for free to whoever wants to

dig in (Cao et al., 2017, 2019; Packer et al., 2019). This is also true in my case: despite capturing a wide array of post-embryonic neural crest derived lineages, I focused primarily on the pigment lineages even though they constitute only a quarter of my data set. While these data will certainly provide experimental and grant-writing fodder within my thesis labs, other researchers studying these cell types could use these data to identify new markers and test various hypotheses in silico. Because analysis of scRNA-seq data sets is time consuming and somewhat challenging, maximum utility of data for other researchers requires an emphasis on transparency of experimental design, quality control metrics, and clear metadata annotations. Additionally, more and more sc-genomic data sets are becoming available for the same tissue types across species and disease states such that researchers with their own data sets may want to compare with publicly available ones. Feasibility of these analyses is improving with increasingly available computational tools for removing batch effects from technical variation across labs, researchers, scRNA-seq platforms, and organisms (Haghverdi et al., 2018; Butler et al., 2018). Thus, the accessibility of high quality scRNA-seq data is no longer the bottleneck for answering biological questions in complex systems. Rather, the challenge is in designing informative follow-up experiments despite seemingly endless possibilities born from analyzing one (or more) of these data sets. For example, pseudotemporal analysis of differentiation in a particular lineage will often provide hundreds of novel factors with interesting dynamics. However, the relative importance of any of these genes for the process is unknown. One way to improve an estimate of causality for a given gene from the scRNA-seq data alone is to add perturbations to the system being measured. Increased assay sensitivity and lowered costs that facilitate larger data sets (and thus more power) will also improve inference. An underappreciated aspect of analyzing scRNA-seq data sets is that the outcomes of cell-type clustering and trajectory analysis are not deterministic, and it can be challenging to evaluate the variety of outcomes. Perhaps initially counterintuitive, more prior knowledge of the system enables more thorough validation of the various outcomes and facilitates generation of more grounded hypotheses for experimental follow-up.

Looking ahead, integration of multi-omic data sets – such as single cell chromatin accessibility (ATAC-seq), histone and TF occupancy (Cut&Tag), spatial orientation, and lineage tracing

(Gestalt, Memoir, others) – will allow for further distillation of candidates for follow-up experimentation. In addition to advances in single cell genomics, improvements in genome editing for forward genetic screens, multi-plexed expression labeling in intact tissues, and high resolution imaging techniques are facilitating experimental progress for unearthing mechanistic insight more efficiently. While we still have a lot of ground to cover, I feel very lucky to be a young scientist at this particular point in time and am excited to see what the future holds.

3.3 FUTURE DIRECTIONS

3.3.1 Towards a comprehensive understanding of TH-dependent pattern formation

In this dissertation, I present a few ways in which we have made progress towards understanding how a global signal, TH, elicits cell-type specific responses in a model of complex pattern formation. Still, there are many unanswered questions, and a major direction of future work in this area will be to dissect the directness of these TH-dependent changes in responding cell types. New and emerging technologies in zebrafish allow for precise, lineage-specific manipulation of genes and pathways of interest. These tools will improve our ability to study the multipotent progenitor cells that give rise to adult pigment cells. They will also enable careful dissection of the role of TRs in each pigment lineage and facilitate cell-type specific forward genetic screens that bypass non-specific consequences of target manipulation.

To date, most of the work in this area focuses on the pigment lineages themselves, but these cells are stratified in a complex environment between the muscle and dermis and surrounded not only by other pigment cells, but likely dozens of other cell types (Hirata et al., 2003; Hawkes, 1974). Very little is known about the cell types present in the surrounding hypodermis and more superficial dermal and epidermal layers, let alone how they change in response to TH during the larval-to-adult transition. In frogs and mammals, TH classically regulates proliferation and homeostasis of the epidermis, and skin abnormalities are used as a diagnostic for hypothyroidism in humans (Antonini et al., 2013). During the same time that adult pigment pattern formation is unfolding in zebrafish, major changes are occurring in the skin: a dense yet transparent collagenous

matrix forms superficially to the hypodermis, bony scales begin to cover the surface of the fish, and the epidermal layers are expanded (Le Guellec et al., 2003; Aman et al., 2018). Future research will hopefully elucidate the extent to which TH plays a role in skin development and how the relationship between pigment cells and their environment shapes the final adult tissue. There are certainly remaining challenges, but new genetic, genomic and imaging technologies coupled with an ever-growing knowledge of skin and pigment biology promise an exciting future towards a comprehensive understanding this system in fish and other organisms.

BIBLIOGRAPHY

Adameyko, I., Lallemend, F., Aquino, J. B., Pereira, J. A., Topilko, P., Müller, T., Fritz, N., Beljajeva, A., Mochii, M., Liste, I., Usoskin, D., Suter, U., Birchmeier, C. and Ernfors, P. (2009). Schwann cell precursors from nerve innervation are a cellular origin of melanocytes in skin. Cell *139*, 366–379.

Aman, A. J., Fulbright, A. N. and Parichy, D. M. (2018). Wnt/β-catenin regulates an ancient signaling network during zebrafish scale development. eLife *7*.

Antonini, D., Sibilio, A., Dentice, M. and Missero, C. (2013). An Intimate Relationship between Thyroid Hormone and Skin: Regulation of Gene Expression. Frontiers in Endocrinology *4*.

Arduini, B. L., Bosse, K. M. and Henion, P. D. (2009). Genetic ablation of neural crest cell diversification. Development *136*, 1987–1994.

Astapova, I. (2016). Role of co-regulators in metabolic and transcriptional actions of thyroid hormone. Journal of Molecular Endocrinology *56*, R73–R97.

Atchley, W. R. and Hall, B. K. (1991). A model for development and evolution of complex morphological structures. Biol. Rev. Camb. Philos. Soc. *66*, 101–157.

Baggiolini, A., Varum, S., Mateos, J. M., Bettosini, D., John, N., Bonalli, M., Ziegler, U., Dimou, L., Clevers, H., Furrer, R. and Sommer, L. (2015). Premigratory and Migratory Neural Crest Cells Are Multipotent In Vivo. Cell Stem Cell *16*, 314–322.

Bagnara, J. T. and Matsumoto, J. (2006). Comparative Anatomy and Physiology of Pigment Cells in Nonmammalian Tissues. In The Pigmentary System, (Nordlund, J. J., Boissy, R. E., Hearing, V. J., King, R. A., Oetting, W. S. and Ortonne, J.-P., eds), pp. 11–59. Blackwell Publishing Ltd Oxford, UK.

Bagnara, J. T., Taylor, J. D. and Hadley, M. E. (1968). The dermal chromatophore unit. J. Cell Biol. *38*, 67–79.

Barrallo-Gimeno, A., Holzschuh, J., Driever, W. and Knapik, E. W. (2004). Neural crest survival and differentiation in zebrafish depends on mont blanc/tfap2a gene function. Development *131*, 1463–1477.

Baxter, L. L., Watkins-Chow, D. E., Pavan, W. J. and Loftus, S. K. (2018). A curated gene list for expanding the horizons of pigmentation biology. Pigment Cell Melanoma Res. .

Becht, E., McInnes, L., Healy, J., Dutertre, C.-A., Kwok, I. W. H., Ng, L. G., Ginhoux, F. and Newell, E. W. (2018). Dimensionality reduction for visualizing single-cell data using UMAP. Nat. Biotechnol. .

Beirl, A. J., Linbo, T. H., Cobb, M. J. and Cooper, C. D. (2014). oca2 Regulation of chromatophore differentiation and number is cell type specific in zebrafish. Pigment Cell Melanoma Res. *27*, 178–189.

Bendall, S. C., Davis, K. L., Amir, E.-A. D., Tadmor, M. D., Simonds, E. F., Chen, T. J., Shenfeld, D. K., Nolan, G. P. and Pe'er, D. (2014). Single-cell trajectory detection uncovers progression and regulatory coordination in human B cell development. Cell *157*, 714–725.

Blondel, V. D., Guillaume, J.-L., Lambiotte, R. and Lefebvre, E. (2008). Fast unfolding of communities in large networks. Journal of Statistical Mechanics: Theory and Experiment *2008*, P10008.

Braasch, I., Brunet, F., Volff, J.-N. and Schartl, M. (2009). Pigmentation pathway evolution after whole-genome duplication in fish. Genome Biol. Evol. *1*, 479–493.

Braasch, I., Peterson, S. M., Desvignes, T., McCluskey, B. M., Batzel, P. and Postlethwait, J. H. (2015). A new model army: Emerging fish models to study the genomics of vertebrate Evo-Devo. J. Exp. Zool. B Mol. Dev. Evol. *324*, 316–341.

Brent, G. A. (2012). Mechanisms of thyroid hormone action. J. Clin. Invest. *122*, 3035–3043.

Briggs, J. A., Weinreb, C., Wagner, D. E., Megason, S., Peshkin, L., Kirschner, M. W. and Klein, A. M. (2018). The dynamics of gene expression in vertebrate embryogenesis at single-cell resolution. Science *360*, eaar5780.

Bronner, M. E. and Simões-Costa, M. (2016). The Neural Crest Migrating into the Twenty-First Century. In Current Topics in Developmental Biology pp. 115–134. Elsevier.

Brown, D. D. and Cai, L. (2007). Amphibian metamorphosis. Dev. Biol. *306*, 20–33.

Buchholz, D. R., Hsia, S.-C. V., Fu, L. and Shi, Y.-B. (2003). A dominant-negative thyroid hormone receptor blocks amphibian metamorphosis by retaining corepressors at target genes. Mol. Cell. Biol. *23*, 6750–6758.

Budi, E. H., Patterson, L. B. and Parichy, D. M. (2008). Embryonic requirements for ErbB signaling in neural crest development and adult pigment pattern formation. Development *135*, 2603–2614.

Budi, E. H., Patterson, L. B. and Parichy, D. M. (2011). Post-embryonic nerve-associated precursors to adult pigment cells: genetic requirements and dynamics of morphogenesis and differentiation. PLoS Genet. *7*, e1002044.

Butler, A., Hoffman, P., Smibert, P., Papalexi, E. and Satija, R. (2018). Integrating single-cell transcriptomic data across different conditions, technologies, and species. Nature Biotechnology *36*, 411–420.

Camargo-Sosa, K., Colanesi, S., Müller, J., Schulte-Merker, S., Stemple, D., Patton, E. E. and Kelsh, R. N. (2019). Endothelin receptor Aa regulates proliferation and differentiation of Erb-dependent pigment progenitors in zebrafish. PLOS Genetics *15*, e1007941.

Campinho, M. A., Saraiva, J., Florindo, C. and Power, D. M. (2014). Maternal Thyroid Hormones Are Essential for Neural Development in Zebrafish. Molecular Endocrinology *28*, 1136–1149.

Cao, J., Packer, J. S., Ramani, V., Cusanovich, D. A., Huynh, C., Daza, R., Qiu, X., Lee, C., Furlan, S. N., Steemers, F. J., Adey, A., Waterston, R. H., Trapnell, C. and Shendure, J. (2017). Comprehensive single-cell transcriptional profiling of a multicellular organism. Science *357*, 661–667.

Cao, J., Spielmann, M., Qiu, X., Huang, X., Ibrahim, D. M., Hill, A. J., Zhang, F., Mundlos, S., Christiansen, L., Steemers, F. J., Trapnell, C. and Shendure, J. (2019). The single-cell transcriptional landscape of mammalian organogenesis. Nature *566*, 496–502.

Ceinos, R. M., Guillot, R., Kelsh, R. N., Cerdá-Reverter, J. M. and Rotllant, J. (2015). Pigment patterns in adult fish result from superimposition of two largely independent pigmentation mechanisms. Pigment cell & melanoma research *28*, 196–209.

Ceol, C. J., Houvras, Y., Jane-Valbuena, J., Bilodeau, S., Orlando, D. A., Battisti, V., Fritsch, L., Lin, W. M., Hollmann, T. J., Ferré, F., Bourque, C., Burke, C. J., Turner, L., Uong, A., Johnson, L. A., Beroukhim, R., Mermel, C. H., Loda, M., Ait-Si-Ali, S., Garraway, L. A., Young, R. A. and Zon, L. I. (2011). The histone methyltransferase SETDB1 is recurrently amplified in melanoma and accelerates its onset. Nature *471*, 513–517.

Chang, J., Wang, M., Gui, W., Zhao, Y., Yu, L. and Zhu, G. (2012). Changes in thyroid hormone levels during zebrafish development. Zoolog. Sci. *29*, 181–184.

Chatonnet, F., Guyot, R., Benoit, G. and Flamant, F. (2013). Genome-wide analysis of thyroid hormone receptors shared and specific functions in neural cells. Proceedings of the National Academy of Sciences *110*, E766–E775.

Chinenov, Y. and Kerppola, T. K. (2001). Close encounters of many kinds: Fos-Jun interactions that mediate transcription regulatory specificity. Oncogene *20*, 2438–2452.

Choi, J., Suzuki, K.-I. T., Sakuma, T., Shewade, L., Yamamoto, T. and Buchholz, D. R. (2015). Unliganded thyroid hormone receptor α regulates developmental timing via gene repression in Xenopus tropicalis. Endocrinology *156*, 735–744.

Coller, H. A., Sang, L. and Roberts, J. M. (2006). A new description of cellular quiescence. PLoS Biol. *4*, e83.

Curran, K., Lister, J. A., Kunkel, G. R., Prendergast, A., Parichy, D. M. and Raible, D. W. (2010). Interplay between Foxd3 and Mitf regulates cell fate plasticity in the zebrafish neural crest. Dev. Biol. *344*, 107–118.

D'Agati, G., Beltre, R., Sessa, A., Burger, A., Zhou, Y., Mosimann, C. and White, R. M. (2017). A defect in the mitochondrial protein Mpv17 underlies the transparent casper zebrafish. Dev. Biol. *430*, 11–17.

Darzynkiewicz, Z., Traganos, F. and Melamed, M. R. (1980). New cell cycle compartments identified by multiparameter flow cytometry. Cytometry *1*, 98–108.

Dimri, G. P., Lee, X., Basile, G., Acosta, M., Scott, G., Roskelley, C., Medrano, E. E., Linskens, M., Rubelj, I. and Pereira-Smith, O. (1995). A biomarker that identifies senescent human cells in culture and in aging skin in vivo. Proc. Natl. Acad. Sci. U. S. A. *92*, 9363–9367.

Djurdjevič, I., Kreft, M. E. and Sušnik Bajec, S. (2015). Comparison of pigment cell ultrastructure and organisation in the dermis of marble trout and brown trout, and first description of erythrophore ultrastructure in salmonids. J. Anat. *227*, 583–595.

Dooley, C. M., Mongera, A., Walderich, B. and Nüsslein-Volhard, C. (2013a). On the embryonic origin of adult melanophores: the role of ErbB and Kit signalling in establishing melanophore stem cells in zebrafish. Development *140*, 1003–1013.

Dooley, C. M., Schwarz, H., Mueller, K. P., Mongera, A., Konantz, M., Neuhauss, S. C. F., Nüsslein-Volhard, C. and Geisler, R. (2013b). Slc45a2 and V-ATPase are regulators of melanosomal pH homeostasis in zebrafish, providing a mechanism for human pigment evolution and disease. Pigment Cell Melanoma Res. *26*, 205–217.

Dutton, K. A., Pauliny, A., Lopes, S. S., Elworthy, S., Carney, T. J., Rauch, J., Geisler, R., Haffter, P. and Kelsh, R. N. (2001). Zebrafish colourless encodes sox10 and specifies non-ectomesenchymal neural crest fates. Development *128*, 4113–4125.

Ebisuya, M. and Briscoe, J. (2018). What does time mean in development? Development *145*.

Ellerhorst, J. A., Cooksley, C. D., Broemeling, L., Johnson, M. M. and Grimm, E. A. (2003). High prevalence of hypothyroidism among patients with cutaneous melanoma. Oncol. Rep. *10*, 1317–1320.

Engeszer, R. E., Wang, G., Ryan, M. J. and Parichy, D. M. (2008). Sex-specific perceptual spaces for a vertebrate basal social aggregative behavior. Proceedings of the National Academy of Sciences *105*, 929–933.

Eom, D. S., Bain, E. J., Patterson, L. B., Grout, M. E. and Parichy, D. M. (2015). Long-distance communication by specialized cellular projections during pigment pattern development and evolution. Elife *4*.

Eskova, A., Chauvigné, F., Maischein, H.-M., Ammelburg, M., Cerdà, J., Nüsslein-Volhard, C. and Irion, U. (2017). Gain-of-function mutations in Aqp3a influence zebrafish pigment pattern formation through the tissue environment. Development *144*, 2059–2069.

Evans, R. M. and Mangelsdorf, D. J. (2014). Nuclear Receptors, RXR, and the Big Bang. Cell *157*, 255–266.

Fadeev, A., Krauss, J., Frohnhöfer, H. G., Irion, U. and Nüsslein-Volhard, C. (2015). Tight Junction Protein 1a regulates pigment cell organisation during zebrafish colour patterning. Elife *4*.

Farrell, J. A., Wang, Y., Riesenfeld, S. J., Shekhar, K., Regev, A. and Schier, A. F. (2018). Single-cell reconstruction of developmental trajectories during zebrafish embryogenesis. Science *360*.

Flamant, F., Poguet, A.-L., Plateroti, M., Chassande, O., Gauthier, K., Streichenberger, N., Mansouri, A. and Samarut, J. (2002). Congenital Hypothyroid Pax8-/- Mutant Mice Can Be Rescued by Inactivating the TRα Gene. Mol. Endocrinol. *16*, 24–32.

Flamant, F. and Samarut, J. (2003). Thyroid hormone receptors: lessons from knockout and knock-in mutant mice. Trends Endocrinol. Metab. *14*, 85–90.

Frohnhöfer, H. G., Krauss, J., Maischein, H.-M. and Nüsslein-Volhard, C. (2013). Iridophores and their interactions with other chromatophores are required for stripe formation in zebrafish. Development *140*, 2997–3007.

Gans, C. and Northcutt, R. G. (1983). Neural crest and the origin of vertebrates: a new head. Science *220*, 268–273.

Granneman, J. G., Kimler, V. A., Zhang, H., Ye, X., Luo, X., Postlethwait, J. H. and Thummel, R. (2017). Lipid droplet biology and evolution illuminated by the characterization of a novel perilipin in teleost fish. Elife *6*.

Greenhill, E. R., Rocco, A., Vibert, L., Nikaido, M. and Kelsh, R. N. (2011). An Iterative Genetic and Dynamical Modelling Approach Identifies Novel Features of the Gene Regulatory Network Underlying Melanocyte Development. PLoS Genetics *7*, e1002265.

Grøntved, L., Waterfall, J. J., Kim, D. W., Baek, S., Sung, M.-H., Zhao, L., Park, J. W., Nielsen, R., Walker, R. L., Zhu, Y. J., Meltzer, P. S., Hager, G. L. and yann Cheng, S. (2015). Transcriptional activation by the thyroid hormone receptor through ligand-dependent receptor recruitment and chromatin remodelling. Nature Communications *6*.

Haffter, P., Odenthal, J., Mullins, M. C., Lin, S., Farrell, M. J., Vogelsang, E., Haas, F., Brand, M., van Eeden, F. J. M., Furutani-Seiki, M., Granato, M., Hammerschmidt, M., Heisenberg, C.-P., Jiang, Y.-J., Kane, D. A., Kelsh, R. N., Hopkins, N. and Nusslein-Volhard, C. (1996). Mutations affecting pigmentation and shape of the adult zebrafish. Development Genes and Evolution *206*, 260–276.

Haghverdi, L., Lun, A. T. L., Morgan, M. D. and Marioni, J. C. (2018). Batch effects in single-cell RNA-sequencing data are corrected by matching mutual nearest neighbors. Nature Biotechnology *36*, 421–427.

Hamada, H., Watanabe, M., Lau, H. E., Nishida, T., Hasegawa, T., Parichy, D. M. and Kondo, S. (2014). Involvement of Delta/Notch signaling in zebrafish adult pigment stripe patterning. Development *141*, 318–324.

Hawkes, J. W. (1974). The structure of fish skin. Cell and Tissue Research *149*, 147–158.

Higdon, C. W., Mitra, R. D. and Johnson, S. L. (2013). Gene expression analysis of zebrafish melanocytes, iridophores, and retinal pigmented epithelium reveals indicators of biological function and developmental origin. PLoS One *8*, e67801.

Hirata, M., Nakamura, K.-I., Kanemaru, T., Shibata, Y. and Kondo, S. (2003). Pigment cell organization in the hypodermis of zebrafish. Dev. Dyn. *227*, 497–503.

Hörlein, A. J., Näär, A. M., Heinzel, T., Torchia, J., Gloss, B., Kurokawa, R., Ryan, A., Kamei, Y., Söderström, M. and Glass, C. K. (1995). Ligand-independent repression by the thyroid hormone receptor mediated by a nuclear receptor co-repressor. Nature *377*, 397–404.

Hultman, K. A., Bahary, N., Zon, L. I. and Johnson, S. L. (2007). Gene Duplication of the zebrafish kit ligand and partitioning of melanocyte development functions to kit ligand a. PLoS Genet. *3*, e17.

Ilicic, T., Kim, J. K., Kolodziejczyk, A. A., Bagger, F. O., McCarthy, D. J., Marioni, J. C. and Teichmann, S. A. (2016). Classification of low quality cells from single-cell RNA-seq data. Genome Biol. *17*, 29.

Inoue, S., Kondo, S., Parichy, D. M. and Watanabe, M. (2014). Tetraspanin 3c requirement for pigment cell interactions and boundary formation in zebrafish adult pigment stripes. Pigment Cell Melanoma Res. *27*, 190–200.

Irion, U., Frohnhöfer, H. G., Krauss, J., Çolak Champollion, T., Maischein, H.-M., Geiger-Rudolph, S., Weiler, C. and Nüsslein-Volhard, C. (2014). Gap junctions composed of connexins 41.8 and 39.4 are essential for colour pattern formation in zebrafish. Elife *3*, e05125.

Irion, U., Singh, A. P. and Nüsslein-Volhard, C. (2016). The Developmental Genetics of Vertebrate Color Pattern Formation: Lessons from Zebrafish. Curr. Top. Dev. Biol. *117*, 141–169.

Iwashita, M., Watanabe, M., Ishii, M., Chen, T., Johnson, S. L., Kurachi, Y., Okada, N. and Kondo, S. (2006). Pigment pattern in jaguar/obelix zebrafish is caused by a Kir7.1 mutation: implications for the regulation of melanosome movement. PLoS Genet. *2*, e197.

Johnson, S. L., Africa, D., Walker, C. and Weston, J. A. (1995). Genetic control of adult pigment stripe development in zebrafish. Dev. Biol. *167*, 27–33.

Kague, E., Gallagher, M., Burke, S., Parsons, M., Franz-Odendaal, T. and Fisher, S. (2012). Skeletogenic fate of zebrafish cranial and trunk neural crest. PLoS One *7*, e47394.

Kaufman, C. K., Mosimann, C., Fan, Z. P., Yang, S., Thomas, A. J., Ablain, J., Tan, J. L., Fogley, R. D., van Rooijen, E., Hagedorn, E. J., Ciarlo, C., White, R. M., Matos, D. A., Puller, A.-C., Santoriello, C., Liao, E. C., Young, R. A. and Zon, L. I. (2016). A zebrafish melanoma model reveals emergence of neural crest identity during melanoma initiation. Science *351*, aad2197.

Kelsh, R. N., Brand, M., Jiang, Y.-J., Heisenberg, C.-P., Lin, S., Haffter, P., Odenthal, J., Mullins, M. C., Van Eeden, F., Furutani-Seiki, M. et al. (1996). Zebrafish pigmentation mutations and the processes of neural crest development. Development *123*, 369–389.

Kelsh, R. N., Schmid, B. and Eisen, J. S. (2000). Genetic analysis of melanophore development in zebrafish embryos. Dev. Biol. *225*, 277–293.

Kelsh, R. N., Sosa, K. C., Owen, J. P. and Yates, C. A. (2017). Zebrafish adult pigment stem cells are multipotent and form pigment cells by a progressive fate restriction process: Clonal analysis identifies shared origin of all pigment cell types. Bioessays *39*.

Kiefer, C., Sumser, E., Wernet, M. F. and Von Lintig, J. (2002). A class B scavenger receptor mediates the cellular uptake of carotenoids in Drosophila. Proc. Natl. Acad. Sci. U. S. A. *99*, 10581–10586.

Kivioja, T., Vähärautio, A., Karlsson, K., Bonke, M., Enge, M., Linnarsson, S. and Taipale, J. (2011). Counting absolute numbers of molecules using unique molecular identifiers. Nature Methods *9*, 72–74.

Knight, R. D., Nair, S., Nelson, S. S., Afshar, A., Javidan, Y., Geisler, R., Rauch, G.-J. and Schilling, T. F. (2003). lockjaw encodes a zebrafish tfap2a required for early neural crest development. Development *130*, 5755–5768.

Kodric-Brown, A. (1985). Female preference and sexual selection for male coloration in the guppy (Poecilia reticulata). Behavioral Ecology and Sociobiology *17*, 199–205.

Koopman, R., Schaart, G. and Hesselink, M. K. (2001). Optimisation of oil red O staining permits combination with immunofluorescence and automated quantification of lipids. Histochem. Cell Biol. *116*, 63–68.

Krauss, J., Astrinidis, P., Frohnhöfer, H. G., Walderich, B. and Nüsslein-Volhard, C. (2013). transparent, a gene affecting stripe formation in Zebrafish, encodes the mitochondrial protein Mpv17 that is required for iridophore survival. Biol. Open *2*, 703–710.

Kurz, D. J., Decary, S., Hong, Y. and Erusalimsky, J. D. (2000). Senescence-associated (beta)-galactosidase reflects an increase in lysosomal mass during replicative ageing of human endothelial cells. J. Cell Sci. *113 (Pt 20)*, 3613–3622.

Lang, M. R., Patterson, L. B., Gordon, T. N., Johnson, S. L. and Parichy, D. M. (2009). Basonuclin-2 requirements for zebrafish adult pigment pattern development and female fertility. PLoS Genet. *5*, e1000744.

Larson, T. A., Gordon, T. N., Lau, H. E. and Parichy, D. M. (2010). Defective adult oligodendrocyte and Schwann cell development, pigment pattern, and craniofacial morphology in puma mutant zebrafish having an alpha tubulin mutation. Dev. Biol. *346*, 296–309.

Le Guellec, D., Morvan-Dubois, G. and Sire, J.-Y. (2003). Skin development in bony fish with particular emphasis on collagen deposition in the dermis of the zebrafish (Danio rerio). International Journal of Developmental Biology *48*, 217–231.

Lee, B. Y., Han, J. A., Im, J. S., Morrone, A., Johung, K., Goodwin, E. C., Kleijer, W. J., DiMaio, D. and Hwang, E. S. (2006). Senescence-associated beta-galactosidase is lysosomal beta-galactosidase. Aging Cell *5*, 187–195.

Lee, H.-O., Levorse, J. M. and Shin, M. K. (2003). The endothelin receptor-B is required for the migration of neural crest-derived melanocyte and enteric neuron precursors. Developmental Biology *259*, 162–175.

Leikam, C., Hufnagel, A. L., Otto, C., Murphy, D. J., Mühling, B., Kneitz, S., Nanda, I., Schmid, M., Wagner, T. U., Haferkamp, S., Bröcker, E.-B., Schartl, M. and Meierjohann, S. (2015). In vitro evidence for senescent multinucleated melanocytes as a source for tumor-initiating cells. Cell Death & Disease *6*, e1711–e1711.

Levy, C., Khaled, M. and Fisher, D. E. (2006). MITF: master regulator of melanocyte development and melanoma oncogene. Trends in Molecular Medicine *12*, 406–414.

Lister, J. A. (2019). Larval but not adult xanthophore pigmentation in zebrafish requires GTP cyclohydrolase 2 (gch2) function. Pigment Cell & Melanoma Research .

Lister, J. A., Close, J. and Raible, D. W. (2001). Duplicate mitf Genes in Zebrafish: Complementary Expression and Conservation of Melanogenic Potential. Developmental Biology *237*, 333–344.

Lister, J. A., Lane, B. M., Nguyen, A. and Lunney, K. (2011). Embryonic expression of zebrafish MiT family genes tfe3b, tfeb, and tfec. Dev. Dyn. *240*, 2529–2538.

Lister, J. A., Robertson, C. P., Lepage, T., Johnson, S. L. and Raible, D. W. (1999). nacre encodes a zebrafish microphthalmia-related protein that regulates neural-crest-derived pigment cell fate. Development *126*, 3757–3767.

Luo, R., An, M., Arduini, B. L. and Henion, P. D. (2001). Specific pan-neural crest expression of zebrafish Crestin throughout embryonic development. Dev. Dyn. *220*, 169–174.

Macosko, E. Z., Basu, A., Satija, R., Nemesh, J., Shekhar, K., Goldman, M., Tirosh, I., Bialas, A. R., Kamitaki, N., Martersteck, E. M. et al. (2015). Highly parallel genome-wide expression profiling of individual cells using nanoliter droplets. Cell *161*, 1202–1214.

Mahalwar, P., Walderich, B., Singh, A. P. and Nüsslein-Volhard, C. (2014). Local reorganization of xanthophores fine-tunes and colors the striped pattern of zebrafish. Science *345*, 1362–1364.

Mahony, C. B., Fish, R. J., Pasche, C. and Bertrand, J. Y. (2016). tfec controls the hematopoietic stem cell vascular niche during zebrafish embryogenesis. Blood *128*, 1336–1345.

Marelli, F., Carra, S., Agostini, M., Cotelli, F., Peeters, R., Chatterjee, K. and Persani, L. (2016). Patterns of thyroid hormone receptor expression in zebrafish and generation of a novel model of resistance to thyroid hormone action. Molecular and Cellular Endocrinology *424*, 102–117.

Matsumoto, J. (1965). Studies on fine structure and cytochemical properties of erythrophores in swordtail, Xiphophorus helleri, with special reference to their pigment granules (Pterinosomes). J. Cell Biol. *27*, 493–504.

McInnes, L., Healy, J., Saul, N. and Großberger, L. (2018). UMAP: Uniform Manifold Approximation and Projection. JOSS *3*, 861.

McMenamin, S. K., Bain, E. J., McCann, A. E., Patterson, L. B., Eom, D. S., Waller, Z. P., Hamill, J. C., Kuhlman, J. A., Eisen, J. S. and Parichy, D. M. (2014). Thyroid hormone-dependent adult pigment cell lineage and pattern in zebrafish. Science *345*, 1358–1361.

McMenamin, S. K. and Parichy, D. M. (2013). Metamorphosis in teleosts. Curr. Top. Dev. Biol. *103*, 127–165.

Minchin, J. E. N. and Hughes, S. M. (2008). Sequential actions of Pax3 and Pax7 drive xanthophore development in zebrafish neural crest. Dev. Biol. *317*, 508–522.

Mosimann, C., Kaufman, C. K., Li, P., Pugach, E. K., Tamplin, O. J. and Zon, L. I. (2011). Ubiquitous transgene expression and Cre-based recombination driven by the ubiquitin promoter in zebrafish. Development *138*, 169–177.

Nagao, Y., Takada, H., Miyadai, M., Adachi, T., Seki, R., Kamei, Y., Hara, I., Taniguchi, Y., Naruse, K., Hibi, M., Kelsh, R. N. and Hashimoto, H. (2018). Distinct interactions of Sox5 and Sox10 in fate specification of pigment cells in medaka and zebrafish. PLoS Genet. *14*, e1007260.

Nandi-Munshi, D. and Taplin, C. E. (2015). Thyroid-Related Neurological Disorders and Complications in Children. Pediatric Neurology *52*, 373–382.

Nord, H., Dennhag, N., Muck, J. and von Hofsten, J. (2016). Pax7 is required for establishment of the xanthophore lineage in zebrafish embryos. Mol. Biol. Cell *27*, 1853–1862.

Obika, M. (1993). Formation of pterinosomes and carotenoid granules in xanthophores of the teleost Oryzias latipes as revealed by the rapid-freezing and freeze-substitution method. Cell Tissue Res. *271*, 81–86.

Odenthal, J., Rossnagel, K., Haffter, P., Kelsh, R. N., Vogelsang, E., Brand, M., van Eeden, F. J., Furutani-Seiki, M., Granato, M., Hammerschmidt, M., Heisenberg, C. P., Jiang, Y. J., Kane, D. A., Mullins, M. C. and Nüsslein-Volhard, C. (1996). Mutations affecting xanthophore pigmentation in the zebrafish, Danio rerio. Development *123*, 391–398.

Opdecamp, K., Nakayama, A., Nguyen, M., Hodgkinson, C. A., Pavan, W. J. and Arnheiter, H. (1997). Melanocyte development in vivo and in neural crest cell cultures: crucial dependence on the Mitf basic-helix-loop-helix-zipper transcription factor. Development *124*, 2377–2386.

Orr-Weaver, T. L. (2015). When bigger is better: the role of polyploidy in organogenesis. Trends Genet. *31*, 307–315.

Packer, J. and Trapnell, C. (2018). Single-Cell Multi-omics: An Engine for New Quantitative Models of Gene Regulation. Trends in Genetics *34*, 653–665.

Packer, J. S., Zhu, Q., Huynh, C., Sivaramakrishnan, P., Preston, E., Dueck, H., Stefanik, D., Tan, K., Trapnell, C., Kim, J., Waterston, R. H. and Murray, J. I. (2019). A lineage-resolved molecular atlas of C. elegans embryogenesis at single cell resolution. bioRxiv .

Parichy, D. M., Elizondo, M. R., Mills, M. G., Gordon, T. N. and Engeszer, R. E. (2009a). Normal table of postembryonic zebrafish development: staging by externally visible anatomy of the living fish. Dev. Dyn. *238*, 2975–3015.

Parichy, D. M., Elizondo, M. R., Mills, M. G., Gordon, T. N. and Engeszer, R. E. (2009b). Normal table of postembryonic zebrafish development: staging by externally visible anatomy of the living fish. Dev. Dyn. *238*, 2975–3015.

Parichy, D. M., Mellgren, E. M., Rawls, J. F., Lopes, S. S., Kelsh, R. N. and Johnson, S. L. (2000a). Mutational analysis of endothelin receptor b1 (rose) during neural crest and pigment pattern development in the zebrafish Danio rerio. Dev. Biol. *227*, 294–306.

Parichy, D. M., Ransom, D. G., Paw, B., Zon, L. I. and Johnson, S. L. (2000b). An orthologue of the kit-related gene fms is required for development of neural crest-derived xanthophores and a subpopulation of adult melanocytes in the zebrafish, Danio rerio. Development *127*, 3031–3044.

Parichy, D. M., Rawls, J. F., Pratt, S. J., Whitfield, T. T. and Johnson, S. L. (1999). Zebrafish sparse corresponds to an orthologue of c-kit and is required for the morphogenesis of a subpopulation of melanocytes, but is not essential for hematopoiesis or primordial germ cell development. Development *126*, 3425–3436.

Parichy, D. M. and Spiewak, J. E. (2015). Origins of adult pigmentation: diversity in pigment stem cell lineages and implications for pattern evolution. Pigment Cell Melanoma Res. *28*, 31–50.

Parichy, D. M., Turner, J. M. and Parker, N. B. (2003). Essential role for puma in development of postembryonic neural crest-derived cell lineages in zebrafish. Developmental Biology *256*, 221–241.

Patil, C. and Walter, P. (2001). Intracellular signaling from the endoplasmic reticulum to the nucleus: the unfolded protein response in yeast and mammals. Curr. Opin. Cell Biol. *13*, 349–355.

Patterson, L. B., Bain, E. J. and Parichy, D. M. (2014). Pigment cell interactions and differential xanthophore recruitment underlying zebrafish stripe reiteration and Danio pattern evolution. Nat. Commun. *5*, 5299.

Patterson, L. B. and Parichy, D. M. (2013). Interactions with iridophores and the tissue environment required for patterning melanophores and xanthophores during zebrafish adult pigment stripe formation. PLoS Genet. *9*, e1003561.

Patton, E. E. and Zon, L. I. (2001). The art and design of genetic screens: zebrafish. Nature Reviews Genetics *2*, 956–966.

Petersen, J. and Adameyko, I. (2017). Nerve-associated neural crest: peripheral glial cells generate multiple fates in the body. Current Opinion in Genetics & Development *45*, 10–14.

Petratou, K., Subkhankulova, T., Lister, J. A., Rocco, A., Schwetlick, H. and Kelsh, R. N. (2018). A systems biology approach uncovers the core gene regulatory network governing iridophore fate choice from the neural crest. PLoS Genet. *14*, e1007402.

Pijuan-Sala, B., Griffiths, J. A., Guibentif, C., Hiscock, T. W., Jawaid, W., Calero-Nieto, F. J., Mulas, C., Ibarra-Soria, X., Tyser, R. C. V., Ho, D. L. L., Reik, W., Srinivas, S., Simons, B. D., Nichols, J., Marioni, J. C. and Göttgens, B. (2019). A single-cell molecular map of mouse gastrulation and early organogenesis. Nature *566*, 490–495.

Porazzi, P., Calebiro, D., Benato, F., Tiso, N. and Persani, L. (2009). Thyroid gland development and function in the zebrafish model. Molecular and Cellular Endocrinology *312*, 14–23.

Qiu, X., Hill, A., Packer, J., Lin, D., Ma, Y.-A. and Trapnell, C. (2017a). Single-cell mRNA quantification and differential analysis with Census. Nat. Methods *14*, 309–315.

Qiu, X., Mao, Q., Tang, Y., Wang, L., Chawla, R., Pliner, H. A. and Trapnell, C. (2017b). Reversed graph embedding resolves complex single-cell trajectories. Nat. Methods *14*, 979–982.

Quigley, I. K., Turner, J. M., Nuckels, R. J., Manuel, J. L., Budi, E. H., MacDonald, E. L. and Parichy, D. M. (2004). Pigment pattern evolution by differential deployment of neural crest and post-embryonic melanophore lineages in Danio fishes. Development *131*, 6053–6069.

R Core Team (2017). R: A Language and Environment for Statistical Computing.

Raposo, G., Marks, M. S. and Cutler, D. F. (2007). Lysosome-related organelles: driving post-Golgi compartments into specialisation. Current Opinion in Cell Biology *19*, 394–401.

Regneri, J., Klotz, B., Wilde, B., Kottler, V. A., Hausmann, M., Kneitz, S., Regensburger, M., Maurus, K., Götz, R., Lu, Y., Walter, R. B., Herpin, A. and Schartl, M. (2018). Analysis of the putative tumor suppressor gene cdkn2ab in pigment cells and melanoma of Xiphophorus and medaka. Pigment Cell & Melanoma Research *32*, 248–258.

Riabowol, K., Schiff, J. and Gilman, M. Z. (1992). Transcription factor AP-1 activity is required for initiation of DNA synthesis and is lost during cellular aging. Proc. Natl. Acad. Sci. U. S. A. *89*, 157–161.

Robertson, G., McGee, C., Dumbarton, T., Croll, R. and Smith, F. (2007). Development of the swimbladder and its innervation in the zebrafish, Danio rerio. Journal of Morphology *268*, 967–985.

Rosenberg, A. B., Roco, C. M., Muscat, R. A., Kuchina, A., Sample, P., Yao, Z., Graybuck, L. T., Peeler, D. J., Mukherjee, S., Chen, W., Pun, S. H., Sellers, D. L., Tasic, B. and Seelig, G. (2018). Single-cell profiling of the developing mouse brain and spinal cord with split-pool barcoding. Science *360*, 176–182.

Salis, P., Roux, N., Soulat, O., Lecchini, D., Laudet, V. and Frédérich, B. (2018). Ontogenetic and phylogenetic simplification during white stripe evolution in clownfishes. BMC Biology *16*.

Santos, J. C., Coloma, L. A. and Cannatella, D. C. (2003). Multiple, recurring origins of aposematism and diet specialization in poison frogs. Proceedings of the National Academy of Sciences *100*, 12792–12797.

Shah, A. N., Davey, C. F., Whitebirch, A. C., Miller, A. C. and Moens, C. B. (2015). Rapid reverse genetic screening using CRISPR in zebrafish. Nat. Methods *12*, 535–540.

Shah, M., Orengo, I. F. and Rosen, T. (2006). High prevalence of hypothyroidism in male patients with cutaneous melanoma. Dermatol. Online J. *12*, 1.

Sharan, S. K., Thomason, L. C., Kuznetsov, S. G. and Court, D. L. (2009). Recombineering: a homologous recombination-based method of genetic engineering. Nat. Protoc. *4*, 206–223.

Sheets, L., Ransom, D. G., Mellgren, E. M., Johnson, S. L. and Schnapp, B. J. (2007). Zebrafish melanophilin facilitates melanosome dispersion by regulating dynein. Curr. Biol. *17*, 1721–1734.

Shi, Y.-B. (1999). Amphibian Metamorphosis: From Morphology to Molecular Biology. Wiley-Liss.

Shi, Y.-B. (2013). Chapter Ten - Unliganded Thyroid Hormone Receptor Regulates Metamorphic Timing via the Recruitment of Histone Deacetylase Complexes. In Current Topics in Developmental Biology, (Rougvie, A. E. and O'Connor, M. B., eds), vol. 105, pp. 275–297. Academic Press.

Singh, A. P., Dinwiddie, A., Mahalwar, P., Schach, U., Linker, C., Irion, U. and Nüsslein-Volhard, C. (2016). Pigment Cell Progenitors in Zebrafish Remain Multipotent through Metamorphosis. Dev. Cell *38*, 316–330.

Singh, A. P., Schach, U. and Nüsslein-Volhard, C. (2014). Proliferation, dispersal and patterned aggregation of iridophores in the skin prefigure striped colouration of zebrafish. Nat. Cell Biol. *16*, 607–614.

Sisley, K., Curtis, D., Rennie, I. G. and Rees, R. C. (1993). Loss of heterozygosity of the thyroid hormone receptor B in posterior uveal melanoma. Melanoma Res. *3*, 457–461.

Spiewak, J. E., Bain, E. J., Liu, J., Kou, K., Sturiale, S. L., Patterson, L. B., Diba, P., Eisen, J. S., Braasch, I., Ganz, J. and Parichy, D. M. (2018). Evolution of Endothelin signaling and diversification of adult pigment pattern in Danio fishes. PLoS Genet. *14*, e1007538.

Suster, M. L., Abe, G., Schouw, A. and Kawakami, K. (2011). Transposon-mediated BAC transgenesis in zebrafish. Nat. Protoc. *6*, 1998–2021.

Takayama, S., Hostick, U., Haendel, M., Eisen, J. and Darimont, B. (2008). An F-domain introduced by alternative splicing regulates activity of the zebrafish thyroid hormone receptor α. General and Comparative Endocrinology *155*, 176–189.

Thisse, C., Thisse, B. and Postlethwait, J. H. (1995). Expression of snail2, a second member of the zebrafish snail family, in cephalic mesendoderm and presumptive neural crest of wild-type and spadetail mutant embryos. Dev. Biol. *172*, 86–99.

Toews, D. P. L., Hofmeister, N. R. and Taylor, S. A. (2017). The Evolution and Genetics of Carotenoid Processing in Animals. Trends Genet. *33*, 171–182.

Toomey, M. B., Lopes, R. J., Araújo, P. M., Johnson, J. D., Gazda, M. A., Afonso, S., Mota, P. G., Koch, R. E., Hill, G. E., Corbo, J. C. and Carneiro, M. (2017). High-density lipoprotein receptor SCARB1 is required for carotenoid coloration in birds. Proc. Natl. Acad. Sci. U. S. A. *114*, 5219–5224.

Toomey, M. B. and McGraw, K. J. (2007). Modified saponification and HPLC methods for analyzing carotenoids from the retina of quail: implications for its use as a nonprimate model species. Invest. Ophthalmol. Vis. Sci. *48*, 3976–3982.

Trapnell, C., Cacchiarelli, D., Grimsby, J., Pokharel, P., Li, S., Morse, M., Lennon, N. J., Livak, K. J., Mikkelsen, T. S. and Rinn, J. L. (2014). The dynamics and regulators of cell fate decisions are revealed by pseudotemporal ordering of single cells. Nat. Biotechnol. *32*, 381–386.

Tzur, A., Moore, J. K., Jorgensen, P., Shapiro, H. M. and Kirschner, M. W. (2011). Optimizing Optical Flow Cytometry for Cell Volume-Based Sorting and Analysis. PLoS ONE *6*, e16053.

Usui, Y., Kondo, S. and Watanabe, M. (2018). Melanophore multinucleation pathways in zebrafish. Dev. Growth Differ. *60*, 454–459.

Van de Putte, T., Maruhashi, M., Francis, A., Nelles, L., Kondoh, H., Huylebroeck, D. and Higashi, Y. (2003). Mice lacking ZFHX1B, the gene that codes for Smad-interacting protein-1, reveal a role for multiple neural crest cell defects in the etiology of Hirschsprung disease-mental retardation syndrome. Am. J. Hum. Genet. *72*, 465–470.

Vella, K. R., Ramadoss, P., e Sousa, R. H. C., Astapova, I., Ye, F. D., Holtz, K. A., Harris, J. C. and Hollenberg, A. N. (2014). Thyroid Hormone Signaling In Vivo Requires a Balance between Coactivators and Corepressors. Molecular and Cellular Biology *34*, 1564–1575.

Wagner, D. E., Weinreb, C., Collins, Z. M., Briggs, J. A., Megason, S. G. and Klein, A. M. (2018). Single-cell mapping of gene expression landscapes and lineage in the zebrafish embryo. Science *360*, 981–987.

Watanabe, M., Iwashita, M., Ishii, M., Kurachi, Y., Kawakami, A., Kondo, S. and Okada, N. (2006). Spot pattern of leopard Danio is caused by mutation in the zebrafish connexin41.8 gene. EMBO Rep. *7*, 893–897.

Watanabe, M. and Kondo, S. (2015). Is pigment patterning in fish skin determined by the Turing mechanism? Trends Genet. *31*, 88–96.

Williams, J. S., Hsu, J. Y., Rossi, C. C. and Artinger, K. B. (2018). Requirement of zebrafish pcdh10a and pcdh10b in melanocyte precursor migration. Dev. Biol. .

Zhang, Y. M., Zimmer, M. A., Guardia, T., Callahan, S. J., Mondal, C., Di Martino, J., Takagi, T., Fennell, M., Garippa, R., Campbell, N. R., Bravo-Cordero, J. J. and White, R. M. (2018). Distant Insulin Signaling Regulates Vertebrate Pigmentation through the Sheddase Bace2. Dev. Cell *45*, 580–594.e7.

Ziegler, I. (2003). The pteridine pathway in zebrafish: regulation and specification during the determination of neural crest cell-fate. Pigment Cell Res. *16*, 172–182.

Ziller, C., Dupin, E., Brazeau, P., Paulin, D. and Le Douarin, N. M. (1983). Early segregation of a neuronal precursor cell line in the neural crest as revealed by culture in a chemically defined medium. Cell *32*, 627–638.

VITA

Lauren M. Saunders grew up in Geneva, Illinois. She graduated from St. Olaf College in Northfield, MN with a B.A. in Biology and Asian Studies. While at St. Olaf, she studied intracellular nutrient homeostasis in *Tetrahymena thermophila* in the lab of Eric Cole. Before starting graduate school, Lauren discovered her love of developmental biology in the lab of Victoria Bautch at the University of North Carolina at Chapel Hill studying blood vessel morphogenesis in response to Notch and BMP signaling. When not in lab, Lauren spends her time in the mountains, doing at-home fermentation experiments, and making new pottery to contain her ever-growing collection of plants.